



Turun yliopisto
University of Turku

PHOTON UPCONVERTING NANOPHOSPHORS:

Unique Reporters for Optical Biosensing

Riikka Arppe

University of Turku

Faculty of Mathematics and Natural Sciences

Department of Biochemistry

Analytical Biotechnology

National Doctoral Programme of Advanced Diagnostic Technologies and Applications, DIA-NET

Doctoral Programme in Molecular Life Sciences, DPMLS

Supervised by

Professor Tero Soukka, PhD
Department of Biochemistry / Biotechnology
University of Turku
Turku, Finland

Adjunct Professor Mika Lastusaari, PhD
Department of Chemistry
Laboratory of Materials Chemistry and
Chemical Analysis
University of Turku
Turku, Finland

Reviewed by

Harri Takalo, PhD
Innotrac Diagnostics Oy
Turku, Finland

Artur Bednarkiewicz, PhD
Institute of Low Temperature and
Structure Research
Polish Academy of Sciences
Wroclaw Research Centre EIT+
Wroclaw, Poland

Opponent

Professor Dmitri B. Papkovsky, PhD
School of Biochemistry and Cell Biology
University College Cork
Cavanagh Pharmacy Building, 1.28
College Road, Cork
Ireland

The originality of this thesis has been checked in accordance with the University of Turku quality assurance system using the Turnitin OriginalityCheck service.

ISBN 978-951-29-6181-8 (PRINT)

ISBN 978-951-29-6182-5 (PDF)

ISSN 0082-7002

Painosalama Oy - Turku, Finland 2015

Remember kids, the only difference between
screwing around and science is writing it down.

- Adam Savage

CONTENTS

CONTENTS	4
LIST OF ORIGINAL PUBLICATIONS	6
ABBREVIATIONS.....	7
ABSTRACT	9
TIIVISTELMÄ.....	10
1 INTRODUCTION.....	11
2 REVIEW OF THE LITERATURE	13
2.1 Photon upconverting nanophosphors.....	13
2.1.1 Composition and upconversion mechanisms	13
2.1.2 Synthesis of nanophosphors.....	18
2.1.3 Luminescent properties.....	20
2.1.4 Surface chemistry	26
2.1.5 Characterization of UCNPs.....	33
2.2 Applications in homogeneous sensing	34
2.2.1 Upconversion resonance energy transfer	34
2.2.2 Optical (bio)chemical and temperature sensors	35
2.2.3 Bioanalytical assays	38
3 AIMS OF THE STUDY	41
4 SUMMARY OF MATERIALS AND METHODS	42
4.1 Upconverting nanophosphor bioconjugates	42
4.1.1 UCNP materials and their characterization.....	42
4.1.2 Surface modification and bioconjugation	42
4.2 High gradient magnetic separation	44
4.3 Homogeneous assays using UCNPs	45
4.3.1 pH-nanosensor	45
4.3.2 Whole blood folic acid assay	46
4.4 Instrumentation for luminescence measurements	47

4.4.1 Plate readers	47
4.4.2 Spectral analysis	48
4.4.3 Time-domain lifetime analysis	48
4.4.4 Imaging	49
5 SUMMARY OF RESULTS AND DISCUSSION.....	50
5.1 Upconverting nanophosphor bioconjugates	50
5.1.1 UCNPs	50
5.1.2 Surface modification and bioconjugation of the UCNPs	51
5.1.3 Purification of bioconjugated UCNPs	54
5.2 Homogeneous assays using UCNPs	56
5.2.1 pH-nanosensor	57
5.2.2 Whole blood folic acid assay	61
5.3 Quenching effect of water on photon upconversion.....	63
6 CONCLUSIONS AND FUTURE PROSPECTS	69
ACKNOWLEDGEMENTS	72
REFERENCES	75
ORIGINAL PUBLICATIONS	87

LIST OF ORIGINAL PUBLICATIONS

This thesis is based on the following original publications, referred to in the text by the Roman numerals (I–IV).

- I Riikka Arppe, Oskari Salovaara, Leena Mattsson, Satu Lahtinen, Timo Valta, Terhi Riuttamäki and Tero Soukka (2013). High gradient magnetic separation of upconverting lanthanide nanophosphors based on their intrinsic paramagnetism. *Journal of Nanoparticle Research* **15**: 1883.
- II Riikka Arppe, Tuomas Näreoja, Sami Nylund, Leena Mattsson, Sami Koho, Jessica M. Rosenholm, Tero Soukka and Michael Schäferling (2014). Photon upconversion sensitized nanoprobes for sensing and imaging of pH. *Nanoscale* **6**: 6837–6843.
- III Riikka Arppe, Leena Mattsson, Krista Korpi, Sami Blom, Qi Wang, Terhi Riuttamäki and Tero Soukka (2015). Homogeneous assay for whole blood folate using photon upconversion. *Analytical Chemistry* **87**: 1782–1788.
- IV Riikka Arppe, Iko Hyppänen, Niina Perälä, Riikka Peltomaa, Martin Kaiser, Christian Würth, Simon Christ, Ute Resch-Genger, Michael Schäferling and Tero Soukka (2015). Quenching of the upconversion luminescence of NaYF₄: Yb³⁺, Er³⁺ and NaYF₄: Yb³⁺, Tm³⁺ nanophosphors by water: the role of the sensitizer Yb³⁺ in non-radiative relaxation. *Nanoscale*, **7**: 11746–11757.

In addition, unpublished data are included.

The original publications have been reproduced with the permission of the copyright holders.

ABBREVIATIONS

AF680	Alexa Fluor 680
APTE	addition of photons by transfer of energy
ATP	adenosine triphosphate
BSA	bovine serum albumin
CCD	charge coupled device
ConA	concanavalin A
CTAB	cetyltrimethylammonium bromide
DMEM	<i>Dulbecco's Modified Eagle's medium</i>
DMF	dimethylformamide
DTT	dithiothreitol
EDC	1-ethyl-3-(3-dimethylaminopropyl)carbodiimide hydrochloride
EDTA	ethylenediamine tetraacetic acid
EDS	energy-dispersive spectrometer
EDX	energy-dispersive X-ray spectroscopy
EELS	electron energy loss spectrometer
EMU	energy migration-mediated upconversion
ESA	excited state absorption
ETU	energy transfer upconversion
FBP	folate binding protein
FCS	fetal calf serum
FRET	Förster resonance energy transfer
GSA	ground state absorption
HAADF	high-angle annular dark-field
HGMS	high gradient magnetic separation
HPLC	high-performance liquid chromatography
HR-TEM	high-resolution transmission electron microscope
ICP-AES	inductively coupled plasma atomic emission spectroscopy
ICP-MS	inductively coupled plasma mass spectrometry
IR	infrared
Mab	monoclonal antibody
MIP	molecularly imprinted polymer
MMP-2	matrix metalloproteinase-2
MRSA	methicillin-resistant <i>Staphylococcus aureus</i>
NIR	near infrared
NOBF ₄	nitrosonium tetrafluoroborate
OA	oleic acid
ODE	1-octadecene
OM	oleylamine
PA	photon avalanche
PAA	poly(acrylic acid)
PAH	poly(allylamine hydrochloride)
PEG	polyethylene glycol

Abbreviations

PEI	polyethyleneimine
PMAO	poly(maleic anhydride-alt-1-octadecene)
PMT	photomultiplier tube
PSA	prostate-specific antigen
PSS	poly(sodium 4-styrenesulfonate)
PVP	polyvinylpyrrolidone
QY	quantum yield
SEM	scanning electron microscope
STED	stimulated emission depletion
STEM	scanning transmission microscope
sulfo-NHS	<i>N</i> -hydroxysulfosuccinimide sodium salt
TAMRA	carboxytetramethylrhodamine
TEM	transmission electron microscope
TEOS	tetraethyl orthosilicate
TGA	thermogravimetric analysis
TMED	(<i>N</i> -(3-trimethoxysilyl)propyl)ethylene diamine
TMOS	tetramethyl orthosilicate
TOPO	trioctylphosphine oxide
UCNP	upconverting nanophosphor
UCPL	upconversion photoluminescence
UC-RET	upconversion resonance energy transfer

ABSTRACT

Upconversion photoluminescence is a unique property of mostly certain inorganic materials, which are capable of converting low-energy infrared radiation into a higher-energy emission at visible wavelengths. This anti-Stokes shift enables luminescence detection without autofluorescence, which makes the upconverting materials a highly suitable reporter technology for optical biosensing applications. Furthermore, they exhibit long luminescence lifetime with narrow bandwidths also at the optical window of biomaterials enabling luminescence measurements in challenging sample matrices, such as whole blood.

The aim of this thesis was to study the unique properties and the applicability of nano-sized upconverting phosphors (UCNPs) as reporters in biosensing applications. To render the inorganic nanophosphors water-dispersible and biocompatible, they were subjected to a series of surface modifications starting with silica-encapsulation and ending with a bioconjugation step with an analyte-recognizing biomolecule. The paramagnetism of the lanthanide dopants in the nanophosphors was exploited to develop a highly selective separation method for the UCNP-bioconjugates based on the magnetic selectivity of the high gradient magnetic separation (HGMS) system.

The applicability of the nano-sized UCNPs as reporters in challenging sample matrices was demonstrated in two homogeneous sensing applications based on upconversion resonance energy transfer (UC-RET). A chemosensor for intracellular pH was developed exploiting UC-RET between the UCNP and a fluorogenic pH-sensitive dye with strongly increasing fluorescence intensity in decreasing pH. The pH-independent emission of the UCNPs at 550 nm was used for referencing. The applicability of the pH-nanosensor for intracellular pH measurement was tested in HeLa cells, and the acidic pH of endosomes could be detected with a confocal fluorescence microscope. Furthermore, a competitive UC-RET-based assay for red blood cell folic acid was developed for the measurement of folate directly from a whole blood sample. The optically transparent window of biomaterials was used in both the excitation and the measurement of the UC-RET sensitized emission of a near-infrared acceptor dye to minimize sample absorption, and the anti-Stokes detection completely eliminated the Stokes-shifted autofluorescence.

The upconversion photoluminescence efficiency is known to be dependent on crystallite size, because the increasing surface-to-volume ratio of nano-sized UCNPs renders them more susceptible to quenching effects of the environment than their bulk counterpart. Water is known to efficiently quench the luminescence of lanthanide dopants. In this thesis, the quenching mechanism of water was studied using luminescence decay measurements. Water was found to quench the luminescence of UCNPs by increasing the non-radiative relaxation of the excited state of Yb^{3+} sensitizer ion, which had a very strong quenching effect on upconversion luminescence intensity.

TIIVISTELMÄ

Käänteisviritteinen fotoluminesenssi on lähinnä tiettyjen epäorgaanisten nanomateriaalien ainutlaatuinen ominaisuus, jossa matalaenergistä infrapunasäteilyä muutetaan korkeampienergisiksi näkyvän aallonpituuden emissioksi. Tämä Stokesin siirtymän vastainen fotoluminesenssi mahdollistaa mittaamisen ilman autofluoresenssia, minkä takia käänteisvirittetyt materiaalit soveltuvat leimoiksi optisiin biosensorisovelluksiin. Lisäksi ne tuottavat pitkäikäistä emissiota kapeilla kaistanleveyksillä myös aallonpituusalueilla, jotka biomateriaaleissa ovat optisesti läpinäkyviä, ja mahdollistavat näin luminesenssimittaukset myös hankalista näytemateriaaleista, kuten kokoverestä.

Väitöskirjan tarkoituksena oli tutkia nanokokoisten käänteisviritteisten partikkelien ainutlaatuisia ominaisuuksia ja niiden käyttöä leimoina biosensorisovelluksissa. Nanopartikkelit pinnoitettiin silikalla ja analyyttejä tunnistavilla biomolekyyleillä. Partikkelien sisältämien lantanidi-ionien paramagneettisuutta käytettiin hyväksi kehitettäessä erittäin selektiivistä erotusmenetelmää biomolekyyli-pinnoitettujen partikkeleiden puhdistusta varten. Menetelmä perustui korkean gradientin magneettiseen erotteluun.

Nanopartikkeleiden käyttöä leimoina hankalissa näytemateriaaleissa tutkittiin kehittämällä kaksi käänteisviritteisen luminesenssin resonanssienergiansiirtoon perustuvaa, erotusvapaata sovellusta. Väitöskirjassa kehitettiin kemiallinen sensori solunsisäisen pH:n tutkimiseen. Sensori perustui resonanssienergiansiirtoon nanopartikkelin ja pH-herkän pienmolekyylivärin välillä. pH-nanosensorin soveltuvuutta solunsisäisen pH:n mittaamiseen tutkittiin HeLa-soluilla, joiden endosomien hapan pH pystyttiin havaitsemaan fluoresenssimikroskoopin avulla. Väitöskirjassa kehitettiin myös kilpaileva pesuvaiheeton määrittäminen, jolla punasolujen foolihappopitoisuus voidaan mitata suoraan kokoverinäytteestä. Biologisten materiaalien optisesti läpinäkyviä valon aallonpituuksia käytettiin sekä käänteisviritteisten nanopartikkelien virittämiseen että resonanssienergiansiirron vastaanottajapienvärin emission mittaamiseen, jotta pystyttiin minimoimaan kokoverinäytteen valon absorptio. Lisäksi Stokesin siirtymän vastainen fotoluminesenssi mahdollisti mittaamisen ilman autofluoresenssia.

Käänteisviritteisen fotoluminesenssin tehokkuuden tiedetään olevan kidekokoriippuvainen, koska nanokokoisten partikkeleiden suuri pinnan ja tilavuuden välinen suhde altistaa partikkelit ympäristön luminesenssia sammuttaville vaikutuksille. Vesi sammuttaa tehokkaasti lantanidien luminesenssia, ja väitöskirjassa tutkittiin sen mekanismia tarkemmin luminesenssin elinikämittausten avulla. Veden havaittiin sammuttavan voimakkaasti käänteisviritteisten nanopartikkeleiden luminesenssia lisäämällä Yb^{3+} herkistimen virittyneen tilan säteilemätöntä purkautumista.

1 INTRODUCTION

Optical biosensing includes both chemical sensing and bioanalytical assays, which can be further categorized into heterogeneous or homogeneous assays. In heterogeneous assays the label signal is detected after the specific binding reaction is separated from interfering assay components with washing steps. The binding reaction is performed on a solid surface. Homogeneous assays are simple “mix-and-measure” type of tests, in which the detection is based on the modulation of the optical signal upon a specific biomolecular recognition of the analyte. Bioanalytical assays employ, for example, enzymes, antibodies, or oligonucleotides as the analyte recognition moieties, and chemosensors require indicator dyes, whose optical properties change in the presence of the chemical analytes, such as pH, ions, or gases. Luminescence provides the transduction of the recognition event into a measurable optical signal. Luminescence is the primary tool in the detection of chemical and biochemical analytes in medical diagnostics due to high sensitivity and fast response (Hemmilä, 1985). However, conventional luminescent labels suffer from autofluorescence background and the high absorption of light at ultraviolet and visible wavelengths by the biological sample material, which limits the sensitivity.

Photon upconverting nanophosphors (UCNPs) represent an exciting new reporter technology with unique optical properties. Unlike conventional fluorescent labels, they are able to produce visible emission upon excitation with near-infrared radiation. This is possible via a sequential absorption of two or more low-energy photons to produce one higher-energy photon (Auzel, 1966). The anti-Stokes photoluminescence enables detection with low background even in biological material, because autofluorescence is totally eliminated by spectral separation. Furthermore, the light absorption by the biological sample at near-infrared wavelengths is minimal. The long luminescence lifetime of UCNPs with narrow bandwidths makes UCNPs ideal donors for upconversion resonance energy transfer (UC-RET) -based homogeneous applications.

The applicability of photon upconversion for sensitive bioanalytical detection has already been proved with bulk phosphor material (Kuningas *et al.*, 2007; Riuttamäki and Soukka, 2014). However, the large particle size caused problems, such as large signal variation and high background in homogeneous assays originating from non-proximity-based reabsorptive energy transfer from the particle core, as only the dopants located on the particle surface are able to transfer energy to acceptors via dipole-dipole interaction (Riuttamäki *et al.*, 2011). Thereafter, synthetic methods for the production of nanosized upconverting materials have been established. The decreasing particle size should improve the specific activity of these reporters and provide new possibilities for their exploitation, such as intracellular sensing. With particle size in the nano-range, the whole volume of the UCNP is in the range for UC-RET, which should improve the signal-to-background ratio of homogeneous assays increasing their sensitivity. However, the surface quenching effects are also stronger

in nano-sized UCNPs attributing to their low luminescence quantum yield, which has an opposite impact on the signal-to-background ratio (Boyer and van Veggel, 2010). Thus, the optimal nanocrystal size for homogeneous sensing is a trade-off between the high UC-RET efficiency and the low luminescence intensity.

2 REVIEW OF THE LITERATURE

2.1 Photon upconverting nanophosphors

2.1.1 Composition and upconversion mechanisms

Upconversion mechanisms

In contrast to “conventional” fluorescence, in which one higher-energy photon is absorbed and one lower-energy photon is emitted, photon upconversion is a process in which two or more low-energy photons are absorbed sequentially by the UCNP, and subsequently one higher-energy photon is emitted. This thesis concentrates only on the most efficient upconversion mechanisms which are commonly exploited with upconverting nanophosphors, including excited state absorption (ESA), energy transfer upconversion (ETU) and photon avalanche (PA) (Figure 1). All of these processes take advantage of metastable intermediate excited energy levels for temporary energy storage. Thus, low excitation power densities are required, unlike in those processes, where no intermediate levels exist, such as cooperative sensitization, second harmonic generation, and two-photon absorption. (Auzel, 2004; Wang and Liu, 2009)

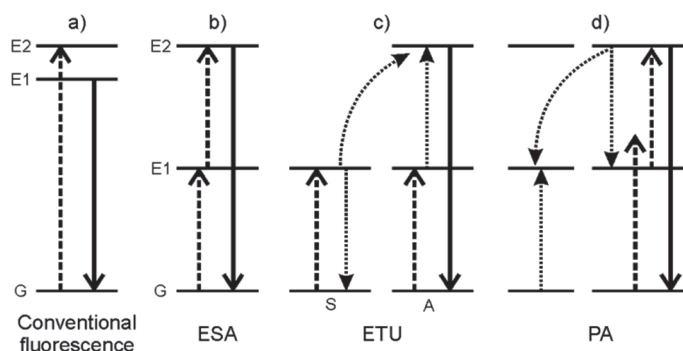


Figure 1. Simplified energy diagrams of a) “conventional” fluorescence mechanism, and b-d) upconversion photoluminescence mechanisms. Dashed, solid, and dotted lines represent photon absorption, photon emission and energy transfer processes, respectively. *ESA*, excited state absorption; *ETU*, energy transfer upconversion; *PA*, photon avalanche; *S*, sensitizer; *A*, activator; *G*, ground state; *E1*, *E2*, excited energy state. Based on figures by Wang and Liu (2009) and Dong *et al.* (2015).

The *excited state absorption* (ESA) can occur if the energy gaps between three or more subsequent energy levels of a single ion are very similar and if the intermediate levels are metastable. A monochromatic light source excites the ion from the ground state *G* to the first metastable energy level *E1* in a process called ground state absorption (GSA). A second pump photon promotes the ion further to a higher-lying energy state *E2* via the ESA process. Thereafter, upconversion emission occurs via radiative transition from *E2* to *G*. (Auzel, 2004; Wang and Liu, 2009) Lanthanide ions with a ladder-like energy level structure are highly suitable emitters for the singly-

doped upconverting nanophosphors. Most commonly used lanthanides are Er^{3+} , Tm^{3+} , and Ho^{3+} . The major parameters affecting upconversion in a system with a single dopant are the distance between two neighboring ions and the absorption cross-section of the ion. With the equally separated energy levels, cross-relaxation processes (Figure 2) can occur between two neighboring ions in high doping concentrations, resulting in the quenching of the excitation energy. The absorptivity of most lanthanides is low leading to low pump efficiency (Li *et al.*, 2015). Thus, the ESA process is the least efficient of the three upconversion processes (Haase and Schäfer, 2011). The quantum efficiency is in the order of 10^{-5} (Auzel, 2004). However, ESA or GSA is also involved in both ETU and PA mechanisms.

To enhance upconversion efficiency, another ion with a larger absorption cross-section is co-doped to the upconverting nanophosphors as a sensitizer to absorb the excitation energy. In *energy transfer upconversion* (ETU), also called *addition of photons by transfer of energy* (APTE) (Auzel, 1966), two neighboring ions, a sensitizer and an activator, both absorb a pump photon of a same energy populating their metastable levels E1 via the GSA mechanism. An energy transfer process from the sensitizer to the activator further promotes the activator ion to a higher-lying emitting energy state E2 while the sensitizer relaxes back to the ground state. The energy transfer process is a non-radiative, dipole-dipole resonant interaction (Figure 2) and, thus, the distance between the two ions affects the energy transfer efficiency and further, the upconversion efficiency. The inter-ion distance is determined by the dopant concentration. The ETU process is 100-fold more efficient than ESA and most frequently used in upconverting nanomaterials. (Wang and Liu, 2009).

The energy transfer processes involved in photon upconversion are illustrated in Figure 2. If the $G \rightarrow E1$ transitions of the sensitizer and activator are in resonance, i.e., the energy difference between the two levels are equal, a resonant non-radiative energy transfer may occur. However, if a small energy mismatch exists between the pair, the energy transfer must be phonon-assisted to meet the resonance condition. A cross-relaxation can occur in a pair of two neighboring ions of the same kind (or with similar energy level spacing), in which one of the ions is in its higher excited state. An energy transfer between the two ions brings both ions to the E1 energy state. Cross-relaxation is the cause of concentration quenching, because its rate increases in increasing ion concentrations as the distance of the two neighboring ions become shorter. (Auzel, 2004; Chen and Zhao, 2012)

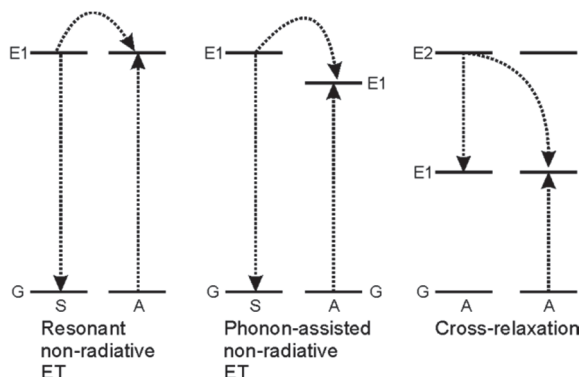


Figure 2. Energy transfer processes in UCNP. *ET*, energy transfer; *S*, sensitizer; *A*, activator; *G*, ground state; *E1*, *E2*, excited energy state. Based on a figure by Auzel (2004).

The third upconversion process is called *photon avalanche* (PA) which was first discovered by Chivian *et al.* (1979) in Pr^{3+} -based infrared quantum counters. Photon avalanche features an unusual pump mechanism requiring non-resonant, higher pump intensity. The process starts with the population of *E1* level by a weak, non-resonant GSA followed by a resonant ESA populating the higher-lying emitting *E2* energy level. Thereafter, a cross-relaxation between the excited ion and a neighboring ground-state ion occurs resulting in both ions populating the intermediate energy level *E1*. The two ions then again populate the level *E2* via ESA to further initiate cross-relaxation, leading to a looping process. Thus, the upconversion emission produced by photon avalanche is very strong. The PA process is considered to be the most efficient upconversion process. However, the emission response is delayed due to the looping processes with a rise time up to a few seconds. Also the weak GSA and the high pump threshold limit the use of PA. (Joubert, 1999; Wang and Liu, 2009; Zheng *et al.*, 2015) In fact, only a few nanomaterials have shown PA-based upconversion (Deng *et al.*, 2008).

Another novel, efficient upconversion mechanism is *energy migration-mediated upconversion* (EMU), which involves four types of luminescent centers located in separate layers. The luminescent ions are either sensitizers, accumulators, migrators, or activators. (Wang *et al.*, 2011b) To eliminate deleterious cross-relaxation processes between the activator and the accumulator ions, this mechanism requires a core-shell structure for the upconverting nanophosphors, which lies out of the scope of this thesis.

Composition of upconverting nanophosphors

Upconverting nanophosphors comprise the inorganic host lattice and the lanthanide dopant ions, which act as luminescent centers. Lanthanides comprise lanthanum and the f-block elements ranging from cerium to lutetium. Together with scandium and yttrium, they are also known as the rare earth elements. The chemical properties of lanthanides are similar due to the 4f-orbitals, which are shielded by the filled 5s and

5p shells and do not, therefore, play a role in chemical bonding. The unique luminescent properties of lanthanides originate from the f–f transitions, which are parity forbidden according to the Laporte selection rule. When lanthanides are placed in a coordinating environment, such as in an inorganic crystal, the f–f transitions become partly allowed due to the crystal-field coupling, which induces further splitting of the lanthanide electronic energy levels. These transitions are called *induced electric dipole transitions*, which are weaker than the fully allowed transitions found in organic chromophores. This is the reason for the long lifetimes of lanthanide luminescence in complexes. (Liu, 2015; Werts, 2005) The physical properties of lanthanides include their paramagnetism, due to the fact that all lanthanides have unpaired f-electrons. (Evans and Tew, 1981; Greenwood and Earnshaw, 1997; Werts, 2005)

Most lanthanide ions possess multiple metastable energy levels, which makes them highly suitable activators in upconverting nanophosphors. Theoretically, photon upconversion is possible with most lanthanide ions. Their intermediate and excited energy levels should be spaced equally to facilitate ESA and energy transfer processes. The most common and most efficient activators are Er^{3+} , Tm^{3+} , and Ho^{3+} , which all have ladder-like energy level diagrams with large enough spacing to reduce the probability of non-radiative multiphonon relaxations. However, the ladder-like arrangement of the energy levels can also lead to deleterious cross-relaxation processes when the ion-to-ion distance of dopants in the host lattice decreases. Thus, the concentration of the activators must be kept low to avoid the concentration quenching effects. The upper limit for activator concentrations in UCNPs is 3 mol% for Er^{3+} and 0.5 mol% for Tm^{3+} . (Haase and Schäfer, 2011; Wang and Liu, 2009)

The absorption cross-section of most lanthanides is low due to the forbidden nature of f–f transitions leading to poor excitation efficiency. The efficiency can be enhanced by co-doping the UCNPs with a sensitizer ion possessing larger absorption cross-section in the NIR region, to take advantage of the ETU process. Yb^{3+} has a relatively large absorption cross-section at 980 nm ($9.11 \times 10^{-21} \text{ cm}^2$) (Dong *et al.*, 2015) and a simple energy level diagram with only one excited energy state, which is well resonant with the transitions of the common activator ions facilitating energy transfer. The concentration of Yb^{3+} can be kept high without the deleterious cross-relaxations processes, normally at ~20 mol%. This increases the absorption probability of NIR photons. (Dong *et al.*, 2015; Heer *et al.*, 2004; Suyver *et al.*, 2006)

The energy level diagrams of two of the most common dopant combinations, $\text{Yb}^{3+}/\text{Er}^{3+}$ and $\text{Yb}^{3+}/\text{Tm}^{3+}$ are presented in Figure 3. In this thesis, mostly only these two dopant combinations are discussed. Both systems take advantage of the ETU system with Yb^{3+} as the sensitizer and Er^{3+} or Tm^{3+} as the activator. Both activators produce emission at multiple wavelengths, depending on the number of excitation photons. The luminescent properties of upconverting nanophosphors are presented in more detail in section 2.1.3. An alternative energy level diagram for $\text{Yb}^{3+}/\text{Er}^{3+}$ co-

doped β -NaYF₄ nanomaterials has been recently introduced, explaining that the red emission is a product of three photon pump processes (Anderson *et al.*, 2014).

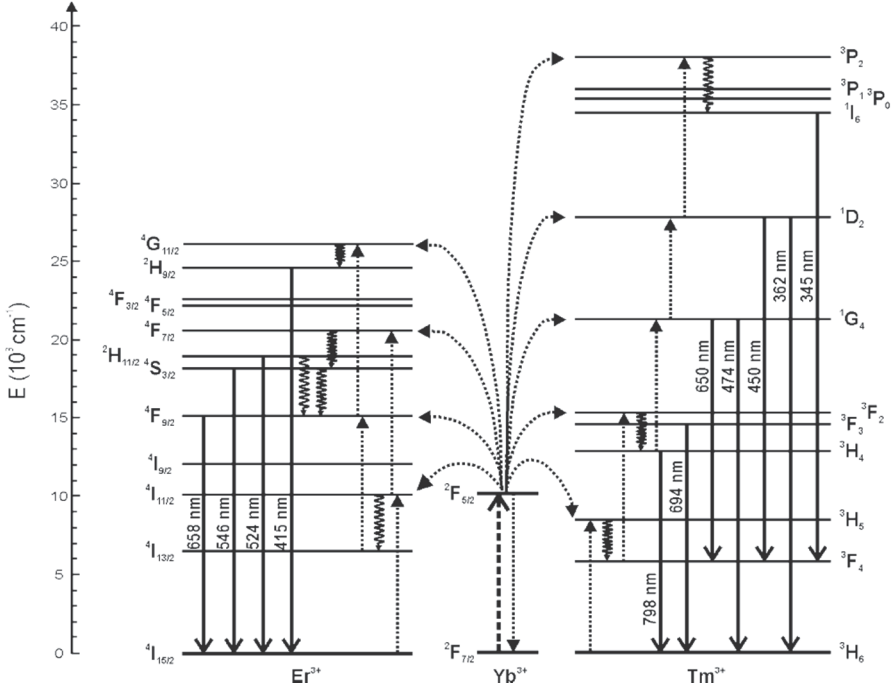


Figure 3. Energy level diagrams of upconversion processes in Yb³⁺/Er³⁺ and Yb³⁺/Tm³⁺ co-doped materials. Dashed, solid, dotted and wavy arrows represent photon absorption, photon emission, energy transfer and relaxation processes, respectively. Based on a figure by Dong *et al.* (2015).

In addition to the crystal-field induced electric dipole transitions enhancing the lanthanide luminescence probability in a crystalline host material, the functions of the host lattice are to bring the optical centers into optimal positions with respect to ion-to-ion distance and spatial arrangement, and to protect the lanthanide ions from the quenching effects of environment. (Li *et al.*, 2015; Liu, 2015) An optimal host material should be optically transparent, chemically and thermally stable, have high tolerance for luminescent centers, and possess low phonon energy (Chen *et al.*, 2013; Dong *et al.*, 2015). Phonon-induced non-radiative relaxation is one of the dominant quenching mechanisms of photon upconversion. Multiple phonons are able to “bridge” the energy difference between two energy levels of a dopant ion through non-radiative energy transfer. If the energy of the gap is less than six phonon energies, the non-radiative pathways will dominate. (van Dijk and Schuurmans, 1983) Thus, optimally low phonon energy of the host lattice is a prerequisite for efficient photon upconversion.

Heavy halides (chlorides, bromides, and iodides) exhibit low phonon energies (<300 cm⁻¹) but they suffer from low chemical stability. Metal oxides are chemically stable but their phonon energy is high (>500 cm⁻¹) (Diamente *et al.*, 2007). Fluoride

materials are both chemically stable and have low phonon energy ($\sim 350\text{ cm}^{-1}$) which is why they are most commonly used host matrices for upconverting nanophosphors. (Suyver *et al.*, 2006; Wang and Liu, 2009) Phonon energy in a host lattice can be reduced by minimizing lattice defects. The sizes of the cation sites in the host lattice must match the ionic radii of the dopants. (DaCosta *et al.*, 2014) Cations, such as Na^+ , Ca^{2+} , and Y^{3+} , have closely matched cationic radii with lanthanide dopant ions and, thus, host materials based on them resist the formation of crystal defects. (Haase and Schäfer, 2011) Also inorganic compounds of some other alkaline earth ions (Sr^{2+} , Ba^{2+}) and transition metal ions (Zr^{4+} , Ti^{4+}), with ionic size close to lanthanides, have been used as host lattices. (Wang and Liu, 2009) Crystal defects can also act as luminescence quenching sites.

Also the crystallite size and crystal structure of the host lattice have a large impact on the efficiency of photon upconversion processes. For example, a hexagonal $\beta\text{-NaYF}_4$ host lattice enables more efficient upconversion than a cubic $\alpha\text{-NaYF}_4$, due to the shorter cation-cation distances and the lower symmetry of the hexagonal crystal which increases the crystal field strength (DaCosta *et al.*, 2014; Liu, 2015). In fact, $\beta\text{-NaYF}_4$ -based upconverting nanophosphors are considered to be the most efficient upconverting materials known to date. (Aebischer *et al.*, 2006; Krämer *et al.*, 2004; Suyver *et al.*, 2005c) The impact of crystallite size on photon upconversion efficiency is discussed in section 2.1.3.

2.1.2 Synthesis of nanophosphors

Recently, methods to synthesize nanosized upconverting materials have emerged. One of the major challenges in the preparation of upconverting nanophosphors is the reproducibility of monodispersed particles with a narrow size-distribution, uniform shape and chemical composition, phase-purity, and solubility to either organic or aqueous solvents. Most of the methods use organic solvents as the medium in the synthesis. (DaCosta *et al.*, 2014) In this thesis, only the most widely used methods for the controlled preparation of high-quality UCNPs are introduced. They include thermal decomposition, a method based on rare-earth oleates, and hydro(solvo)thermal method. These methods differ from each other mostly with respect to the precursor materials used.

One of the most commonly used method for the preparation of UCNPs is thermal decomposition, or the thermolysis of organometallic precursors, typically metal- and Ln^{3+} -trifluoroacetates (Boyer *et al.*, 2006; Mai *et al.*, 2006; Yi and Chow, 2006). A high-boiling organic solvent, such as 1-octadecene (ODE), with the trifluoroacetate precursors and oleic acid (OA) or oleylamine (OM) as surface ligands, is heated above the precursor decomposition temperature ($>300^\circ\text{C}$). The decomposition is observed as a release of gases. After cooling, the hydrophobic UCNP products can be isolated by centrifugation and dispersed to organic solvents. The surface ligands OA and OM contain polar head groups that can coordinate to the growing nanocrystal during the reaction, and a long hydrocarbon tail, which extends into the organic solvent and,

therefore, offers repulsive interactions with other nanocrystals. The surface ligands also control the growth of the nanocrystal by blocking the expansion of the lattice. (Haase and Schäfer, 2011) The thermal decomposition method, therefore, provides a straightforward means for the synthesis of nanophosphors with well-defined and controlled size and shape (Ye *et al.*, 2010). However, the drawbacks of the methods include the toxicity and air-sensitivity of the metal precursors requiring a continuous flow of inert gas. The precursors are also expensive. The generated by-products, such as fluorinated and oxyfluorinated carbon species, are toxic (Chen *et al.*, 2014; Liu *et al.*, 2013e). Furthermore, the temperature window for the decomposition is quite narrow (<10 °C) causing difficulties in reproducibility (Liu *et al.*, 2009). Still, the method has been applied in the fabrication of, e.g., β -NaYF₄ (Ye *et al.*, 2010; Yi and Chow, 2006), LiYF₄ (Mahalingam *et al.*, 2009), KGdF₄ (Wong *et al.*, 2011), and BaYF₅ (Vetrone *et al.*, 2009) nanomaterials.

In 2008, a similar method was described using *in situ* prepared rare earth oleates as the precursors (Li and Zhang, 2008). This method has also been called high-temperature co-precipitation (DaCosta *et al.*, 2014; Liu *et al.*, 2013e). The synthesis is also performed in high-boiling ODE with, typically, OA as the surface ligand. Lanthanides are added as chlorides, and a heating to 160 °C generates Ln³⁺ oleates. NaOH and NH₄F are added before a second heating step to 300 °C as the source of Na⁺ and F⁻, respectively. The surface ligand-capped UCNPs are isolated via centrifugation. Instead of ODE, also liquid paraffin has been used, and OA can be replaced by trioctylphosphine oxide (TOPO) or stearic acid (Li and Zhang, 2008; Liang *et al.*, 2011). The method has been described as “user-friendly”, it provides easy phase and size control, and the Ln³⁺ precursors are readily available at a lower price than the trifluoroacetates, and furthermore, they are not toxic. In addition to the preparation of β -NaYF₄ nanophosphors (Li and Zhang, 2008; Liang *et al.*, 2011; Wang *et al.*, 2010b), this method has been applied to the synthesis of, e.g., LiYF₄ (Wang *et al.*, 2010d), NaLuF₄ (Yang *et al.*, 2012), and KMnF₃ (Wang *et al.*, 2011c) nanomaterials.

The third synthetic method is called hydro(solvo)thermal synthesis, which is also a solution-based method. In contrast to the above methods, hydro(solvo)thermal synthesis exploits pressure and temperature provided by an autoclave. The increased pressure offers the possibility to produce highly crystalline nanophosphors at lower temperatures. By applying pressure, the solubility and the reactivity of the precursors can be increased. Typical precursors are rare earth nitrates, and the solvent is water, ethanol, sodium ethoxide, or acetic acid. Also chelating ligands and surfactants, such as oleic acid, ethylenediamine tetraacetic acid (EDTA), or cetyltrimethylammonium bromide (CTAB) can be used to tune the morphology of the nanophosphor products (Zeng *et al.*, 2005; Zhang *et al.*, 2007). The reagents are mixed and transferred to a Teflon-lined autoclave and heated to 140–200 °C. The hydro(solvo)thermal synthesis produces upconverting nanophosphors with controlled size and shape at low temperatures and mild conditions, and with a good dispersibility in solution (Wang and Liu, 2009). The disadvantages include the need for specialized reaction vessels. A hydrothermal synthesis method of upconverting nanomaterial La₂(MoO₄)₃: Yb³⁺,

Er^{3+} was published already in 2002 (Yi *et al.*, 2002). The synthesis of hexagonal phase NaYF_4 was reported a little later (Zeng *et al.*, 2005). The synthesis of, e.g., NaLuF_4 (Yang *et al.*, 2013) and BaGdF_5 (Zeng *et al.*, 2012) nanomaterials has also been reported.

To yield water-dispersible UCNPs straight from the synthesis, hydrophilic molecules such as citrate (Zhao *et al.*, 2008), 6-aminohexanoic acid (Cao *et al.*, 2011), poly(acrylic acid) (PAA) (Wang *et al.*, 2010e; Wang *et al.*, 2011e), polyvinylpyrrolidone (PVP) (Li and Zhang, 2006), or polyethyleneimine (PEI) (Wang and Liu, 2008) can be added to the synthesis reaction. They all act as growth-controlling agents by coordinating to the lanthanide ions and, at the same time, rendering the synthesized nanophosphors water-dispersible.

2.1.3 Luminescent properties

Spectral properties

The 4f electrons of lanthanides are shielded by the complete 5s and 5p shells, which results in narrow emission peaks. The 4f electrons do not participate in chemical bonding and, thus, the emission is also stable against photobleaching (Wang *et al.*, 2010a; Werts, 2005). The upconversion photoluminescence spectra of both $\text{Yb}^{3+}/\text{Er}^{3+}$ and $\text{Yb}^{3+}/\text{Tm}^{3+}$ -doped nanophosphors are illustrated in Figure 4. The main emission peaks of erbium are located at 524 nm, 546 nm, and 658 nm. Thulium activator emits at multiple wavelengths: 345 nm, 362 nm, 450 nm, 474 nm, 650 nm, 694 nm, and 798 nm. The emission peak wavelengths of the activators are unaffected by the chemical composition of the host material. However, the relative intensities and peak ratios can be manipulated by tuning the combination of host and different dopants; the dopant concentration; the phase, size, and shape of the nanophosphor; and the surface ligands. The use of multiple lanthanides as dopants offers the possibility to cover the whole visible spectrum with several emission peaks. The adjustment of the dopant concentration changes the dopant–dopant interaction, leading to increased cross-relaxation or back-transfer processes, which might quench the intensity of one peak and enhance another. For example, the increase of Yb^{3+} concentration can lead to energy back-transfer from Er^{3+} to Yb^{3+} , causing changes in peak ratios (Wang and Liu, 2008). The crystal structure of a UCNP affects the excitation process and, therefore, also the emission transitions. For example, the red peak dominates the upconversion luminescence spectrum of $\alpha\text{-NaYF}_4$, but the green peak intensity at 540 nm is relatively stronger, compared to other emissions, in $\beta\text{-NaYF}_4$. This is due to the symmetry reduction in $\beta\text{-NaYF}_4$, which enhances the f–f transitions (Krämer *et al.*, 2004). (Wang and Liu, 2014)

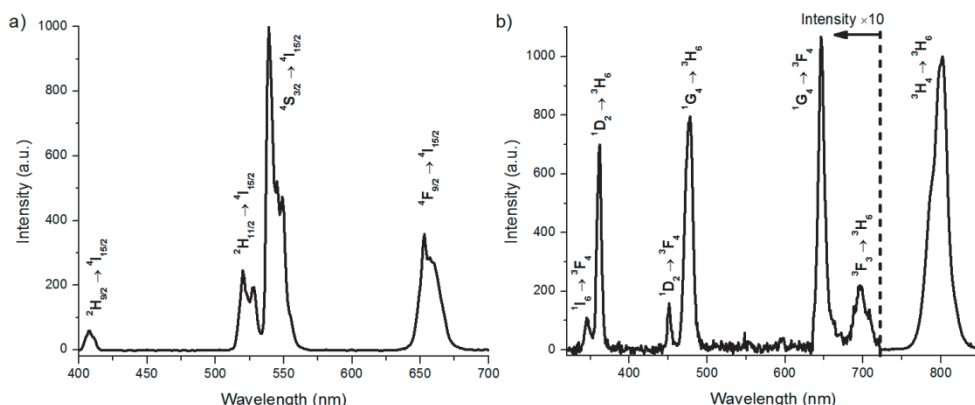


Figure 4. Upconversion photoluminescence spectra and the radiative transitions of a) NaYF₄: Yb³⁺, Er³⁺ and b) NaYF₄: Yb³⁺, Tm³⁺ nanophosphors upon excitation at 980 nm. Adapted from figures by Vuojola *et al.* (2012) and Valta *et al.* (2015).

Photon upconversion is an anti-Stokes process, as the UCNPs are excited at 980 nm while emitting at visible wavelengths. The anti-Stokes shifts are, therefore, very large enabling the detection of emission without crosstalk from the excitation light. The NIR excitation also reduces scattering. In view of bioanalytical and biological applications, the anti-Stokes shift offers a unique opportunity to detect the upconverted emission without the Stokes shifted autofluorescence of the biological material. (Corstjens *et al.*, 2005; Hampl *et al.*, 2001) Furthermore, some of the emission peaks are located at the optical window of biomaterials above 600 nm, where biological material does not attenuate the emission or excitation by light absorption (Kuningas *et al.*, 2007). Especially the 800 nm peak of thulium-doped UCNPs is widely used in bioimaging applications due to the large penetration depth of the NIR radiation (Nyk *et al.*, 2008).

The 980 nm excitation of Yb³⁺ can cause problems in bioanalytical and biological applications where aqueous matrices are required, because water absorbs at NIR wavelengths. This can lead to the overheating of the matrix which is especially troublesome in bioimaging applications. (Zhan *et al.*, 2011) Hence, steps have been taken towards adjusting the excitation of UCNPs to wavelengths where the water absorption is minimal. This has been achieved by adding another sensitizer, Nd³⁺, to the UCNPs. Nd³⁺ can be excited with 808 nm radiation: subsequently the energy is transferred to Yb³⁺, which further transfers the energy to the activator. Water absorption is minimal at 808 nm and, thus, the heating of aqueous matrices can be avoided. The Nd³⁺/Yb³⁺ co-doped shell is usually synthesized around a Yb³⁺/Er³⁺ co-doped core material to avoid the deleterious energy transfer between Nd³⁺ and Er³⁺ (Wang *et al.*, 2013a).

Another interesting, novel approach to shift the excitation to shorter wavelengths and, at the same time, enhance the upconversion photoluminescence of UCNPs is a so-

called broadband dye-sensitized upconversion. An organic near-infrared dye is used as an antenna to absorb the excitation radiation at ~806 nm, after which the energy is transferred to the β -NaYF₄: Yb³⁺, Er³⁺ UCNP, which then emits the upconverted emission at green and red wavelengths. The use of a near-infrared dye antenna increases the absorptivity and broadens the absorption spectrum of the upconverting system and results in enhanced upconversion photoluminescence. (Zou *et al.*, 2012)

Lifetime and quantum yield

The lifetime of an excited state depends on the rates of both radiative and non-radiative depopulations. The radiative rate is mostly determined by the electronic structure of the lanthanide ion. (Wermuth *et al.*, 1998) The f-f transitions are forbidden according to the parity selection rule and, thus, the luminescence of lanthanides is characterized by long lifetimes. (Wang *et al.*, 2010a; Werts, 2005) The forbidden f-f transitions are also the reason for the low absorption cross-section of lanthanides (Wang and Liu, 2014). The rate of the non-radiative depopulation w_0 , i.e., the multiphonon relaxation processes, obeys the “gap rule” (Equation 1) (Riseberg and Moos, 1968; Wermuth *et al.*, 1998)

$$w_0 \propto \beta e^{-\alpha p} \quad (1)$$

where α and β are parameters associated with the host material, and $p = \Delta E/\hbar\omega$ is the number of phonons of energy $\hbar\omega$ required to bridge the energy gap ΔE between the initial and final energy states. (Riseberg and Moos, 1968; Wermuth *et al.*, 1998) In lanthanides, multiphonon relaxation is dominant when $p < 5$ (Wermuth *et al.*, 1998). The highest phonon energy of fluorides is ~350 cm⁻¹ and, therefore, bridging the gap of, e.g., ⁴F_{9/2} → ⁴I_{9/2} energy levels of Er³⁺ dopant (~2650 cm⁻¹) would require 7.5 fluoride phonons. Therefore, the radiative depopulation is dominant and red emission is obtained in fluoride materials. However, higher energy oscillators are present in solvents and on the surface of the nanocrystal, and they enhance the non-radiative relaxation processes. Thus, nanosized Er³⁺-doped UCNPs exhibit shorter lifetimes than larger crystals, the lifetime of the red emission being usually longer than that of the green emission (Lim *et al.*, 2010; Shan *et al.*, 2010b; Wang *et al.*, 2009b; Zhao *et al.*, 2013). The lifetimes of a 13.9-nm-diameter β -NaYF₄: 20 % Yb³⁺, 2 % Er³⁺ at green emission wavelengths have been reported to be 39 μ s and 93 μ s, and at red emission 88 μ s and 222 μ s, whereas ~500-nm-diameter bulk phosphor exhibited lifetimes of 406 μ s and 493 μ s for green and red emission, respectively (Wang *et al.*, 2009b). In another publication, the lifetimes of 110 μ s and 240 μ s for the green and red emission were reported for 18-nm-diameter β -NaYF₄: 20 % Yb³⁺, 2 % Er³⁺ nanophosphors (Shan *et al.*, 2010b). The lifetime of the 800 nm emission of 6.6-nm-diameter NaYF₄: 30 % Yb³⁺, 0.5 % Tm³⁺ nanophosphor in hexane was reported to be 65 μ s (Qiu *et al.*, 2014). The decay times of 450 nm, 476 nm, 646 nm, and 800 nm emissions of β -NaYF₄: 17 % Yb³⁺, 3 % Tm³⁺ samples were reported to be 87 μ s, 143 μ s, 164 μ s, and 185 μ s, respectively (Li *et al.*, 2007).

Because photon upconversion is a nonlinear optical process, the luminescence intensity is dependent on the excitation power density, following the Equation 2

$$I(UCPL) \propto P_{exc}^n. \quad (2)$$

where I is the intensity of upconversion photoluminescence, P is the power of excitation pump laser, and n is the number of excitation photons required to produce the upconversion photoluminescence (UCPL); n can be obtained from the slope of a log–log plot of intensity vs. excitation power density. (Pollnau *et al.*, 2000; Suyver *et al.*, 2005b) The slopes for red and green emission of $\text{Yb}^{3+}/\text{Er}^{3+}$ co-doped nanophosphor are typically ~ 2.5 and ~ 2.1 , respectively (Shan *et al.*, 2010a; Wang *et al.*, 2009b). The emissions of NaYF_4 : 30 % Yb^{3+} , 0.5 % Tm^{3+} core-shell nanophosphors at 345 nm, 360 nm, 450 nm, 475 nm, 654 nm, and 802 nm exhibit excitation power dependencies to the power of 4.8, 3.7, 3.7, 2.9, 3.1, and 2.0, respectively (Qiu *et al.*, 2014). At high excitation power densities the slope of the curve is saturated to one, irrespective of the number of energy transfer steps (Suyver *et al.*, 2005b).

Also the luminescence quantum yield (QY) is strongly dependent on the excitation power density due to the competition between the ETU rate and the linear rate of the depopulation of the intermediate states (Liu *et al.*, 2013c). The quantum yield is defined as the ratio of the number of emitted photons to the number of absorbed photons. For an n -photon UC-process, the theoretical maximum for QY is $100 / n$ %, e.g., for a two-photon process, the maximum QY is 50 %. However, the observed QYs of UCNPs are usually much lower due to the energy losses in UC processes. (Boyer and van Veggel, 2010) The QY of UCNPs must be analyzed by using the absolute QY measurement due to the power dependency and the lack of standardized UCNP reference materials for a relative measurement method (see section 2.1.5).

The absolute QYs of the green emission of NaYF_4 : 20 % Yb^{3+} , 2 % Er^{3+} nanophosphors in the size range of 10–100 nm at 150 W cm^{-2} power density were reported to be between 0.005–0.3 %, while a QY of 3 % was measured for a bulk phosphor at 20 W cm^{-2} (Boyer and van Veggel, 2010). The excitation power densities were chosen from the beginning of the saturation region of the power dependency curve to obtain the maximum possible QY. However, to compare the results between different studies, Xu *et al.* (2013) suggested that the whole power density dependence of QY should be reported instead of providing QYs at one specific power density. As a fast approach, Liu *et al.* (2013c) suggested that the QY of a nanophosphor should be reported by using a power density, at which the ETU rate and the linear decay rate have an equal contribution to the depopulation of the intermediate state of the activator. They reported a QY of 0.45 % for the 800 nm emission peak of a 33-nm-diameter NaYF_4 : Yb^{3+} , Tm^{3+} at the balancing power density 3.8 W cm^{-2} where the QY is half of the maximum QY. (Liu *et al.*, 2013c)

Wilhelm *et al.* (2015) reported a luminescence QY of 0.35 % at a power density of 150 W cm^{-2} for 22.7-nm-diameter OA-coated β -NaYF₄: Yb³⁺, Er³⁺ UCNPs dispersed in cyclohexane. When the OA-capping was changed to citrate via ligand exchange and the resulted hydrophilic UCNPs were dispersed in aqueous solution, the QY decreased by half. This decrease illustrates the environmental sensitivity of upconversion photoluminescence and especially the quenching effect of water (Bogdan *et al.*, 2011; Wang *et al.*, 2010c).

Size-dependency and environmental sensitivity

The upconversion photoluminescence efficiency is known to be particle size-dependent. Unlike quantum confinement, which is the reason for the size-dependent emission wavelength of quantum dots, the effect of UCNP size on the luminescence intensity is believed to be due to surface quenching effects, which become more prominent with decreasing size and increasing surface-to-volume ratio. (Schietinger *et al.*, 2009; Shan *et al.*, 2010b; Wang *et al.*, 2010c; Zhao *et al.*, 2013) In addition, with a decrease in the nanophosphor size, the number of emitting ions decreases and, furthermore, a larger portion of the emitters is located near the surface. Therefore, it is believed that the upconversion photoluminescence in nanosized materials is more inefficient than in bulk materials (Wang and Liu, 2009). However, decreasing the size of UCNPs below 10 nm while maintaining the strong luminescence intensity is of growing interest for, e.g., imaging purposes (Gargas *et al.*, 2014; Ostrowski *et al.*, 2012). Thus, understanding the impact of nanophosphor size on the upconversion luminescence efficiency is vital, but contradicting suggestions on the underlying mechanisms have been reported.

The size-dependency in upconversion luminescence intensity has been suggested to originate from surface effects due to the strong vibrational energies of ligands, surfactants or surrounding solvent (Shan *et al.*, 2010b; Zhao *et al.*, 2013), phonon-mediated energy transfer processes (Liu, 2015; Schietinger *et al.*, 2009), or increased surface defect density (Zhao *et al.*, 2013). Non-radiative deactivation is considered to be the dominant factor influencing the upconversion photoluminescence of nanophosphors due to the small energy gaps of lanthanide excited states and the large proportion of surface dopant ions in incomplete coordination environments (Wang and Liu, 2009).

The non-radiative rate in a homogeneous crystalline material with small defect density obeys the “gap rule” as introduced above. Thus, the highest vibrational modes in the nanocrystal interior, surface, or in the surrounding solvents determine the rate of the radiative and non-radiative depopulations. (Riseberg and Moos, 1968; Wermuth *et al.*, 1998; Zhao *et al.*, 2013) The high energy of OH- and CH-vibrations of surface ligands or solvents can bridge the gap between the energy levels of lanthanides offering a non-radiative relaxation pathway (Monguzzi *et al.*, 2009). The energy of an excited lanthanide ion is transferred to the isoenergetic vibrational states (or overtones) of the vibrational bond. (Ermolaev and Sveshnikova, 1994; Förster, 1948; Stavola and

Dexter, 1979) The high-energy vibrational modes of OH-groups ($3200\text{--}3600\text{ cm}^{-1}$) in water can quench Er^{3+} activator ions by facilitating the multiphonon relaxation of $^2\text{H}_{11/2}/^4\text{S}_{3/2} \rightarrow ^4\text{F}_{9/2}$ and $^4\text{I}_{11/2} \rightarrow ^4\text{I}_{13/2}$ transitions. Both these relaxation pathways favor the population of the red emitting $^4\text{F}_{9/2}$ state either directly or via a $^4\text{I}_{13/2} \rightarrow ^4\text{F}_{9/2}$ transition at the expense of the green emission. Thus, the red-to-green emission peak ratio increases in the presence of water. (Bogdan *et al.*, 2011; Boyer *et al.*, 2010) In heavy water (D_2O), the non-radiative pathways are reduced because the OD vibrates at a lower frequency ($\sim 2500\text{ cm}^{-1}$) (Max and Chapados, 2009) and, therefore, the upconversion luminescence intensity increases when compared to the luminescence in water. (Bogdan *et al.*, 2011)

In organic solvents or in a dry sample, the enhancement of the green emission peak in relation to the red with decreasing nanocrystal size has been observed. Schietinger *et al.* (2009) and Lim *et al.* (2010) suggested that the size-dependent mechanism involves differing number of phonons available in the individual crystals for multiphonon relaxation processes. There are not enough low-frequency phonons in very small nanocrystals to efficiently populate the red-emitting level via phonon-assisted energy transfer and, thus, the green luminescence is relatively enhanced. This is also called phonon confinement, which status as the dominant mechanism affecting upconversion has, however, been debated as in most of the reports the measurements were performed at a low temperature or from a solid-state sample without surface vibrators (Shan *et al.*, 2010b; Wang *et al.*, 2010c).

Crystalline defects provide additional channels for non-radiative recombination. The defect density increases with decreasing nanocrystal size. Especially in $<10\text{ nm}$ cubic NaYF_4 nanophosphors, the defect density is high and the non-radiative relaxation processes dominate. Zhao *et al.* (2013) also observed that, because of different defect densities, the decay rates on the surface of hexagonal NaYF_4 nanophosphors differ from the decay rates in the core. Furthermore, the larger defect density in cubic nanocrystals explains the weaker upconversion luminescence in relation to the higher quality hexagonal nanophosphors.

In addition to the surface quencher-caused deactivation of the dopants located on or near the surface of the nanophosphor, the energy of the dopants located in the UCNF core can migrate a long distance to the dopant on the surface and be quenched. Energy migration is prominent in UCNPs due to the high concentration of Yb^{3+} sensitizer ions with simple energy level scheme and long excited state lifetime enabling an efficient energy transfer between ions. (Auzel, 2004; Chen *et al.*, 2014) Gargas *et al.* (2014) suggested that the entire volume of an 8-nm nanophosphor is energetically coupled to the surface via Yb–Yb migration. Chen *et al.* (2014) proposed that the NIR excitation energy can travel a distance up to 10 nm long. Therefore, an efficient surface passivation is a prerequisite to prevent quenching on the nanophosphor surface to obtain a bright upconversion photoluminescence in nanosized UCNPs. The passivation can be achieved through surface coating with an inorganic shell or a polymer coating, which is discussed in section 2.1.4. By covering a luminescent

nanophosphor core with a thin inactive inorganic shell, the surface quenching effects have been shown to reduce. (Su *et al.*, 2012) For example, the introduction of a ~2.5-nm NaGdF₄ shell on a 15-nm β -NaGdF₄: Yb³⁺, Tm³⁺ core decreased the quenching efficiency that 20 vol% water in Igepal CO-520/ethanol solution had on the upconversion luminescence from 80 % for the core-only material to 35 % for core-shell material, when compared to the luminescence intensities in the absence of water. (Wang *et al.*, 2010c) Furthermore, NaYF₄: Yb³⁺, Er³⁺/Tm³⁺@NaYF₄ core-shell material in chloroform also showed increased upconversion luminescence when compared to the core-only material suggesting a quenching effect of the surface dopants on the luminescence of the core-only material (Yi and Chow, 2007). Prorok *et al.* (2014) showed an upconversion photoluminescence intensity enhancement of up to ~40-fold when growing either NaYF₄ or CaF₂ shell around a 25-nm α -NaYF₄:40 % Tb³⁺, 20 % Yb³⁺ core.

Also the shape of the UCNP nanocrystal has been reported to have an impact on the upconversion photoluminescence efficiency. It was stated that differently shaped nanocrystals with identical surface-to-volume ratios could have different lattice energy, ion density, defect density, and multiphonon relaxation processes. (Shan *et al.*, 2010a; Shan *et al.*, 2010b)

In addition to the strong quenching effect of water on upconversion photoluminescence, aqueous solutions of heavy metal ions have also been reported to quench the emission of Er³⁺-doped UCNPs. The most efficient quenchers were Fe²⁺ and Hg²⁺. Also the luminescence of Tm³⁺ or Ho³⁺-doped UCNPs were shown to be quenched by the presence of Cu²⁺, Fe³⁺, or Pb²⁺ ions. (Saleh *et al.*, 2011b)

2.1.4 Surface chemistry

Most synthetic methods yield hydrophobic UCNPs with a long-chain ligand capping as described in section 2.1.2. However, to use UCNPs as labels in biological and bioanalytical applications, they must be rendered water-dispersible and colloidally stable in aqueous solutions (Boyer *et al.*, 2010). Additionally, many applications require the conjugation of a capturing biomolecule for which functional groups, such as hydroxyl, amine, maleimide, epoxide, carboxylic acid, or phosphonate groups, need to be added on the UCNP surface (Sedlmeier and Gorris, 2015). Furthermore, the surface coating should preferably protect the luminescent lanthanide ions from the quenching effect of water to yield high upconversion efficiency for the bioanalytical applications. Naccache *et al.* (2009) suggested that a larger surface ligand, such as PAA, can shield the UCNP from water molecules better than a small, linear molecule, such as azelaic acid, although the comparison was only made visually from 980 nm excited dispersions. The typically used surface coating routes are silanization, ligand exchange, ligand attraction, layer-by-layer method, and ligand oxidation.

Silica coating

The most widely used surface chemistry method for UCNPs is surface silanization, in which a SiO_2 shell is polymerized around the nanophosphor (Figure 5). Silica is optically transparent, chemically stable, highly biocompatible, and easily functionalized. Furthermore, unlike other surface coating methods, silanization utilizes covalent bonds, thus increasing the stability of the coating. There are two methods for silica coating: the Stöber method (Stöber *et al.*, 1968) and the reverse microemulsion method. The Stöber method is used when the UCNPs are readily hydrophilic; they are dispersed in low molecular weight alcohol, most commonly ethanol, where tetraalkyl orthosilicates are hydrolyzed in the presence of ammonia. The thickness of the silica shell, although this is difficult, can be controlled by the reaction time or temperature, the amount of the tetraalkyl orthosilicates, or by the addition of PVP (Graf *et al.*, 2003; Johnson *et al.*, 2010). The functionalization of the silica can be performed by adding an organosilane to the Stöber reaction or by forming an additional silica shell with the organosilanes in a subsequent silanization step. (Graf *et al.*, 2003; Johnson *et al.*, 2010; Li and Zhang, 2006; Mader *et al.*, 2010) It is also possible to perform silanization in toluene in which the oleic acid-capped UCNPs are readily dispersible. The resulting silica shell is very thin because as soon as the UCNP surface is coated with silica, the particles become insoluble to toluene and they precipitate. (Jana *et al.*, 2007; Pääkilä *et al.*, 2012)

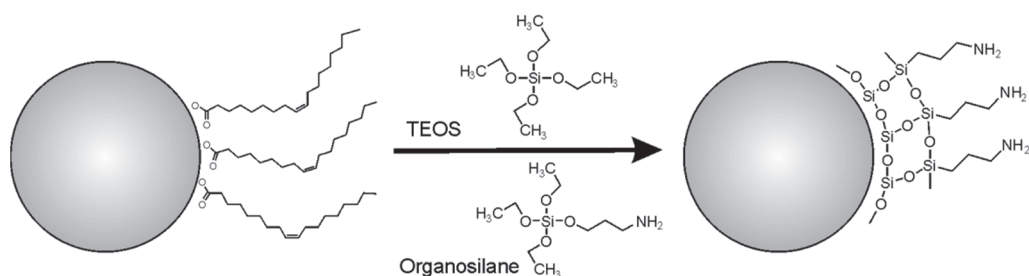


Figure 5. Schematic of the silica coating method. A functionalized silica shell is polymerized around an OA-capped UCNP from TEOS monomers and organosilanes containing functional groups. *TEOS*, tetraethylorthosilicate. Figure not drawn to scale. Modified from a figure by Wang and Liu (2009).

The most popular method for the silanization of upconverting nanophosphors is the reverse microemulsion method which is often performed on the oleic acid-capped hydrophobic UCNPs. In this method, reverse micelles are formed from detergents, such as Triton X-100 or Igepal CO-520 (Santra *et al.*, 2001), in nonpolar solvents, such as cyclohexane. Each micelle encapsulates (preferably) a single hydrophobic nanophosphor and serves as a nanoreactor for the growth of the silica shell. If, however, multiple nanophosphors are located in a micelle, the method produces a common silica shell around them. (Darbandi and Nann, 2006) Ammonia is added as catalyst and the thickness of the silica shell is controlled by the amount of silicates, the reaction time, and the size of the reverse micelles, i.e., the amount of detergents. The reaction time can be in the range of 2–48 h. Functionalization can be performed either

simultaneously with the hydrolyzation of, e.g., tetraethyl orthosilicate (TEOS) by adding an organosilane to the reaction, or in an additional silanization step with the organosilanes after the first silica shell is formed. (Abdul Jalil and Zhang, 2008; Li *et al.*, 2008; Rantanen *et al.*, 2009; Wilhelm *et al.*, 2013) The most commonly used organosilanes for the functionalization of the silica shell contain amine groups ((3-aminopropyl)-triethoxysilane and *N*-[3-(trimethoxysilyl)propyl]-ethylenediamine) (Jiang *et al.*, 2009; Rantanen *et al.*, 2009), carboxylic acid groups (carboxyethylsilanetriol) (Liu *et al.*, 2013b), and alkyne or azide groups (azidopropyl triethoxysilane or O-(propargyloxy)-*N*-(triethoxysilylpropyl)urethane, respectively) (Mader *et al.*, 2010; Rubner *et al.*, 2012), but also *N*-succinimidyl ester (Wilhelm *et al.*, 2013) or epoxy groups (Saleh *et al.*, 2011a) have been used.

For sensing or photodynamic therapy applications, also a mesoporous silica shell can be formed on the surface of UCNPs with the pore size in the nanometer range. The pores are formed by adding, e.g., a surfactant CTAB as a capping ligand or introducing it during the silanization reaction. CTAB is later removed by calcination or with a solvent, which leads to a porous silica shell. The sensing indicator dyes or photosensitizers can then be incorporated into the pores. (Liu *et al.*, 2012a; Qian *et al.*, 2009)

In addition to the possible coating of multiple nanophosphors in one silica shell, the limitations of surface silanization include buffer-dependent aggregation (Bagwe *et al.*, 2006; Bogdan *et al.*, 2011; Jana *et al.*, 2007; Johnson *et al.*, 2010), and increased nonspecific binding through electrostatic interactions, because at physiological pH silanol groups have a negative charge whereas the functional groups, such as amine, are positively charged (Bagwe *et al.*, 2006). Also, the size of the nanophosphor is increased by the growth of a silica layer. However, as already mentioned above, the silica encapsulation is stable and does not detach from the UCNPs surface, as covalent bonds are utilized.

Ligand exchange

Ligand exchange is another widely used method for the surface coating of UCNPs producing a very thin, even a monomolecular surface layer. In this method, the original hydrophobic surface ligand, usually oleic acid, is displaced by another, bifunctional hydrophilic ligand with which bioconjugation can be performed. The requirement for the ligand exchange is that the incoming hydrophilic ligand must bind to the UCNP surface with a higher affinity than the original one. Ligands are usually bound to the lanthanide ions via coordination bonds, whose strength of interaction increase in the order $-\text{SH}$, $-\text{NH}_2$, $-\text{COOH}$, $-\text{PO}_3\text{H}$ (Muhr *et al.*, 2014). Polydentate ligands offer much better stability than monodentate ligands by reducing desorption rates (DaCosta *et al.*, 2014). Ligand exchange can be performed with either one- or two-step strategy (Figure 6).

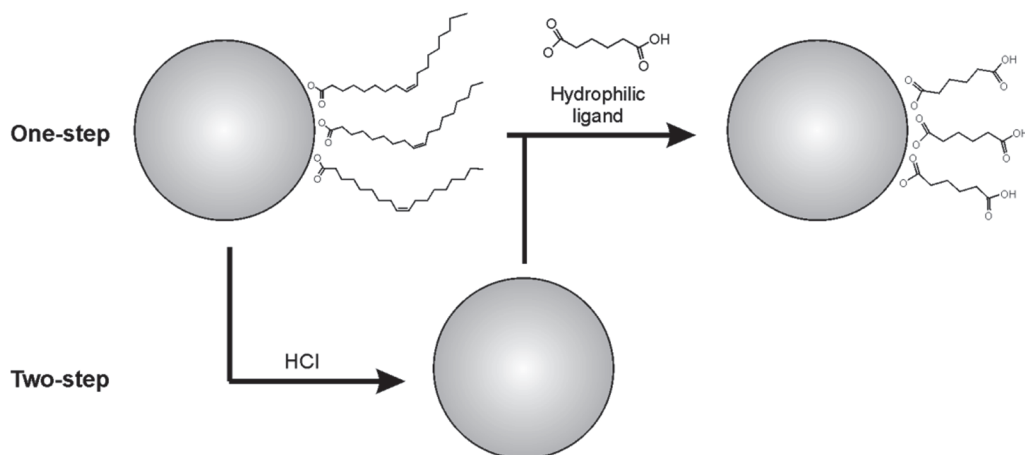


Figure 6. Schematic of the coating of OA-capped UCNP with the ligand exchange method performed in either one-step or two-step strategy. The original hydrophobic ligand is replaced by a hydrophilic ligand. Figure not drawn to scale. Modified from figures by Zhang *et al.* (2009) and Bogdan *et al.* (2011).

In the single-step method, the original ligand is directly replaced by adding an excess of the new hydrophilic ligand in a reaction that can last for up to several days usually at elevated temperatures. (Zhang *et al.*, 2009) One of the first reports of direct ligand exchange for OA-capped UCNPs was with hexanedioic acid, which coordinated to the lanthanides with its carboxylic acid at one end while the carboxyl group on the other end was free for bioconjugation. The six-carbon chain was just long enough to reduce the risk of both carboxylic groups coordinating to the UCNP surface and short enough to ensure good water-dispersibility. (Zhang *et al.*, 2009) A small polydentate citrate molecule has been widely used as the incoming ligand (Cao *et al.*, 2010; Liu *et al.*, 2013d; Wu *et al.*, 2009; Zhou *et al.*, 2011). Because coordination bond is the strongest with a phosphate group, Li *et al.* (2013) managed to bind double-stranded DNA sequence directly to the UCNP surface via ligand exchange. Also larger polymers, such as PAA (Naccache *et al.*, 2009; Xiong *et al.*, 2010); PVP (Johnson *et al.*, 2010); and polyethylene glycol (PEG) with terminal functionalities (Boyer *et al.*, 2010; Liebherr *et al.*, 2012; Yi and Chow, 2006), or branched dendrimers, such as poly(amidoamine) (Bogdan *et al.*, 2010) can be used in ligand exchange. A much better anchoring can be achieved with PEG-*b*-PAA block copolymer, which coordinates to the surface via PAA-moieties, while the PEG part promotes water-dispersibility and prevents aggregation (Kamimura *et al.*, 2008).

In the two-step method, the original ligand is first completely removed. The oleic acid ligand can be removed by dissolving the UCNPs into HCl, which protonates the carboxylic acid groups of OA, subsequently causing it to detach from the surface (Bogdan *et al.*, 2011; Zhou *et al.*, 2014). The excess OA is then removed by washing; the resulting bare UCNPs are water-dispersible. The acid washing requires only ~2 h for complete OA detachment. Another strategy for the removal of OA or oleylamine is the use of nitrosonium tetrafluoroborate (NOBF₄) which efficiently displaces OA and

covers the UCNP surface with BF_4^- molecules (Dong *et al.*, 2011). Another similar ligand is called the Meerwein's salt (Et_3OBF_4) (Rosen *et al.*, 2012). The dispersion of BF_4^- -coated UCNP in dimethylformamide (DMF) is stable for months without observed aggregation or precipitation. The NOBF_4 method is very fast, as the exchange process occurs in minutes. In the second step, the new hydrophilic ligand is introduced. Ligands such as PVP (Dong *et al.*, 2011), PAA (Esipova *et al.*, 2012), citrate (Zhou *et al.*, 2014), poly(allylamine) (Wang *et al.*, 2013b), lysine (Liu *et al.*, 2013a), 2-aminoethyl dihydrogen phosphate (Liu *et al.*, 2012b), and HS-PEG- NH_2 (Ni *et al.*, 2014) have been used as the incoming surface-capping molecule.

The surface modification via ligand exchange produces highly monodispersed, colloidally stable, water-dispersible UCNP containing functional groups for bioconjugation. However, as only coordination bonds are involved, the detachment of the new ligand is also possible in certain environments, depending on the coordinating group and the number of them. For example, the multidentate ligands, such as citrate or EDTA in blood samples can possibly replace the ligand capping. Aggregation and crosslinking of individual UCNP can occur depending on the size and amount of the ligand used, as well as on other factors, such as the buffer salt concentration. The size of the ligand also affects the efficiency of shielding the UCNP surface from water molecules (Naccache *et al.*, 2009).

Ligand attraction and layer-by-layer method

In the ligand attraction method, the original OA-capping is maintained and an amphiphilic block copolymer is adsorbed on top of it to form a bilayer through hydrophobic interactions between the hydrocarbon chains of the OA and the polymer (Figure 7a). The hydrophilic part of the copolymer enables dispersion in water and subsequent biomolecule conjugation. (Sperling and Parak, 2010) Both synthetic and biological amphiphilic co-polymers have been used (Jiang *et al.*, 2013). An example of the biological co-polymers is phospholipid, which is highly biocompatible. There is a large variety of functionalities and chain lengths available for phospholipids. (Li *et al.*, 2012; Yao *et al.*, 2014) The synthetic amphiphilic co-polymers include poly(maleic anhydride-alt-1-octadecene) (PMAO) (Jiang *et al.*, 2012; Wang *et al.*, 2011a) and PAA modified with long alkyl chains (Yi and Chow, 2007). The hydrophobic moiety of the co-polymer coating should efficiently prevent the quenching effect of water.

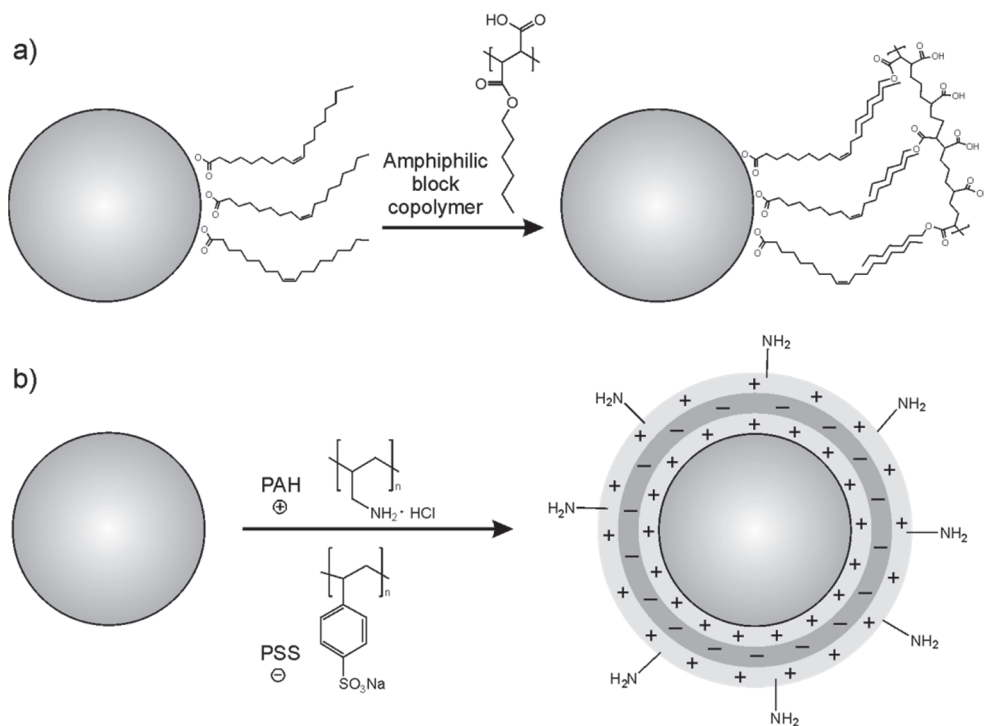


Figure 7. Schematics of the coating of UCNPs with the a) ligand attraction method and b) the layer-by-layer method. PAH, poly(allylamine hydrochloride); PSS, poly(sodium 4-styrenesulfonate). Figure not drawn to scale. Modified from a figure by Wang *et al.* (2011d).

The layer-by-layer method involves an alternate electrostatic adsorption of oppositely charged polyions (Figure 7b). Usually poly(allylamine hydrochloride) (PAH) and poly(sodium 4-styrenesulfonate) (PSS) are used (Wang *et al.*, 2005). This method provides a precise control over the coating thickness and charge. However, a buffered medium can cause the aggregation of the coated UCNPs (Budijono *et al.*, 2010).

Other surface modification methods

One of the simplest methods to produce hydrophilic surface coating is the oxidation of the double bond between C9 and C10 in the oleic acid or oleylamine capping ligands to yield a carboxylic acid, epoxy, or aldehyde group. The ligand oxidation can be performed with the Lemieux-von Rudloff reagent (Chen *et al.*, 2008), 3-chloroperoxybenzoic acid (Hu *et al.*, 2008), or ozone (Zhou *et al.*, 2009). The resulting azelaic acid capping from the reaction with the Lemieux-von Rudloff reagent has been shown to have insufficient shielding efficiency from the quenching effect of water molecules (Naccache *et al.*, 2009) and, thus, ligand oxidation is a rarely used surface modification method.

A new surface coating method for hydrophobic UCNPs utilizing UV or visible light upconversion emission to locally photopolymerize a thin polymer shell around an

individual UCNPs was recently introduced by Beyazit *et al.* (2014). A large variety of monomers with various functional groups can be used in the polymerization reaction. A typical example of a monomer for water-dispersible polymer coating is 2-hydroxyethyl methacrylate used together with a cross-linker *N,N'*-ethylenebis(acrylamide) and a molecule containing the functional groups, such as 2-carboxyethyl acrylate for a carboxylic acid group. The absorption wavelength of the initiator system for the photopolymerization reaction must overlap with the emission wavelength of the UCNPs, and this was the case with an initiation system of eosin Y/trimethylamine with NaYF₄: Yb³⁺, Er³⁺ nanophosphors. Beyazit *et al.* further synthesized a second shell of a molecularly imprinted polymer (MIP) on top of the first polymer layer. MIPs are tailor-made synthetic binders with affinities comparable to antibodies and with the ability to specifically recognize and bind target molecules. (Arshady and Mosbach, 1981; Beyazit *et al.*, 2014; Haupt *et al.*, 2012)

Separation methods

The most widely used separation method in surface coating processes is centrifugation with high g-forces (Li and Zhang, 2006; Liu *et al.*, 2013b; Wilhelm *et al.*, 2013). This, however, leads to nanophosphor aggregation and difficult re-dispersion of the precipitate. Ultrasonication is mandatory for the re-dispersion, but may be harmful to the conjugated biomolecules. Wilhelm *et al.* (2013) also used centrifugation to separate the silanized UCNPs from unreacted silanization reagents but, as the final step, they used filtration through a syringe filter with a pore size of 200 nm to get rid of nanophosphor aggregates. Chemical extraction is often used, e.g., to precipitate the silanized UCNPs with acetone from the reverse microemulsion (Abdul Jalil and Zhang, 2008; Darbandi and Nann, 2006; Rantanen *et al.*, 2009). Mader *et al.* (2010) used size-exclusion chromatography (Sephadex LH-60 and Sephadex G-75) to purify silica-coated UCNPs from the excess silanization reagents, unreacted dyes, biomolecules, or catalysts. However, size exclusion chromatography is a highly diluting method, which might be an undesired outcome. Magnetic separation can be used to purify UCNPs in which magnetically susceptible materials are incorporated. For example, the UCNPs material can be synthesized around a Fe₃O₄ magnetite core (Gai *et al.*, 2010; Wilhelm *et al.*, 2011), or an additional paramagnetic lanthanide Gd³⁺ can be co-doped into the nanophosphors (Chen *et al.*, 2012; Li *et al.*, 2009). These magnetic sub-structures, however, compromise the upconversion luminescence efficiency as the entire nanophosphor volume is not optically active. Boyer *et al.* (2010) used dialysis to remove the excess PEG-phosphate ligands after ligand exchange. Hlaváček *et al.* (2014) managed to separate monodispersed silanized UCNPs from aggregates by agarose gel electrophoresis due to the negative charge of the silica. They could also purify bovine serum albumin (BSA)-conjugated silanized UCNPs from excess BSA. However, this method is only applicable to small-scale purification and it requires the extraction of the purified UCNPs from the gel for subsequent applications. Additionally, the visual monitoring of the UCNPs mobility on the gel is impossible without a high-power laser to yield a bright enough emission from the monodispersed UCNPs, or alternatively, a dye-conjugation is required for

visualization. The size of the UCNPs must also be small enough to ensure mobility in the gel.

2.1.5 Characterization of UCNPs

Analytical tools are required to characterize the physical properties, such as size, morphology, crystal structure, elemental composition, and surface chemistry, of the synthesized UCNPs. Uniform size and shape are preferred in bioanalytical applications and the best method for UCNP characterization is electron microscopy, which includes transmission (TEM), scanning (SEM), and scanning transmission electron microscopies (STEM). They utilize a beam of electrons to construct an image of the nanocrystal. (Liu *et al.*, 2015) TEM can also be used to visualize a silica shell around the nanocrystals because of the differences in their electron scattering properties (Abdul Jalil and Zhang, 2008). For very thin surface coatings, a high-resolution TEM (HR-TEM) is required, as it offers a resolution down to atomic level (Erni *et al.*, 2009); high resolution also offers a chance to visualize the crystallographic structure of a single nanocrystal (Wang *et al.*, 2011b). STEM with a high-angle annular dark-field (HAADF) imaging mode is a superior technique for the visualization of the different layers of core-shell nanophosphors (Abel *et al.*, 2011; Zhang *et al.*, 2012a). SEM utilizes the backscattered electrons and is used for imaging nanophosphor surfaces (Zhang *et al.*, 2007).

The crystal structure of the synthesized UCNP is commonly analyzed with powder X-ray diffraction, a method based on the diffraction of scattered X-rays by crystalline materials. (Mai *et al.*, 2006; Wang *et al.*, 2010b) The selected area electron diffraction mode of TEM can also be used for crystal structure analysis when a large number of nanocrystals are illuminated by the electron beam (Liu *et al.*, 2011c; Liu *et al.*, 2015).

The concentration of dopants in a single nanocrystal is usually estimated from the amount and proportions of added lanthanide precursors in the synthesis reaction. However, the dopant concentration of a single nanophosphor can be measured with a HR-TEM equipped with either an energy dispersive spectrometer (EDS) or an electron energy loss spectrometer (EELS) (Abel *et al.*, 2011; Wang *et al.*, 2011b; Zhang *et al.*, 2012a). These methods are both qualitative and quantitative, with 2D scanning capability. The elemental composition can also be analyzed from UCNP dispersions with inductively coupled plasma mass spectrometry (ICP-MS) or inductively coupled plasma atomic emission spectroscopy (ICP-AES) (Abdul Jalil and Zhang, 2008; Chatterjee *et al.*, 2008; Liu *et al.*, 2015; Xiong *et al.*, 2010).

The presence of surface ligands can be analyzed with infrared (IR) spectroscopy in which the ligands are identified through their vibrational frequencies (Cao *et al.*, 2011; Wang *et al.*, 2010e). Thermogravimetric analysis (TGA) has also been used; weight changes at certain temperatures indicate the amount and type of surface ligands. However, this method requires a large amount of surface-coated UCNP sample (10-15 mg). (Dong *et al.*, 2011; Gorris *et al.*, 2011; Saleh *et al.*, 2011a; Schäfer *et al.*, 2007)

A useful tool in analyzing the surface functionalization is the measurement of zeta potential, which indicates the sign of the surface charge and whether the UCNPs are colloidally stable in water after the surface modifications. At the same time, the hydrodynamic diameter of the coated nanophosphors can be measured with dynamic light scattering to assess aggregation. (Dong *et al.*, 2011; Sedlmeier and Gorris, 2015; Xiong *et al.*, 2010)

In addition to the physical properties, the characterization of the optical properties of synthesized and surface-coated UCNPs is important. Most of the equipment for the measurement of the upconversion photoluminescence is usually customized from standard instruments by equipping them with a 980-nm laser diode as the excitation source, as very few commercial measurement devices are available (Gnach and Bednarkiewicz, 2012; Soukka *et al.*, 2008). High upconversion emission efficiency and the sufficient shielding of the UCNP surface from the quenching effects of water are preferable in bioanalytical applications and, thus, upconversion luminescence spectrum is normally analyzed both before and after the surface modifications to study the impact of the coating and the aqueous environment on the spectral properties, such as the total emission intensity and the peak ratios (Wilhelm *et al.*, 2015).

As stated above, due to the lack of standard reference materials, the absolute quantum yield, instead of a relative measurement, must be measured for UCNPs. Absolute QY is measured with an integrating sphere. The method has been described by Boyer and van Veggel (2010), Liu *et al.* (2013c), and Würth *et al.* (2013). The lifetimes of the excited states of the activator dopants in UCNPs can be measured either in the time-domain (Anderson *et al.*, 2014; Hyppänen *et al.*, 2009; Suyver *et al.*, 2005a) or in the frequency-domain (Riuttamäki *et al.*, 2011).

2.2 Applications in homogeneous sensing

In homogeneous assays the label signal is modulated by a binding event with an analyte or by enzymatic reaction and, thus, the bound labels need not be separated from the unbound ones, unlike in heterogeneous assays (Hemmilä, 1985). Homogeneous assays are simple and fast to perform, which also simplifies the instrument requirements. However, they are prone to interference from biological sample materials which can limit the assay sensitivity. (Kuningas *et al.*, 2005b; Mathis, 1993; Ullman, 1999)

2.2.1 Upconversion resonance energy transfer

A typical fluorescent homogeneous assay employs Förster resonance energy transfer (FRET) (Förster, 1948) in which the acceptor fluorophore must be in close proximity to the donor fluorophore to enable a non-radiative dipole-dipole interaction between the two. Furthermore, the excitation spectrum of the acceptor dye must overlap with the emission spectrum of the donor for FRET to take place between the two isoenergetic states. Conventional fluorescence techniques suffer from

autofluorescence, scattered excitation light, and light absorption by the sample (Vedvik *et al.*, 2004).

Upconversion resonance energy transfer (UC-RET) is a form of FRET in which an excited upconverting nanophosphor transfers energy to a fluorescent acceptor dye. The NIR excitation and anti-Stokes photoluminescence of UCNPs eliminate autofluorescence and reduce scattering enabling background-free detection. NIR excitation further excludes direct acceptor excitation. The narrow upconversion emission peaks and a large anti-Stokes shift facilitate the specific detection of the acceptor emission without donor crosstalk. (Kuningas *et al.*, 2005b) The UCNP emission peaks above 600 nm (e.g., 660 nm for Er^{3+} -doped UCNPs) are not attenuated due to the light absorption of biological materials and, thus, homogeneous assays can be performed also in optically challenging matrices, such as whole blood (Kuningas *et al.*, 2007). Furthermore, UCNPs do not photobleach, and as the NIR excitation has a high penetration depth, it enables the use of UC-RET-based homogeneous sensing even within cells (Wang *et al.*, 2010a). As UCNPs employ lanthanides, the Förster radius R_0 (the distance at which 50 % of the energy is transferred) can be even longer than 7.5 nm allowing for efficient energy transfer over expanded range (Selvin, 1996). UC-RET is, therefore, a highly suitable tool for homogeneous sensing and bioassays.

2.2.2 Optical (bio)chemical and temperature sensors

Optical chemical sensors provide information about an analyte concentration in an environment through changes in an optical signal generated by reversible recognition events. One of the first applications of UCNPs in optical chemical sensors was introduced by the group of Wolfbeis in 2009 (Sun *et al.*, 2009). The luminescence of $\text{Yb}^{3+}/\text{Er}^{3+}$ or $\text{Yb}^{3+}/\text{Tm}^{3+}$ -doped UCNP materials does not respond directly to chemical or biochemical analytes and, thus, suitable recognition molecules, such as indicator dyes, are required for optical sensing applications. By selecting the indicator dyes so that their absorption spectra overlap with the emission spectrum of the UCNPs, UC-RET can be used for the analyte sensing. The indicator dye needs not be luminescent, as long as its absorbance changes with the analyte concentration. The changing absorbance attenuates the UCNP emission, which can be measured. Furthermore, the measurement of the UC-RET-attenuated UCNP emission peak (or UC-RET-sensitized indicator emission) can be referenced by measuring the UC-RET-independent UCNP emission peak enabling two-wavelength ratiometric referencing. Signal referencing is mandatory for most sensor applications, because the measurement conditions, such as fluctuating light source or indicator concentration, might vary (Meier *et al.*, 2014; Schäferling and Duerkop, 2008).

UC-RET-based optical chemical sensors utilizing indicators whose luminescence properties change in varying pH have been developed for biologically and biochemically important parameters, such as CO_2 (Ali *et al.*, 2010), pH (Sun *et al.*, 2009), and NH_3 (Mader and Wolfbeis, 2010). Achatz *et al.* (2011) employed a luminescent iridium complex for sensing oxygen; the UC-RET-sensitized emission of

the iridium complex was quenched by the presence of O₂. Xie *et al.* (2012; 2013) prepared optical thin films for the detection of pH and metal ions in whole blood. The detection was based on UC-RET between UCNPs and chromoionophores in hydrophobic polymer matrices. These sensor applications, however, employed UCNPs with diameters close to or above 100 nm. In a publication by del Barrio *et al.* (2014), an enzymatic biosensor based on UC-RET between Tm³⁺-doped nanosized UCNP and fluorescein-modified glucose oxidase was developed for the continuous detection of glucose. In all of these sensors, the UCNPs and the indicator dyes were immobilized on thin films. Even though these kinds of planar sensor films enable continuous and reversible measurements (Xie *et al.*, 2012), they are not applicable to, e.g., intracellular sensing purposes.

Completely solution-based, homogeneous sensors based on UCNPs have also been developed. Esipova *et al.* (2012) introduced a homogeneous pH sensor based on UC-RET with porphyrins, which attenuated the red emission peak of Er³⁺-doped UCNP at decreasing pH. Homogeneous sensors detecting ions, such as Hg²⁺ (Kumar and Zhang, 2010; Li and Wang, 2013; Li *et al.*, 2014b), CN⁻ (Yao *et al.*, 2012), Cu²⁺ (Zhang *et al.*, 2012b), Ce⁴⁺ (Zhou *et al.*, 2009) and Cr³⁺ (Liu *et al.*, 2013a) in aqueous solutions have also been developed. The sensor for mercury ions by Kumar *et al.* (2010) did not employ an Hg²⁺-sensing indicator; the ion recognition was performed by a single-stranded oligonucleotide bound to the UCNP surface. Thymine-thymine mismatches can bind Hg²⁺ ions with high selectivity (Miyake *et al.*, 2006). When mercury was present, the oligonucleotide formed a hairpin structure, which intercalated SYBR Green dyes: a UC-RET-sensitized emission of the SYBR Green was detected. Liu *et al.* (2011b) developed an Hg²⁺ sensor for the sensing of intracellular mercury, and Peng *et al.* (2015) reported a sensor for detecting Zn²⁺ in HeLa cells, brain tissue (β-amyloids), or in living zebrafish. Both homogeneous and planar optical chemical sensors based on UC-RET utilizing nanosized (<100 nm) upconverting materials are listed in Table 1.

Table 1. Optical chemical sensors based on UC-RET from UCNP to an indicator dye.

Analyte	Indicator dye	UCNP material diameter	Detection mechanism	Matrix	Reference
Thin films:					
CO ₂	Bromothymol blue	NaYF ₄ :Yb,Er 40–100 nm	Attenuation of UCNP emission spectrum	Gas	(Ali <i>et al.</i> , 2010)
NH ₃	Phenol red	NaYF ₄ :Yb,Er 60–90 nm	Attenuation of green emission of UCNP	Aqueous solution	(Mader and Wolfbeis, 2010)
O ₂	Ir ³⁺ complex	NaYF ₄ :Yb,Tm 80–120 nm	UC-RET-sensitized indicator emission	Gas	(Achatz <i>et al.</i> , 2011)
Glucose	Fluorescein-modified glucose oxidase	NaYF ₄ :Yb,Tm@NaYF ₄ 30 nm	UC-RET-sensitized fluorescein emission	Aqueous solution	(del Barrio <i>et al.</i> , 2014)
Homogeneous:					
pH	Porphyrin	NaYF ₄ :Yb,Er 23 nm	Attenuation of UCNP emission spectrum	Aqueous solution	(Esipova <i>et al.</i> , 2012)
Hg ²⁺	Ruthenium complex	NaYF ₄ :Yb,Er,Tm 17 nm	Attenuation of UCNP emission spectrum	Aqueous solution, in vivo	(Liu <i>et al.</i> , 2011b)
	Thymine-rich DNA + SYBR Green	NaYF ₄ :Yb,Tm ~50 nm	UC-RET-sensitized indicator emission	Aqueous solution	(Kumar and Zhang, 2010)
	Rhodamine B thiolactone	NaYF ₄ :Yb,Er -	Attenuation of green emission of UCNP	Aqueous solution	(Li and Wang, 2013)
	Ruthenium complex	NaYF ₄ :Yb,Er,Tm 10–15 nm	Attenuation of UCNP emission spectrum	Aqueous solution	(Li <i>et al.</i> , 2014b)
CN ⁻	Ir ³⁺ complex	NaYF ₄ :Yb,Ho 20–40 nm	Attenuation of green emission of UCNP	Aqueous solution	(Yao <i>et al.</i> , 2012)
Cu ²⁺	Rhodamin B-hydrazide	NaYF ₄ :Yb,Er -	UC-RET sensitized indicator emission	Aqueous solution	(Zhang <i>et al.</i> , 2012b)
Zn ²⁺	a	NaYF ₄ :Yb,Tm 16 nm	Attenuation of blue emission of UCNP	Aqueous solution, in vivo	(Peng <i>et al.</i> , 2015)
Ce ⁴⁺	MPTEA ^b	NaYF ₄ :Yb,Er 18 nm	Attenuation of UCNP emission spectrum	Aqueous solution	(Zhou <i>et al.</i> , 2009)
Cr ³⁺	dimercapto-succinic acid-capped gold nanoparticles	NaYF ₄ :Yb,Er 70 nm	Attenuation of UCNP emission spectrum	Aqueous solution, urine	(Liu <i>et al.</i> , 2013a)
Glucose	Flavin adenine dinucleotide + glucose oxidase	NaYF ₄ :Yb,Tm@NaYF ₄ 34 nm	Attenuation of blue emission of UCNP	Aqueous solution	(Wilhelm <i>et al.</i> , 2014)

^a(E)-4-(4-(bis(2-(bis(pyridin-2-ylmethyl)amino)ethyl)amino)styryl)-1-methylpyridin-1-ium^b2-(4-aminophenylethyl)-5-methoxy-2-(2-pyridyl)thiazole

In contrast to the sensors listed above, where an indicator dye or other recognition molecule is required, Suyver *et al.* (2005c) showed that the optical properties of NaYF₄:Yb³⁺, Er³⁺ UCNP respond to temperature changes: the intensity ratio of the two green

emission bands at 525 nm and 545 nm of Er^{3+} -doped UCNPs changes with temperature. Since then, many research groups have reported nanothermometers based on UCNPs (Dong and Zink, 2014; Rakov and Maciel, 2012; Sedlmeier *et al.*, 2012; Singh *et al.*, 2009; Vetrone *et al.*, 2010b). Recently, Saleh *et al.* (2011b) noticed that the UCNP emission is quenched by heavy metal ions, and they used this characteristic in the quantification of Cu^{2+} , Hg^{2+} , Pb^{2+} , Cd^{2+} , Co^{2+} , Ag^+ , Fe^{3+} , Zn^{2+} , bromide, and iodide ions.

2.2.3 Bioanalytical assays

Homogeneous UC-RET-based bioanalytical assays employ an analyte-binding biomolecule, such as an antibody or oligonucleotide, as the recognition moiety and a fluorophore-labeled analyte or binding molecule as the acceptor. These assays can also be called biosensors. Homogeneous assays can be categorized as competitive or non-competitive assays. In a competitive assay, the analyte competes with an acceptor-labeled analyte analog for the binding to the recognition moiety. In a non-competitive, or sandwich assay, the analyte is bound by both binders conjugated either to the donor or the acceptor.

The first UC-RET-based homogeneous assays were simultaneously published by Wang *et al.* (2005) and Kuningas *et al.* (2005b). Both assays utilized the strong binding between biotin and (strept)avidin, but the acceptor dye differed. Wang *et al.* utilized avidin-conjugated gold nanoparticles to quench the upconversion photoluminescence when brought into close contact with the biotin-conjugated UCNPs in a sandwich assay, whereas Kuningas *et al.* used biotin-conjugated fluorescent protein B-phycoerythrin as the acceptor with streptavidin-conjugated bulk UCNPs as donors in a competitive assay for biotin. These first reports of UC-RET assays represent the two different detection mechanisms used in homogeneous bioanalytical assays, i.e., the detection of either the sensitized acceptor emission or the quenching of upconversion emission. The latter mechanism requires a highly absorbing gold nanoparticle (Wang *et al.*, 2005) or the strong electron-capturing tendency of π -rich structure of carbon nanoparticles, graphene, and graphene oxide (Li *et al.*, 2014a; Wang *et al.*, 2011e; Wang *et al.*, 2012; Zhang *et al.*, 2011) as the acceptor, because the quenching of nanoparticle luminescence with an organic fluorophore, such as BHQ-1, is very inefficient (He *et al.*, 2013). The use of quenchers as acceptors requires the detection of small changes in high upconversion photoluminescence intensity with usually a relatively large standard deviation produced by the particulate labels. Especially, the efficient quenching of the luminescence of a micrometer size particle is not possible, as only the surface dopants are within the distance required for RET and the particle core produces high intensity background signal (Rantanen *et al.*, 2008). Rantanen *et al.* (2008) resolved this problem with a tandem dye, in which the UC-RET-sensitized acceptor fluorophore further transferred its energy to a quencher molecule. Organic fluorophores (Chen *et al.*, 2008), fluorescent proteins (Vetrone *et al.*, 2010a), and quantum dots (Mattsson *et al.*, 2015) have been used as fluorescent acceptors. The changes in the sensitized acceptor signal are easier to detect, because the signal intensities are lower than that of the upconversion photoluminescence. The homogeneous bioanalytical assays utilizing nanosized (<100 nm) UCNPs and different fluorophores or quenchers as acceptors are listed in Table 2.

Table 2. Homogeneous UC-RET-based bioanalytical assays with nanosized UCNPs.

Acceptor	Analyte	Binder	UCNP material diameter, surface	Type of assay	Reference
Based on the detection of sensitized acceptor emission					
TAMRA ^a	Target DNA	Oligo-nucleotide	NaYF ₄ :Yb,Er 8–14 nm, azelaic acid	Sandwich hybridization	(Chen <i>et al.</i> , 2008)
	Sickle cell disease gene	Oligo-nucleotide	NaYF ₄ :Yb,Er 60–100 nm, silica	Sandwich hybridization	(Kumar <i>et al.</i> , 2009)
	ATP	Aptamer	NaYF ₄ :Yb,Er 20 nm	Competitive	(Song <i>et al.</i> , 2012)
	MRSA DNA sequence	Oligo-nucleotide	NaYF ₄ :Yb,Er 28 nm, citrate	Sandwich hybridization	(Liu <i>et al.</i> , 2013d)
SYBR Green	Target DNA	Oligo-nucleotide	NaYF ₄ :Yb,Tm 20–100 nm, DTPA	Sandwich hybridization	(Kumar and Zhang, 2009)
R-phycoerythrin	ExtrAvidin	Biotin	NaYF ₄ :Yb,Er 18 nm, PEI	Competitive	(Vetrone <i>et al.</i> , 2010a)
Qdot605	Biotin	Streptavidin	NaYF ₄ :Yb,Er 22–36 nm, silica	Competitive	(Mattsson <i>et al.</i> , 2015)
Tandem AF680 + BHQ-3	Caspase-3	Peptide	NaYF ₄ :Yb,Er 80 nm, silica	Enzyme activity	(Vuojola <i>et al.</i> , 2012)
Based on quenching of UCNP emission					
Gold nanoparticles	Avidin	Biotin	NaYF ₄ :Yb,Er 50 nm, LbL	Sandwich	(Wang <i>et al.</i> , 2005)
	Goat antihuman IgG	Rabbit anti-goat IgG + Human IgG	NaYF ₄ :Yb,Er 30–70 nm, silica	Sandwich	(Wang <i>et al.</i> , 2009a)
	Glucose	Con-canavalin A	NaYF ₄ :Yb,Er 30–60 nm, PAA	Competitive	(Peng <i>et al.</i> , 2011)
	Avian influenza virus H7 subtype	Oligo-nucleotide	BaGdF ₅ :Yb,Er 14 nm, PEI	Sandwich hybridization	(Ye <i>et al.</i> , 2014)
	Thrombin	Aptamer	NaYF ₄ :Yb,Tm ~50 nm, PAA	Sandwich	(Yuan <i>et al.</i> , 2014)
Graphene oxide	Glucose	Con-canavalin A	NaYF ₄ :Yb,Er PAA	Competitive	(Zhang <i>et al.</i> , 2011)
	ATP	Aptamer	NaYF ₄ :Yb,Er 29 nm	Competitive	(Liu <i>et al.</i> , 2011a)
	HIV antibody	Peptide	NaYF ₄ :Yb,Er 60 nm	Competitive	(Wu <i>et al.</i> , 2014)
	Kanamycin	Aptamer	NaYF ₄ :Yb,Er 10–20 nm, HDA ^b	Competitive	(Li <i>et al.</i> , 2014a)
Carbon nanoparticles	Thrombin	Aptamer	NaYF ₄ :Yb,Er ~50 nm, PAA	Competitive	(Wang <i>et al.</i> , 2011e)
	Matrix metallo-proteinase-2	Polypeptide	NaYF ₄ :Yb,Er 30–50 nm, PEI	Enzyme activity	(Wang <i>et al.</i> , 2012)
PMPD ^c	Target DNA	Oligo-nucleotide	NaYF ₄ :Yb,Er 20–40 nm, PEI	Competitive	(Wang <i>et al.</i> , 2013c)
BHQ-1	ATP	Split aptamers	NaYF ₄ :Yb,Er 40 nm, PAA	Sandwich	(He <i>et al.</i> , 2013)

^acarboxytetramethylrhodamine, ^bhexanedioic acid, ^cpoly-m-phenylenediamine nanospheres

Homogeneous UC-RET-based assays include ligand binding assays (Mattsson *et al.*, 2015; Wang *et al.*, 2005; Vetrone *et al.*, 2010a), immunoassays (Wang *et al.*, 2009a; Wu *et al.*, 2014), nucleic acid hybridization assays (Chen *et al.*, 2008; Kumar *et al.*, 2009;

Kumar and Zhang, 2009; Liu *et al.*, 2013d; Ye *et al.*, 2014), and enzyme activity assays (Wang *et al.*, 2012; Vuojola *et al.*, 2012). Furthermore, assays based on the binding properties of lectins (Peng *et al.*, 2011; Zhang *et al.*, 2011) and aptamers (He *et al.*, 2013; Li *et al.*, 2014a; Liu *et al.*, 2011a; Song *et al.*, 2012; Wang *et al.*, 2011e; Yuan *et al.*, 2014) have also been developed.

Wang *et al.* (2009a) introduced a homogeneous sandwich immunoassay for goat antihuman IgG, in which the analyte was bound by a UCNP conjugated to rabbit anti-goat IgG and a gold nanoparticle conjugated to human IgG. Liu *et al.* (2013d) demonstrated a nucleic acid hybridization assay for the detection of a methicillin-resistant *Staphylococcus aureus* (MRSA) DNA sequence. Two oligonucleotides complementary to the target sequence were either conjugated to the UCNP surface or labeled with carboxytetramethylrhodamine (TAMRA) dye. Once the target sequence was present, the hybridization reaction brought the two labels together and UC-RET occurred.

Based on the sugar-binding property of a lectin concanavalin A (ConA), Peng *et al.* (2011) presented a competitive homogeneous assay for glucose. The lectin molecules were conjugated to the surface of the UCNP nanophosphor. In the absence of glucose they captured SH- β -cyclodextrin-coated gold nanoparticles, which quenched the upconversion photoluminescence. Because of its higher affinity to ConA, glucose replaced the β -cyclodextrin-coated gold nanoparticles recovering the UCNP emission. Aptamers have also been used as binders for the detection of adenosine triphosphate (ATP) (He *et al.*, 2013; Liu *et al.*, 2011a; Song *et al.*, 2012), thrombin (Wang *et al.*, 2011e; Yuan *et al.*, 2014), and kanamycin (Li *et al.*, 2014a). The fact that only one aptamer exists for each of these analytes makes merely competitive assays possible for their detection (Li *et al.*, 2014a; Wang *et al.*, 2011e). However, by splitting the aptamer in two, a sandwich assay can be developed (He *et al.*, 2013; Yuan *et al.*, 2014).

Kuningas *et al.* (2007) demonstrated the capability of estradiol hormone detection in a whole blood sample with a UC-RET-based homogeneous assay. They utilized the 660-nm emission peak of $\text{La}_2\text{O}_2\text{S}:\text{Yb}^{3+}, \text{Er}^{3+}$ bulk phosphor and a near-infrared acceptor dye Alexa Fluor 680 exploiting only the wavelengths in which whole blood absorption is minimal. This was a major step towards a fast, sensitive, and simple point-of-care testing directly in whole blood of which other fluorescent label molecules are incapable. Wang *et al.* (2012) demonstrated a whole blood enzyme activity assay for matrix metalloproteinase-2 (MMP-2) utilizing the quenching of upconversion photoluminescence of $\text{NaYF}_4:\text{Yb}^{3+}, \text{Er}^{3+}$ nanophosphors by carbon nanoparticles. The UCNP and the carbon nanoparticle were joined by a polypeptide chain which was cleaved by the MMP-2 in the sample. The cleavage separated the two particles and recovered the upconversion emission. For assays performed in blood samples, the stability of the UCNP surface chemistry must be taken into consideration. Blood samples contain anticoagulants and stabilizing agents, such as EDTA, citrate, or heparin, which as polydentate ligands can replace the ligand capping on the UCNPs surface via ligand exchange. In addition, their impact on UCNP aggregation, nonspecific binding, or the stability of the analyte must be analyzed.

3 AIMS OF THE STUDY

The overall aim of this thesis was to study the unique properties of upconverting nanophosphors and to evaluate their potential for homogeneous sensing applications in challenging matrix materials. The purpose was to demonstrate the advantages of nanosized upconverting materials in the field of bioanalytical applications.

More specifically, the aims were:

- I To develop a highly **selective separation method** for bioconjugated upconverting nanophosphors to increase their specific activity by utilizing the intrinsic paramagnetism of the lanthanide dopants.
- II To demonstrate the applicability of upconverting nanophosphors for **sensing and imaging intracellular pH** due to their unique features, including excitation with deeply penetrating near-infrared light, high photostability, and the lack of autofluorescence.
- III To introduce a homogeneous UC-RET-based assay for **the quantification of folic acid in whole blood samples** utilizing the optically transparent window of biological materials for both excitation and autofluorescence-free detection.
- IV To identify **the mechanism behind the high quenching efficiency of water** on the upconversion photoluminescence of nanosized phosphors by the means of luminescence decay measurements.

4 SUMMARY OF MATERIALS AND METHODS

A more detailed description of the materials and methods employed in this study can be found in the original publications (I–IV). A brief summary with some additional information on the materials and methods is presented here.

4.1 Upconverting nanophosphor bioconjugates

4.1.1 UCNP materials and their characterization

The nanocrystalline NaYF₄: Yb³⁺, Er³⁺ materials used in publications I–IV and NaYF₄:Yb³⁺, Tm³⁺ materials used in publication IV were synthesized in organic oils using a modified method based on *in situ* preparation of rare earth oleates described earlier (Wang *et al.*, 2010b). Briefly, methanol solutions of rare earth chlorides (a total of 6 mL) were added to a flask containing 9 mL of oleic acid and 21 mL of octadecene. While stirring, the mixture was heated to 160 °C for 30–40 min after which it was cooled to room temperature. A methanol solution of a mixture of 0.178 g NH₄F and 0.120 g NaOH was added and stirred for 30 min, after which the solution was heated to 310 °C (or 315 °C for Tm³⁺-doped nanophosphors) for 1.5 h. Next, the solution was again cooled down to room temperature and the formed nanophosphors were collected by centrifugation and washed with ethanol.

The molar ratios of Yb³⁺ and Er³⁺ in NaYF₄: Yb³⁺, Er³⁺ nanomaterials out of all rare earth elements were 17 mol% and 3 mol%, respectively. The molar ratios of Yb³⁺ and Tm³⁺ in NaYF₄: Yb³⁺, Tm³⁺ nanomaterials were 20 mol% and 0.5 mol%, respectively.

The shape and size distribution of the synthesized nanophosphors were characterized by imaging with TEM (Tecnai 12 BioTwin, 120 kV, FEI, Oregon, USA; or JEOL JEM-1400+, 80 kV, JEOL, Tokyo, Japan) using Formvar/Carbon 300 mesh copper grids (Agar Scientific Ltd., Stansted, Essex, UK). The average nanocrystal size was calculated by measuring the diameter of >100 particles with ImageJ software, version 1.43s (<http://rsb.info.nih.gov/ij/>).

4.1.2 Surface modification and bioconjugation

The surface of NaYF₄: Yb³⁺, Er³⁺ nanophosphors used in publications I–III were functionalized with silica according to a modified method by Jana *et al.* (2007) and described in publication I. Briefly, the oleic acid-capped UCNPs in 5 mL of toluene were mixed with tetramethyl orthosilicate (TMOS, Sigma-Aldrich, St. Louis, MO) and (*N*-(3-trimethoxysilyl)propyl)ethylene diamine (TMED, Sigma-Aldrich) to produce a thin, hydrophilic silica layer with amine groups (Figure 8). The amine groups were further converted to carboxylic acid groups with glutaric anhydride (Sigma-Aldrich) in publications I and III (Rantanen *et al.*, 2009).

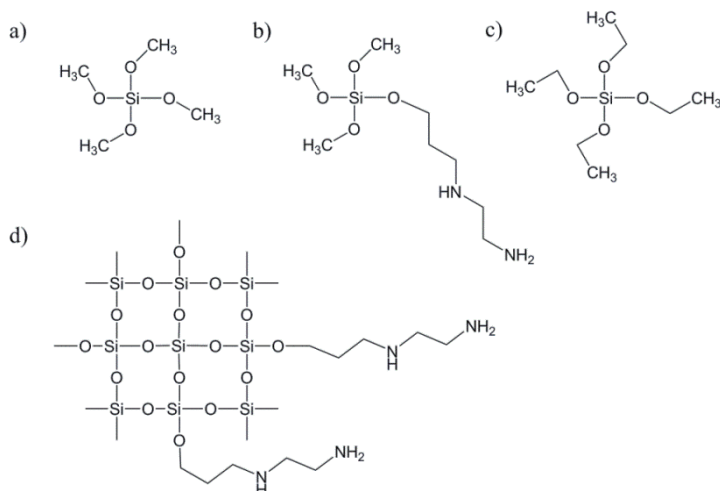


Figure 8. Structures of a) tetramethyl orthosilicate (TMOS), b) (N-(3-trimethoxysilyl)propyl)ethylene diamine (TMED), c) tetraethyl orthosilicate (TEOS) and d) an amino-modified silica polymer.

Monoclonal antibody (Mab) 5A10 against prostate-specific antigen (PSA) (Lilja *et al.*, 1991) (**I**) or folate binding protein (FBP, Scripps Laboratories, Sand Diego, CA) (**III**) was conjugated to the carboxylic acid groups on the surface of the UCNPs via carbodiimide chemistry using 1-ethyl-3-(3-dimethylaminopropyl)carbodiimide hydrochloride (EDC, Fluka, Buchs, Switzerland) and N-hydroxysulfosuccinimide sodium salt (sulfo-NHS, Fluka) (Vuojola *et al.*, 2012). A pH-sensitive dye pHrodo™ Red succinimidyl ester (Molecular Probes, Carlsbad, CA) (**II**) was conjugated to the amine groups of the silica layer in pH 8.5. The protocol is described in more detail in publication **II**.

In publication **IV**, the $\text{NaYF}_4: \text{Yb}^{3+}, \text{Er}^{3+}$ and $\text{NaYF}_4: \text{Yb}^{3+}, \text{Tm}^{3+}$ nanophosphors were washed with HCl to remove the oleic acid capping according to Bogdan *et al.* (2011). Both oleic-acid-capped UCNPs were also surface-modified with a thick silica layer with tetraethyl orthosilicate (TEOS) (Figure 8) using a reverse-microemulsion technique by Wilhelm *et al.* (2013). Both the bare and silanized UCNPs were then dispersed in water or in D_2O as described in more detail in publication **IV**.

The surface-modified UCNPs with the thin silica shell were characterized with HR-TEM and an elemental analysis was performed on a single particle with energy-dispersive X-ray spectroscopy (EDX) with JEOL JEM-2200FS (200 kV, JEOL). Holey-carbon 400 mesh copper grids (Agar Scientific Ltd.) were used for HR-TEM-imaging. The thicker silica shell was imaged with JEOL JEM-1400+ TEM (80 kV, JEOL) using SiO/Formvar 300 mesh copper grids (Agar Scientific Ltd.).

4.2 High gradient magnetic separation

In the original publication **I**, a new and highly selective separation method for bioconjugated UCNP was constructed. The separation method utilized the paramagnetism of the lanthanide ion dopants in UCNP and the amplification of the magnetic field of two permanent supermagnets (110.6×89×19.5 mm, Supermagnete, Germany) by addition of a magnetizable steel wool matrix (grade zero, stainless steel, Oy Teräs-LVI Ab, Finland). The high gradient magnetic separation (HGMS) construct is depicted in Figure 9. The steel wool matrix created strong local magnetic gradients when placed in a column between a pair of strong supermagnets. These magnetic gradients amplified the magnetic field up to 10 000-fold. When bioconjugated UCNP were added to the column containing the matrix, the magnetic field gradients trapped the weakly paramagnetic UCNP, while the excess non-magnetic biomolecules flowed through the column. The captured UCNP were washed and finally eluted from the column by removing the supermagnets and mechanically tapping the column to aid the release of sterically trapped nanophosphors.

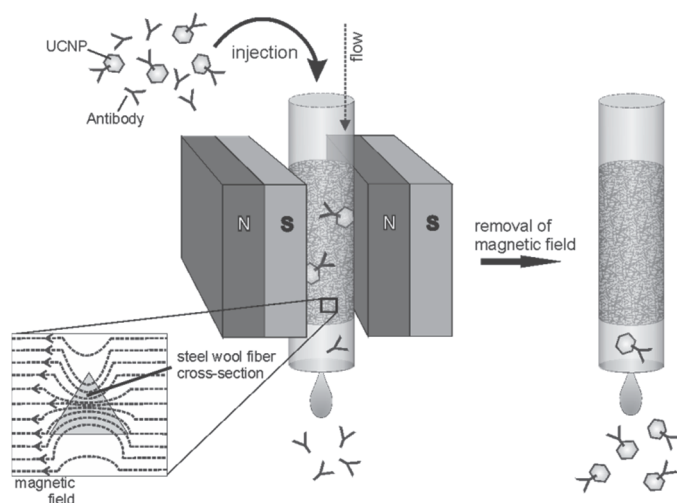


Figure 9. Illustration of the high gradient magnetic separation system for the purification of bioconjugated UCNP from unreacted biomolecules.

Anti-PSA-Mab5A10 was conjugated to UCNP and the UCNPs-bioconjugate was purified from excess antibodies using the high gradient magnetic separation (HGMS). The sample was injected in the column in a 10 mM borate buffer, pH 8.5 with 0.1 % Tween20 and 0.05 % PAA. Using a 0.25 mL min⁻¹ flow rate, the column was washed with 10 mM borate buffer, pH 8.5 with 0.1 % Tween20 for 20 minutes and the wash fractions were collected. For the elution of the trapped UCNP, the magnets were removed and the flow rate was increased to 0.5 mL min⁻¹. The presence of the UCNP in the eluted fractions was characterized by measuring the upconversion luminescence. The presence of bioconjugated or unbound α -PSA-Mab5A10 was

determined with a sandwich immunoassay on rabbit antimouse IgG plates using Tb³⁺-chelate-labeled PSA as a label.

4.3 Homogeneous assays using UCNPs

In this section, the assay principles of the two developed homogeneous UC-RET-based assays are described. In the original publication **II**, a pH-nanosensor was developed and in publication **III**, a competitive homogeneous assay for whole blood folic acid was constructed. The characteristics of the acceptor fluorophores used in the assays are summarized in Table 3.

Table 3. Characteristics of the acceptor fluorophores used in the original publications.

Acceptor	Molecular weight g mol ⁻¹	Excitation λ_{max} nm	Emission λ_{max} nm	Extinction coefficient ϵ cm ⁻¹ M ⁻¹	Manufacturer	Publication
pHrodo TM Red	650	560	585	65 000	Molecular Probes	II
Alexa Fluor 680	1 150	679	702	184 000	Molecular Probes	III

4.3.1 pH-nanosensor

In the original publication **II**, a nanosensor based on UC-RET was constructed for measuring intracellular pH. A fluorogenic pH-dependent dye pHrodoTM Red-NHS ester (Ogawa *et al.*, 2010) was covalently conjugated to the amine groups of the silanized surface of NaYF₄: Yb³⁺, Er³⁺ nanophosphors at pH 8.5. The excess, unbound dye was purified from the conjugate by ultrafiltration with a 30 K Macrosep Advance centrifugal device (Pall Life Sciences, Omega, Ann Arbor, MI). The conjugate was used as a nanosensor to sense the surrounding pH according to the principle illustrated in Figure 10. UC-RET occurs from the UCNP to the acceptor dye upon excitation with 980 nm radiation. The UC-RET-sensitized emission of the dye increases strongly with decreasing pH. The pH-independent emission of the UCNP at 550 nm was used as the reference signal.

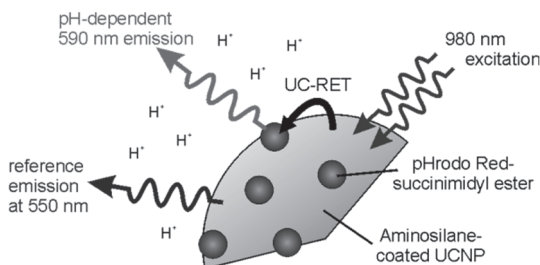


Figure 10. Principle of the UC-RET-based pH-nanosensor.

To study if UC-RET occurs between the UCNP and pHrodoTM Red, the upconversion photoluminescence decays were measured from both aminosilane coated UCNPs and

the dye-UCNP-conjugate. The analysis was performed with a modified plate Chameleon fluorometer as described in section 4.4.3.

The pH-nanosensor was calibrated by measuring the upconversion photoluminescence of the UCNPs at 550 nm and the UC-RET-sensitized emission of the dye at 600 nm at different pH values with a modified plate Chameleon fluorometer (section 4.4.1). The nanosensor conjugate was dispersed in $15 \mu\text{g mL}^{-1}$ concentration in 80 μL of 200 mM phosphate-citrate buffer, pH 7.65, and the pH was adjusted by adding 0.2 M citrate, 1 μL at a time. The pH-titration was also performed in the presence of cellular salt concentration (137 mM NaCl, 2.7 mM KCl) by the addition of 2 M citrate.

For the intracellular imaging of pH, 50 $\mu\text{g mL}^{-1}$ of the nanosensor was added to cultured HeLa cells in *Dulbecco's Modified Eagle's medium* (DMEM, Life Technologies, Carlsbad, CA) with 2 % fetal calf serum (FCS) and incubated for 16 h. The cells were then cultured on glass-bottom 96-well plates and imaged with stimulated emission depletion (STED) super-resolution laser scanning microscope as described in section 4.4.4.

4.3.2 Whole blood folic acid assay

In the original publication **III**, a competitive homogeneous binding assay was constructed for folic acid utilizing UC-RET between $\text{NaYF}_4: \text{Yb}^{3+}, \text{Er}^{3+}$ nanophosphors conjugated to folate binding protein (FBP) and Alexa Fluor 680 (AF680) acceptor-labeled folate analogs. The assay principle is illustrated in Figure 11. The folic acid content of a whole blood sample was analyzed with the developed assay.

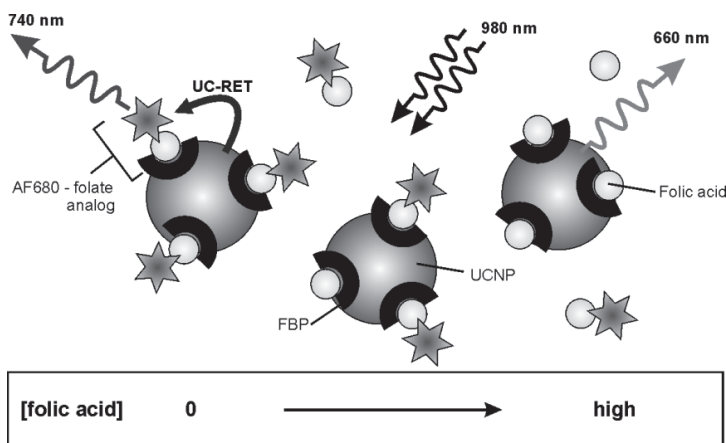


Figure 11. Principle of the UC-RET-based folic acid assay. The folate binding protein (FBP)-conjugated UCNPs donor is excited with 980 nm radiation, and the energy is transferred through upconversion resonance energy transfer (UC-RET) to the AF680 acceptor-labeled folate analog. The folic acid in the sample competes with the AF680-folate analog for binding to the FBP, and the higher the folic acid amount in the sample is, the less UC-RET-sensitized acceptor emission at 740 nm is obtained.

The folate analog N¹⁰-(trifluoroacetyl)pteroic acid (Sigma-Aldrich) was first amine-modified with hexan-1,6-diamine (Sigma-Aldrich) by a method adapted from Adamczyk *et al.* (2004). Next, AF680-NHS ester was conjugated to the amine groups, and the labeled folate analog was isolated with reverse-phase high-performance liquid chromatography (HPLC) (SpectraSYSTEM, Thermo Fisher Scientific, Waltham, MA) using an acetonitrile gradient.

Whole blood samples from a healthy volunteer were pretreated for the assay to release the folic acid content from the red blood cells. Slowly thawed samples were hemolyzed by 20-fold dilution in freshly prepared 0.5 % (w/v) ascorbic acid and mixed for 90 min. Next, 30 μ L of a mixture of 1 M NaOH and 11 mM dithiothreitol (DTT, PerkinElmer Life and Analytical Sciences, Turku, Finland) was added to 300 μ L of lysed blood to denature all proteins in the sample by increasing the pH to \sim 11. Finally, the pH was neutralized by adding 270 μ L of 50 mM borate pH 9.3 with 9 g L⁻¹ NaCl, 3.75 g L⁻¹ BSA, 0.1 g L⁻¹ Tween-40, 0.5 g L⁻¹ NaN₃, and 1 mM DTT. The hemolysed whole blood samples were spiked with folic acid (pteroyl-L-glutamic acid, Sigma-Aldrich) for a recovery analysis.

The standard calibrators of folic acid were treated in the same way as the whole blood samples after lysis to turn the folic acid from the oxygenated form into the reduced form.

The homogeneous assays were performed on black half-area 96-well plates (Corning Incorporated, Corning, NY), protected from light, at room temperature in 50 mM borate buffer, pH 9.3, with 9 g L⁻¹ NaCl, 3.75 g L⁻¹ BSA, 0.1 g L⁻¹ Tween-40, and 0.5 g L⁻¹ NaN₃. The folic acid standard calibrators (0–2400 nM) or spiked pretreated whole blood samples (1:40-dilution, 0, 5 or 10 nM folic acid spikes, corresponding to 0, 200 or 400 nM folic acid in whole blood sample) and FBP-UCNP-conjugate (20 μ g mL⁻¹) were incubated for 30 min, on slow rotation to prevent blood cell sedimentation. Then, AF680-labeled folate analog (12 nM) was added, and the sensitized emission of the acceptor was measured at 740 nm with a modified plate Chameleon fluorometer (see section 4.4.1) after a 30 min incubation on slow rotation.

4.4 Instrumentation for luminescence measurements

4.4.1 Plate readers

In all of the original publications, a modified plate Chameleon reader (Hidex Oy, Turku, Finland) with a 980-nm laser diode as the excitation light source was used for the upconversion photoluminescence intensity and UC-RET measurements on 96-well plates. The emission wavelengths were selected using band-pass filters 535/50 nm and 665/25 nm for the upconversion emissions of NaYF₄: Yb³⁺, Er³⁺ nanomaterials; 600/40 nm and 740/40 nm for UC-RET acceptors pHrodo Red and AF680, respectively; and 470/20 nm, 665/25 nm and 795/5 nm for the emissions of NaYF₄: Yb³⁺, Tm³⁺ nanomaterials. The modifications of the plate Chameleon reader are

described in Soukka *et al.* (2005). The nanophosphors on the well were excited for 2 s and the emission was measured simultaneously.

In the original publication **I**, the fluorescence of the Tb³⁺-chelate was measured in time-resolved manner with a Victor 1420 multilabel counter (PerkinElmer, Wallac Oy, Turku, Finland). The default factory settings for Tb³⁺ measurements were used: excitation 340 nm, emission 545 nm, delay 500 μ s, and gate time 1400 μ s.

4.4.2 Spectral analysis

In the original publication **II**, the upconversion photoluminescence spectrum of NaYF₄: Yb³⁺, Er³⁺ nanomaterials was measured with Cary Eclipse fluorescence spectrophotometer (Agilent Technologies, Santa Clara, CA) equipped with a 980-nm laser diode (~95 mW) (Soukka *et al.*, 2005). The emission spectrum was measured from 500 to 700 nm with a 1 nm data interval, 5 nm emission slit, and S/N mode.

In the original publications **III** and **IV**, the upconversion photoluminescence spectra of both NaYF₄: Yb³⁺, Er³⁺ and NaYF₄: Yb³⁺, Tm³⁺ nanophosphors were measured with a PC2000-CCD optical fiber spectrometer (Ocean Optics, Inc., Dunedin, FL). A fiber-coupled NIR laser diode IFC-975-008 (Optical Fiber Systems Inc., Chelmsford, MA) was used as the excitation light source providing 6 W power at 973 nm. The sample chamber was an aluminum cube equipped with a Peltier element for thermoelectric cooling/heating and a 5-mm quartz NMR tube for liquid samples. In the excitation chamber, a RG850 long-pass filter (Edmund Optics, Barrington, NJ) was used. OOIIrrad software was used to record the spectra.

The PC2000-CCD detector was more red-sensitive than the detector in Cary Eclipse fluorescence spectrophotometer reaching up to 1100 nm. Furthermore, the excitation power density with the PC2000-CCD instrument was also much higher than with the Cary Eclipse fluorescence spectrophotometer, which affects the shape of the measured spectra, i.e., the relative intensities of individual emission peaks.

4.4.3 Time-domain lifetime analysis

In the original publications **II** and **IV**, the modified plate Chameleon fluorometer was used for the time-domain lifetime analysis of the upconversion emission. The lifetime measurement mode was set to repeatedly expose the sample to 2 ms excitation light pulses after which the decay was measured.

In the original publication **IV**, also two other instruments for time-domain lifetime analysis were used. The first one was a modular luminometer with pulsed excitation with NIR laser diode L9418-04 (Hamamatsu Photonics, Hamamatsu City, Japan) providing a 1.2 W maximum power at 976 nm. The optical part was the same as described above for the spectral measurement with PC2000-CCD spectrometer. The emission wavelengths were selected either with band-pass filters 544/10 nm, 650/10

nm, or 470/20 nm, or a long-pass filter with a cutoff at 750 nm. The detector was a head-on R1464 photomultiplier (PMT, Hamamatsu). The PMT signal was amplified in a high-speed current amplifier DHP-100 (Femto Messtechnik GmbH, Germany). The sample was exposed repeatedly to a 20 ms excitation pulse followed by a 30 ms delay period during which the decay was measured. The excitation pulse was cycled 10 000 times.

The instrument for the detection of directly excited luminescence lifetimes of the Yb³⁺ and Er³⁺ dopants in the original publication **IV** was a commercial Edinburgh Instruments spectrofluorometer FSP-920 equipped with a μ -flash lamp 920 H (pulse width 3 μ s) and a red-extended PMT (R2658P) from Hamamatsu; 930 nm or 378 nm excitation was used with 20 or 4 nm band width, respectively. The luminescence lifetimes of 980 nm or 550 nm/655 nm were recorded with 20 nm or 8 nm band widths, respectively.

The decay profiles were analyzed with the exponential decay fitting in Origin 8.0 (Originlab Corporation, Northampton, MA).

4.4.4 Imaging

The pHrodo™ Red-UCNP-conjugate was imaged with a Leica TCS SP5 STED/MP laser scanning microscope (Leica Microsystems GmbH, Germany) with a Spectra-Physics Mai Tai HP Ti:Sapphire NIR/IR laser (Newport, Santa Clara, CA) adjusted to 980 nm as the excitation light source. The laser power was 90 W mm⁻². The upconversion emission of the UCNPs and the sensitized emission of the acceptor dye were scanned from microscope slides at 10 Hz rate with channels 525/50 nm and 585/40 nm with confocal gains of 600 V and 900 V of the PMT, respectively. The microscope image analysis was performed with ImageJ software, version 1.43s (<http://rsb.info.nih.gov/ij/>).

For cell imaging, the Leica SP5 STED/MP microscope was equipped with a 63x water objective with a GaAs-hybrid detector for the sensitized acceptor signal or the standard PMT for the upconversion luminescence (all purchased from Leica) as detectors.

5 SUMMARY OF RESULTS AND DISCUSSION

5.1 Upconverting nanophosphor bioconjugates

5.1.1 UCNPs

The TEM-images of the synthesized $\text{NaYF}_4: \text{Yb}^{3+}, \text{Er}^{3+}$ and $\text{NaYF}_4: \text{Yb}^{3+}, \text{Tm}^{3+}$ show monodispersed sub-40-nm nanophosphors, spherical or rod-like in shape, with a narrow size distribution (Figure 12, Table 4). Their crystal structure was pure hexagonal (data not shown). As the crystal size of UCNPs decreases from bulk to biomolecule scale, the upconversion luminescence intensity is expected to decrease, due to an increasing surface-to-volume ratio enhancing the quenching effects of the environment and surface defects. However, from a bioanalytical application point of view, the nanosized particle labels are beneficial considering their relatively high capacity for bioconjugation, which increases their reactivity. Furthermore, most, if not all, of the particle volume is within the required distance for UC-RET. This decreases the background caused by radiative reabsorption improving the signal-to-background ratios of homogeneous assays. The uniform nanophosphor size and shape reduced the variation in the UC-RET signals.

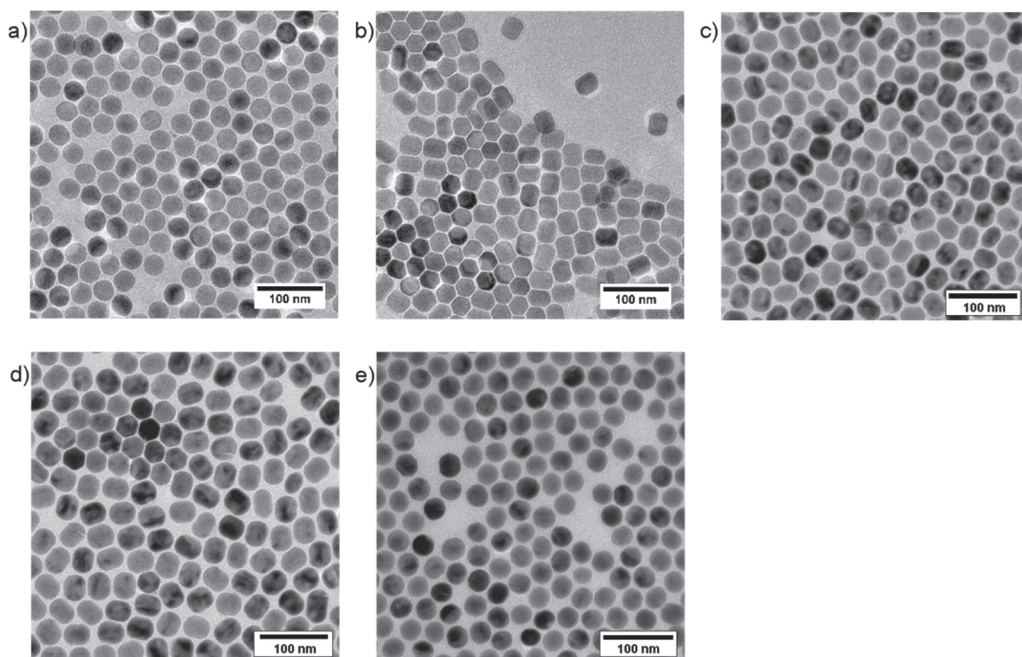


Figure 12. Transmission electron micrographs of $\text{NaYF}_4: \text{Yb}^{3+}, \text{Er}^{3+}$ nanophosphors used in original publication a) I, b) II, c) III, and d) IV, and e) transmission electron micrograph of $\text{NaYF}_4: \text{Yb}^{3+}, \text{Tm}^{3+}$ nanophosphors used in original publication IV. Scale bar 100 nm.

Table 4. The average diameters of the nanophosphors used in the original publications measured with ImageJ from a minimum of a hundred particles.

	Material	Width (nm)	Length (nm)	Publication
a)	NaYF ₄ : Yb ³⁺ , Er ³⁺	32.1 ± 1.0	34.1 ± 0.8	I
b)	NaYF ₄ : Yb ³⁺ , Er ³⁺	28.6 ± 2.2	36.7 ± 1.9	II
c)	NaYF ₄ : Yb ³⁺ , Er ³⁺	29.0 ± 1.6	36.3 ± 3.4	III
d)	NaYF ₄ : Yb ³⁺ , Er ³⁺	31.2 ± 2.2	38.0 ± 1.5	IV
e)	NaYF ₄ : Yb ³⁺ , Tm ³⁺	29.0 ± 1.7	31.5 ± 1.3	IV

The characterization of the synthesized nanophosphors with transmission electron microscopy proved to be invaluable, because the size and shape of the nanophosphors could be immediately seen. Furthermore, the crystal structure of the nanophosphors (determined with X-ray crystallography) correlated well with TEM, so that the hexagonal particles were uniform in both size and shape, whereas the cubic nanophosphors usually had a large size distribution and were variable in shape (data not shown).

5.1.2 Surface modification and bioconjugation of the UCNP

Surface modifications are required to render the inorganic UCNP water-dispersible and to bring functional groups onto their surface for bioconjugation. With an optimal coating, the UCNP are monodispersed and colloidally stable in aqueous solutions, and the surface layer protects the lanthanide ions from the quenching effects of water. The quenching mechanisms of water and the protecting impact of silica are discussed in section 5.3. For the use of UCNP as labels in bioanalytical assays, the surface coating should prevent UCNP aggregation and non-specific binding. For example, electrostatic repulsion can help to prevent aggregation. For homogeneous UC-RET-based assays the surface layer should be as thin as possible to achieve efficient energy transfer, and the capacity to bind the acceptor molecules should be high to achieve strong sensitized acceptor emission intensity.

Silica is widely used for the surface modification of nanoparticles due to its hydrophilicity, optical transparency, ease of functionalization, and biocompatibility. Two silanization methods were applied in this study. In publications **I-III**, a thin silica layer was polymerized onto the UCNP surface using TMOS and TMED as monomers in toluene. To begin with, all components, including the oleic acid-capped UCNP, are soluble in toluene, but as the hydrophilic silica shell is formed around the UCNP, they precipitate out of the nonpolar solvent. Thus, the thickness of the silica shell can be easily controlled. The silanized particles were dispersed in water and characterized with HR-TEM and energy-dispersive X-ray spectroscopy (EDX) to confirm the presence of the silica shell (Figure 13).

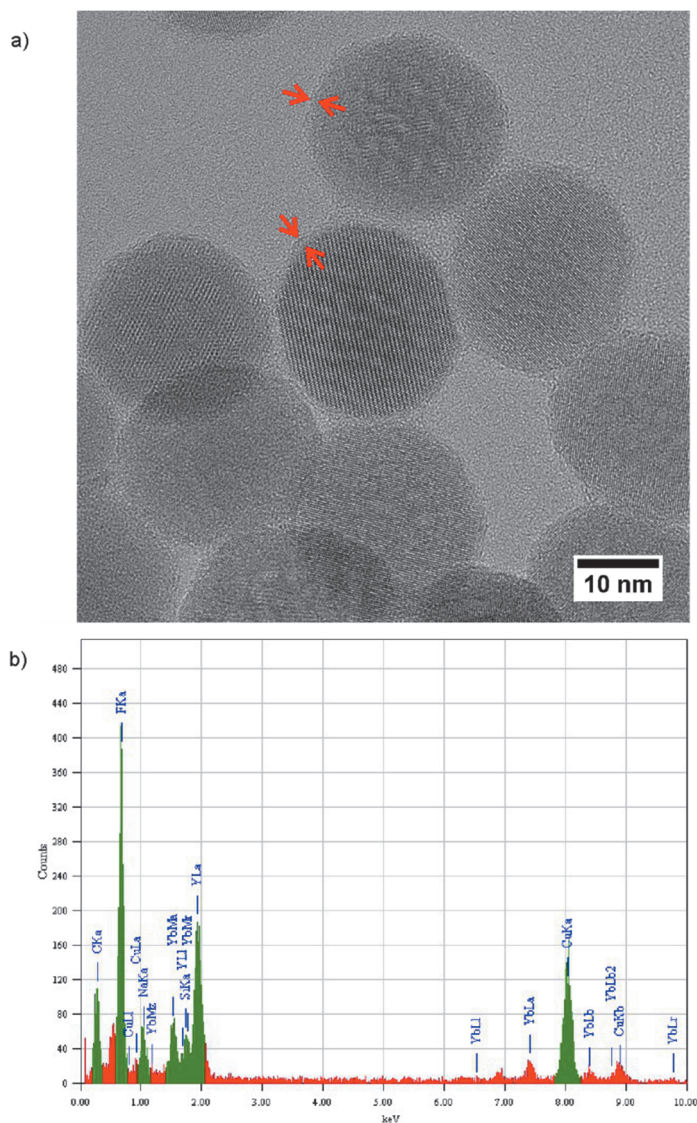


Figure 13. a) High-resolution TEM-image of NaYF₄: Yb³⁺, Er³⁺ nanophosphors with a thin silica layer (indicated with arrows). Scale bar 10 nm. b) EDX analysis of a single UCNP-particle. JEOL JEM-2200FS, 200 kV. (Unpublished)

The silica shell was <1.5 nm thick and it was only visible when imaged with the HR-TEM using high magnification (600 000x). The elemental analysis with EDX confirmed the presence of SiO₂. The nanophosphors were partly agglomerated on the TEM-grid, which may be caused by the TEM-sample preparation method in which a small sample of UCNPs is dropped in water on the hydrophobic grid and then quickly evaporated and dried by adding drops of acetone. Another alternative for the seen agglomeration is that the precipitation during the silanization process is not reversible.

However, the very thin silica shell makes the nanophosphors suitable donors for energy transfer-based assays.

From the elemental analysis of a single nanophosphor it could be calculated that the molar Yb^{3+} concentration in the studied particle was $\sim 17\%$ of the rare earth element content. Er^{3+} ions could not be detected with the EDX due to too low molar concentration. With the HR-TEM, also the crystal lattice structure of UCNPs can be clearly observed due to the sub-Å resolution of the microscope. The distance between two atomic planes of the nanoparticle in the center of the Figure 13a was ~ 0.5 nm.

Another silanization protocol by Wilhelm *et al.* (2013) was used in original publication **IV** in order to produce a thicker silica layer for prevention of water-based quenching. The method was based on reverse microemulsion in which the oleic acid-capped UCNPs were dispersed in cyclohexane with Igepal CO-520 detergent and ammonia acting as catalyst. A silica polymer shell was formed using only TEOS. For the bioconjugation purposes, the silanized nanophosphors can further be functionalized by adding TMED in a separate step; in original publication **IV** this was not necessary. In this method, the silica shell thickness can be controlled with the amount of TEOS and the length of reaction time. The TEM-image shows that the reverse microemulsion method produced a silica layer of ~ 7 nm around individual particles (Figure 14). The nanophosphors were monodispersed on the TEM-grid.

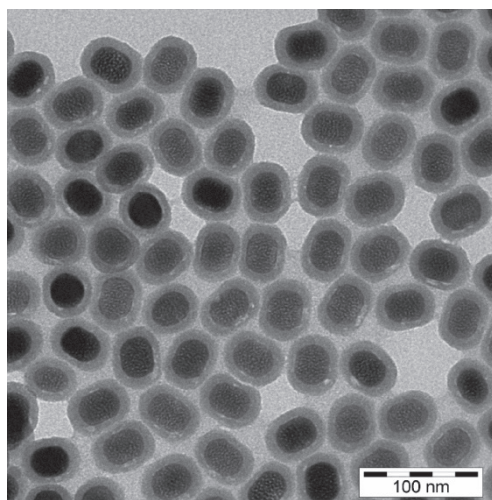


Figure 14. TEM-image of $\text{NaYF}_4: \text{Yb}^{3+}, \text{Er}^{3+}$ nanophosphors with a thick silica layer. Scale bar 100 nm. JEOL JEM-1400+, 80 kV. (Unpublished)

TEM-imaging was the method of choice to characterize the thickness of the polymerized silica shell. However, the images could not reveal the functional group capacity or, in all cases, the uniformity of the silica shell, nor could the colloidal stability be studied with standard TEM due to the sample preparation method with the evaporation step and hydrophobic grids. With cryo-TEM, an analysis of the colloidal stability of UCNPs

in a solvent would be possible, because the sample is frozen quickly with liquid nitrogen and imaged as cooled.

The functional group capacity can be studied by biomolecule conjugation and using the UCNPs conjugates as labels in heterogeneous and homogeneous assays. For example, conjugation to streptavidin is convenient for surface coating characterization because both types of assays can be performed (Kuningas *et al.*, 2005a; Kuningas *et al.*, 2005b). Especially, in homogeneous UC-RET-based assays, the surface layer thickness plays a crucial role. The thinner silica layer enables a more efficient energy transfer (data not shown). Also, a higher binding capacity increases the dynamic range in homogeneous assays and fewer donors are required decreasing also the background caused by radiative reabsorption or a leakage of donor luminescence to the acceptor emission measurement window. In heterogeneous assays, the thicker silica layer has lower nonspecific binding, probably due to the uniform silica layer, which also makes the shape of the UCNPs more round and, therefore, reduces the surface contact area (data not shown). This enables lower detection limits. High binding capacity increases sensitivity, so that if one binder detaches, another one next to it can bind to analyte. The prevention of aggregation and nonspecific binding are the key issues in heterogeneous assays.

Monoclonal antibody against PSA, pH-sensitive dye pHrodo™ Red, or folate binding protein were conjugated to the Er³⁺-doped UCNPs with a thin silica layer in publications I, II, and III, respectively. The anti-PSA-Mab-conjugated UCNPs were used to study a developed separation method based on the paramagnetism of lanthanides (section 5.1.3) and the FBP-conjugated UCNPs were used in the homogeneous whole blood assay for folic acid (section 5.2.2). These conjugation reactions were not optimized or characterized further.

For the pH-sensitive dye conjugation, three different dye amounts in the conjugation reaction were tested: 20, 100, or 200 nmol dye / 1.5 mg of UCNPs. With the largest amount, the dye molecules were conjugated to the surface of the UCNPs too densely which led to concentration quenching of the dye (data not shown). The dye amount of 100 nmol / 1.5 mg of UCNPs was chosen for the pH-nanosensor (section 5.2.1).

5.1.3 Purification of bioconjugated UCNPs

The handling of nanophosphors during the surface modification process can be challenging. Excess reagents and biomolecules must be removed from the UCNPs-solution after each surface modification step to ensure highly responsive labels. The most common method for gathering the UCNPs from solutions was centrifugation which allowed the less dense reagents and biomolecules to remain dispersed. However, centrifugation is time-consuming, as in addition to high g-forces, it also requires approximately 30 minutes to gather the nanophosphors into a precipitate. Furthermore, there is a high risk of losing some of the nanophosphors while removing the solution above the UCNPs-pellet resulting in low yield. The dispersion of the pellet

into a fresh solvent requires efficient sonication with ultrasound, although some aggregates might remain. The ultrasound sonication can also be harmful to the biomolecules conjugated to the UCNPs. Ultrafiltration was used also to filtrate the unreacted biomolecules from the UCNP-bioconjugate solution. However, it was difficult to detach the bioconjugated UCNPs from the filter membrane and redisperse them into solution without aggregation. Nevertheless, for the purification of the pHrodo Red-UCNP-conjugate from excess dye molecules, as described in publication **II**, the ultrafiltration was a convenient and fast method.

All trivalent lanthanide ions are paramagnetic with varying magnetic moments. Especially, Er^{3+} and Ho^{3+} have a high magnetic susceptibility. (Evans and Tew, 1981; Greenwood and Earnshaw, 1997) In the original publication **I**, this intrinsic characteristic of the Er^{3+} -doped nanophosphors was exploited to develop a highly selective separation method for UCNP-bioconjugates without the need of incorporating non-luminescent, magnetic materials inside the UCNP nanophosphor. The separation method was based on strong magnetic field gradients produced in a fibrous ferromagnetic steel wool matrix in a magnetic field. The high gradient magnetic separation (HGMS) system was able to capture even the weakly paramagnetic nanophosphors due to the magnetic field amplified up to 10 000-fold by the matrix. Two permanent supermagnets were used to generate the magnetic field, density of which was measured to be 400 mT.

The developed HGMS-system was used to purify UCNP-Mab5A10-bioconjugate from excess unbound antibodies. A typical elution profile is depicted in Figure 15. In the presence of the magnetic field, only non-magnetic antibodies flowed through. Once the magnets were removed, the antibody-conjugated UCNPs eluted, which could be detected as an increase in both upconversion luminescence and the Tb^{3+} -chelate fluorescence (from Tb^{3+} -labeled PSA) in the collected fractions.

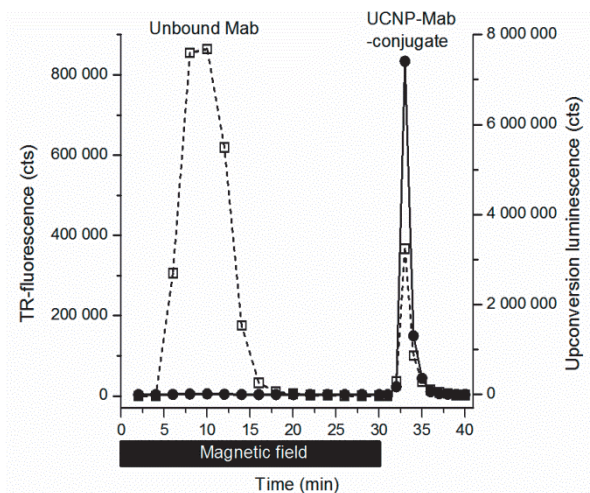


Figure 15. Elution profile of HGMS-purification of Mab5A10-UCNP-conjugate from unbound antibodies. The presence of antibodies was detected by a heterogeneous immunoassay with Tb³⁺-labeled PSA (open symbol, left y-axis). The UCNPs were detected by measuring the upconversion luminescence at 550 nm from the fractions (closed symbols, right y-axis). (I)

In addition to being a highly selective separation method, the HGMS is also fast, convenient, and gentle for the biomolecules. Further, HGMS is a concentrating method unlike most other techniques used for nanoparticle purification. With the HGMS-purified UCNP-bioconjugates, the nonspecific binding and variation in measured signals reduced when compared to bioconjugates purified with ultrafiltration (data not shown). A noteworthy disadvantage of the HGMS method is the use of dangerously strong permanent supermagnets, which need to be handled very carefully. Electromagnets or superconductive electromagnets would be suitable options giving also a possibility to increase the magnetic field density and to scale-up the system.

5.2 Homogeneous assays using UCNPs

Since the resonance energy transfer is a process inversely distance-dependent to the sixth power, only the acceptors that are bound to the UCNP surface can participate in UC-RET. Furthermore, only the activator ions in the UCNP that are within the required distance can transfer their energy to the acceptors. Therefore, the nanosized UCNPs are expected to be more efficient UC-RET-donors than the bulk used previously (Kuningas *et al.*, 2005b; Kuningas *et al.*, 2006; Rantanen *et al.*, 2009; Rantanen *et al.*, 2008; Rantanen *et al.*, 2007). Only the activator ions on the surface of a bulk particle are in the right range for UC-RET and the core volume only produces background luminescence via non-proximity-based reabsorptive energy transfer (Riuttamäki *et al.*, 2011). With nanophosphors, this background is expected to be minimized, because most of the particle volume of the ~30-nm nanophosphor is at the appropriate distance. In addition to the small size, the highly monodispersed and uniform nanophosphors add to the value of the obtained UC-RET signals.

The upconverting nanophosphors were used in two very different applications, which both exploited upconversion resonance energy transfer (UC-RET). In the original publication **II**, a chemosensor for intracellular pH was developed. In the original publication **III**, UC-RET was used for the measurement of folic acid directly in a whole blood sample. The used acceptor dyes were chosen on the basis of their spectral and fluorogenic properties, fluorescence intensity, and stability.

5.2.1 pH-nanosensor

Abnormal acidic intracellular pH values indicate cellular dysfunctions, such as cancer, apoptosis, and cell proliferation. In endosomes and lysosomes the pH is also acidic. The development of optical pH sensors for measuring or imaging intracellular pH is important but challenging. The currently available pH-sensitive probes (Han and Burgess, 2009) are vulnerable to photobleaching and autofluorescence background, and suffer from a poor penetration depth of the shortwave excitation and emission light.

In the original publication **II**, these problems were circumvented by utilizing upconverting nanophosphors as donors and a fluorogenic pH-sensitive pHrodo™ Red dye as acceptor in UC-RET. The dye was covalently conjugated to the aminosilane surface of the UCNPs. The spectral principle of the pH-nanosensor is illustrated in Figure 16. The excitation spectrum of the pHrodo™ Red overlaps with the green emission peaks of the upconverting nanophosphor, and the sensitized emission of the acceptor is measured at wavelengths where the upconversion luminescence is at its minimum. The UC-RET-sensitized fluorescence of the pHrodo™ Red dye increases strongly with decreasing pH, covering a broad dynamic range from pH 8 to pH 4. The pH-independent upconversion photoluminescence at 550 nm was used for referencing. Due to 980-nm excitation, the autofluorescence is spectrally avoided.

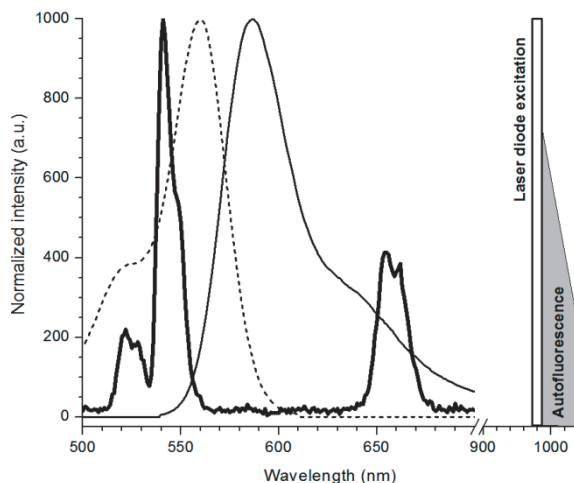


Figure 16. Normalized upconversion photoluminescence spectrum of NaYF₄: Yb³⁺, Er³⁺ nanophosphor (thick solid line) upon 980 nm excitation, and excitation (dotted line) and emission (thin solid line) spectra of pHrodo™ Red acceptor dye. (II)

To study whether UC-RET occurs between the UCNP and pHrodo™ Red, the decay of upconversion photoluminescence at 550 nm was measured for both aminosilane-coated UCNPs and the UCNP-dye conjugate (Figure 17). The decay curves were analyzed using the global fit function of triple exponential decay fitting of Origin 8.0. Two lifetimes (213 μ s and 454 μ s) originating from the emitting ions of the nanophosphors that do not participate in the UC-RET-process were found to be the same. The third lifetime was the main decay component and a decrease in this decay time was found in the UCNP-dye conjugate. The UC-RET-efficiency (η) was 37.7 % which was calculated using the Equation 3.

$$\eta(\text{UC-RET}) = 1 - \frac{\tau(\text{DA})}{\tau(\text{D})} \quad (3)$$

where $\tau(\text{DA})$ is the lifetime of the upconversion photoluminescence of the UCNP-dye conjugate and $\tau(\text{D})$ is the lifetime of the aminosilane-coated UCNP at 550 nm.

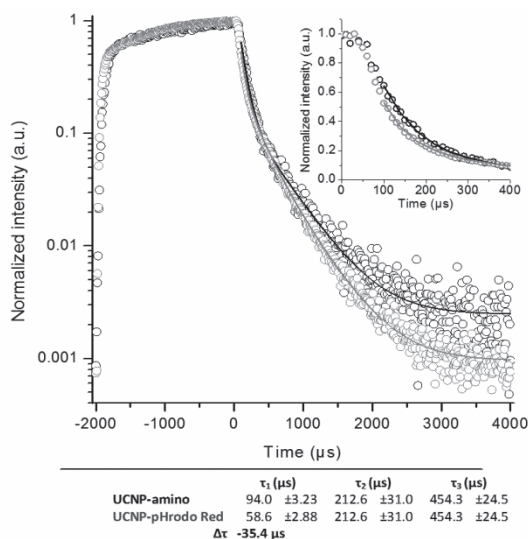


Figure 17. Upconversion photoluminescence decay curves of UCNPs with amino-surface (black) and UCNP-pHrodo Red-conjugate (grey) measured at 550 nm. The time range of 0–400 μ s in linear range is shown in the insert. (II)

A pH-titration was performed for the pH-nanosensor with and without a physiological salt concentration, because ionic strength is known to cause interferences with pH-indicators (Weidgans *et al.*, 2004). The pH-nanosensor produced a linear response between pH 3 and 6.7 (Figure 18). The physiological salt concentration decreased the slope of the response and, therefore, the resolution of the sensor, but the linear range of the response was still approximately in the same pH-range as without salts.

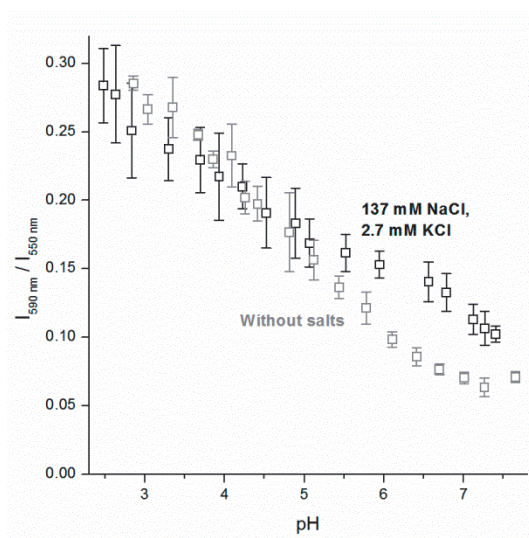


Figure 18. Ratiometric pH-titration curves of UCNP-pHrodo Red with (black) and without (grey) a physiological salt concentration. (II)

To test the applicability of the pH-nanosensor on pH imaging, droplets of the nanosensor in different pHs were scanned with Leica SP5 STED confocal fluorescence microscope at both 590 nm and 550 nm wavelengths at low scanning speed, because of the long luminescence lifetime of UCNP (Figure 19). The STED NIR/IR laser was used for the 980-nm excitation of the UCNP instead of stimulated emission depletion. Single particles could not be resolved but nanophosphor aggregates were visible at both emission channels. The signal response and the applicability of the imaging in ratiometric measurements were assessed. The ratio of the intensity in the red channel (representing the sensitized emission of pHrodo™ Red) and the intensity in the green channel (reference UCNP emission) was calculated giving a linear pH-response. Therefore, it is possible to image pH using the developed nanosensor, provided that extensive calibration experiments are performed.

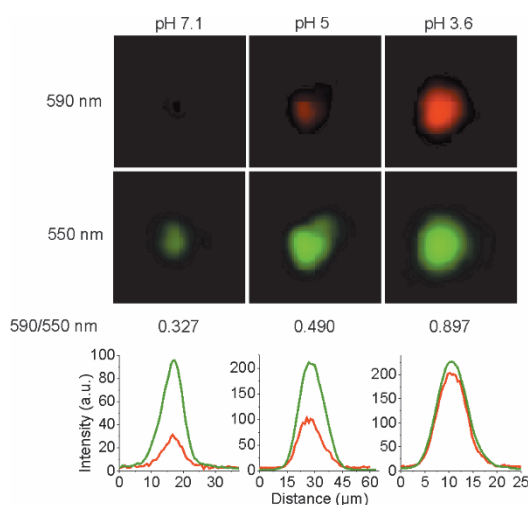


Figure 19. Fluorescence microscopy images of aggregates of UCNP-pHrodo™ Red-conjugate in three pHs and two emission channels. The ratiometric response was calculated from the intensities in the red (sensitized acceptor emission) and green (reference) channels over the whole area of the aggregate spot. The histograms represent the intensity profiles measured for a drawn line over the spot. Reproduced by permission of The Royal Society of Chemistry. (II)

The pH-nanosensors were efficiently taken up by HeLa cells (Figure 20). The particles were clustered in the fluorescence microscopy images, which was probably caused by endosomal compartmentalization. Both late endosomes and larger vesicular bodies would lead to the observed nanoparticle clusters (Prabhakar *et al.*, 2013). The yellow color in the superimposed image indicates a stronger red signal, i.e., an acidic pH, which also suggests compartmentalization inside endosomes. The silica-coated pH-nanosensor is cell-permeable and no cytotoxic effects were observed over a period of 16 h.

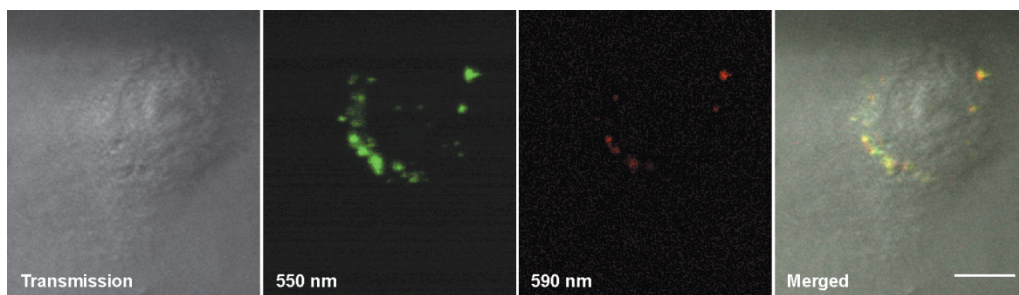


Figure 20. pH-nanosensor in HeLa cells. Transmission microscope image of a HeLa cell (left) and the fluorescence images of the green upconversion emission (550 nm) and the red-sensitized acceptor emission (590 nm) of the nanosensors internalized by the cell. The right image shows the transmission image superimposed with the fluorescence images. Scale bar 10 μm . Reproduced by permission of The Royal Society of Chemistry. (II)

No autofluorescence or photobleaching of the pH-nanosensor was detected. NIR-excitation offers deep penetration of light into tissue. However, the sensitivity of the pH response could be improved by increasing the number of pHrodo™ Red dyes on the UCNP surface by, e.g., introducing more amine groups with PEI-coating, and therefore, increasing the efficiency of UC-RET. This requires careful optimization to prevent the concentration quenching of the dye.

5.2.2 Whole blood folic acid assay

Folic acid has a role in both amino acid and nucleic acid synthesis in cells (Appling, 1991). Folic acid (Vitamin B9) deficiency has been linked to an increased risk of vascular diseases, cancer, and birth defects (Botto *et al.*, 1999; Choi and Mason, 2000; Robinson *et al.*, 1998). The folic acid in serum represents the dietary intake whereas the folate stored in red blood cells reflects the tissue folate levels, which should be analyzed for folate deficiency diagnosis (Amos *et al.*, 1994). Most available binding assays for folate are based on folate binding protein (FBP) and they are usually competitive and heterogeneous. Only a few homogeneous assays for folate are available, only one of which uses whole blood as a sample (Engel and Khanna, 1992; Khanna *et al.*, 1989). Homogeneous assays are simple and fast to perform, but the strong light absorption by whole blood limits the use of conventional fluorescent labels.

In the original publication **III**, a fluorescence-based homogeneous assay for whole blood folic acid was constructed using UCNPs as donors and Alexa Fluor 680 (AF680) as acceptor. The spectral principle of the assay is illustrated in Figure 21. The lysed whole blood absorbs strongly at wavelengths below 600 nm. However, the 660-nm emission peak of the $\text{NaYF}_4:\text{Yb}^{3+}, \text{Er}^{3+}$ nanophosphor is not significantly attenuated by the whole blood absorption. The excitation spectrum of the AF680 acceptor dye overlaps with the red emission peak of the nanophosphor, and the sensitized emission of the acceptor is measured at 740 ± 20 nm where both upconversion photoluminescence and whole blood absorption are at a minimum. The

980-nm excitation and the anti-Stokes measurement enable a total spectral avoidance of autofluorescence, which occurs at wavelengths above 980 nm.

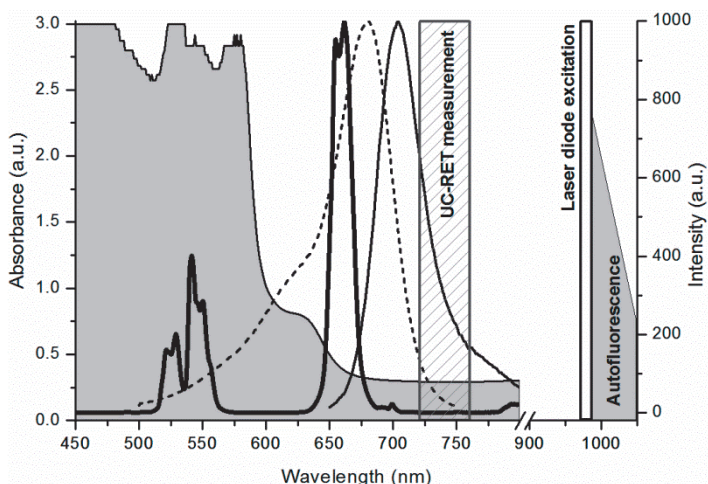


Figure 21. Normalized upconversion photoluminescence spectrum of NaYF₄: Yb³⁺, Er³⁺ nanophosphor (thick solid line) upon 980 nm excitation, and excitation (dotted line) and emission (thin solid line) spectra of Alexa Fluor 680 acceptor dye overlaid together with the absorption spectrum of 1:20-diluted whole blood in 0.5 % ascorbic acid (grey filled area). The sensitized emission of the acceptor is measured at 740±20 nm, using a band-pass emission filter and continuous laser excitation at 980 nm. Autofluorescence is completely spectrally avoided due to the anti-Stokes measurement. (III)

The folic acid in red blood cells is bound by deoxyhemoglobin and they are in the form of polyglutamates, which in serum are deconjugated to monoglutamates, due to pteroyl- γ -glutamylcarboxy-peptidase (Herbert *et al.*, 1962; Perry and Chanarin, 1977). To release the folate from the red blood cells so that it can be analysed in an assay, the whole blood sample needs to be hemolysed and pretreated to enable the deconjugation. Furthermore, the endogeneous folate binders of blood must also be denatured. Finally, the pH of the pretreated hemolysate must be adjusted to ~9.3, where the FBP has equal affinity to both 5-methyltetrahydrofolate (the predominant form of folate in serum) and folic acid (pteroyl-L-glutamic acid), which was used as standard calibrator (Givas and Gutcho, 1975). The same pH was used in the assays.

The standard curve was obtained with 20 μ g/mL FBP-UCNPs and 12 nM AF680-folate analog (Figure 22). The IC₅₀-value was 6 nM, which corresponds to a whole blood folate concentration of 240 nM (when multiplied by the dilution factor of 40). The limit of detection was 1 nM (40 nM in whole blood), defined as the mean of the sensitized emission of zero calibrator subtracted by three times the standard deviation. The measurable concentration range was two orders of magnitude, and the concentration coefficients of variation (CV%) were below 20 % at the folic acid concentration range of 3.2–100 nM, corresponding to whole blood folate concentrations of 128–4000 nM. According to Snow *et al.* (1999), the lower limit of the reference range of serum folate is ~6.8 nM and that of red blood cell folate is 340–

567 nM. According to ARCHITECT Folate Assay (Abbott Diagnostics, Chicago, IL), the normal folic acid reference range is 285–1475 nM in red blood cells and 7–46.5 nM in serum. A wide dynamic range in measuring whole blood folic acid is more important than low LOD. Thus, with its wide dynamic range, the developed homogeneous folate assay met the requirements for folate deficiency analysis.

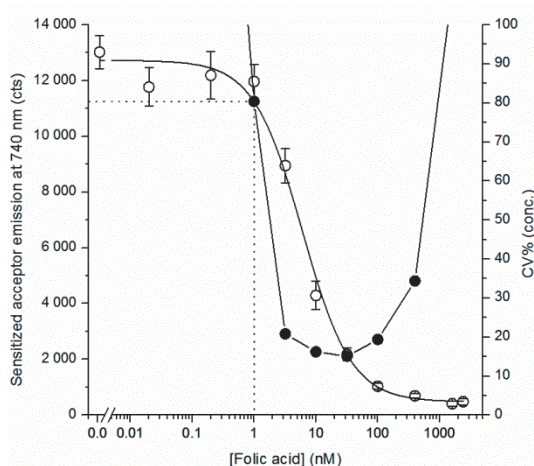


Figure 22. Calibration curve (open symbols) and concentration coefficient of variation percentage (CV%) profile (filled symbols) of the homogeneous folic acid assay. The dotted line indicates the limit of detection (LOD). (III)

The folic acid content and the analytical recovery were measured in a whole blood sample with a hematocrit value of 49 %, to study the reliability of the developed homogeneous assay. The whole blood sample was spiked with two folic acid concentrations, 200 or 400 nM, and the analytical recoveries were calculated by subtracting the endogenous folate amount (0-spiked) from the found amount and dividing it by the spiked amount. The mean endogenous whole blood folic acid concentration of the sample was 148 nM. The hematocrit-corrected amount was 302 nM/mL of packed cells. The analytical recoveries from spiked blood samples were 112–114 %. Thus, all added folic acid was found by the assay, and no major interfering matrix effect was present. The recovery-% of over 100 % could be explained by the spiked folate species being folic acid (pteroyl-L-glutamic acid), whereas the predominant endogenous folate form in serum is *N*-5-methyltetrahydrofolate. Even though the pH of the assay was set to ~9.3, where FBP has the same binding affinity toward both folate species, there might have been differences in pH in local environments.

5.3 Quenching effect of water on photon upconversion

The upconversion photoluminescence efficiency and intensity are known to be particle size-dependent. The nano-sized UCNPs luminesce much more weakly than their bulk

counterparts due to the decreased number of emitting ions and increased surface-to-volume ratio making them more prone to environmental quenching effects. (Schietinger *et al.*, 2009; Shan *et al.*, 2010b; Zhao *et al.*, 2013) The size-dependency may originate from phonon-mediated energy transfer processes (Liu, 2015; Schietinger *et al.*, 2009), surface effects based on the strong vibrational energies of solvent or surfactants (Shan *et al.*, 2010b; Zhao *et al.*, 2013), or increased surface defect density (Zhao *et al.*, 2013).

Water strongly quenches the luminescence of lanthanide ions and also lanthanide-doped nanocrystals. It has been suggested that the main mechanism of luminescence quenching of upconverting nanophosphors is the high-energy vibrational modes of OH-groups ($3200\text{--}3600\text{ cm}^{-1}$) causing increased multiphonon relaxation of the excited or intermediate energy states of lanthanides. (Boyer *et al.*, 2010) OH-vibrations facilitate the multiphonon relaxation of $^4\text{I}_{11/2} \rightarrow ^4\text{I}_{13/2}$ and $^2\text{H}_{11/2}/^4\text{S}_{3/2} \rightarrow ^4\text{F}_{9/2}$ transitions in Er^{3+} ion as illustrated in the energy level diagram in Figure 3 (Bogdan *et al.*, 2011; Boyer *et al.*, 2010).

To study the mechanism of water-based quenching, the luminescence intensities and decays of both Er^{3+} and Tm^{3+} -doped nanophosphors with a silica shell and without any surface-capping ligands (i.e., “bare”) were studied in water and in D_2O (i.e., “heavy water”) in the original publication IV. The bare nanophosphors were water dispersible after the oleic acid was removed from the surface and, thus, the luminescent properties could be measured from colloidal dispersions. D_2O vibrates at lower frequency ($\sim 2500\text{ cm}^{-1}$) and, therefore, it was used as the reference solvent for the water-based quenching. The upconversion photoluminescence spectra upon 980-nm excitation reveal that the luminescence was quenched up to 86 % by water in this measurement setting (Figure 23). Using the modified plate Chameleon fluorometer, the quenching efficiency of water reached 99.9 %. The red-to-green peak ratio in $\text{NaYF}_4: \text{Yb}^{3+}, \text{Er}^{3+}$ nanophosphors also increased in water when compared to D_2O . This is due to the multiphonon relaxations of $^4\text{I}_{11/2} \rightarrow ^4\text{I}_{13/2}$ and $^2\text{H}_{11/2}/^4\text{S}_{3/2} \rightarrow ^4\text{F}_{9/2}$ in water, both of which favor the population of the red emission energy state $^4\text{F}_{9/2}$. Similar quenching efficiency of water was observed in $\text{NaYF}_4: \text{Yb}^{3+}, \text{Tm}^{3+}$ nanophosphors. Silanization seemed to protect the luminescence of $\text{NaYF}_4: \text{Yb}^{3+}, \text{Tm}^{3+}$ nanophosphors more efficiently than that of the Er^{3+} -doped crystals.

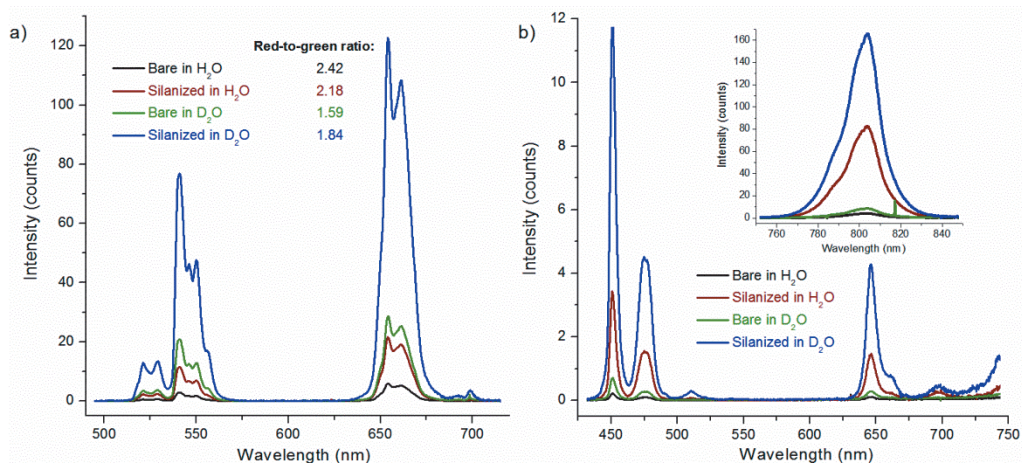


Figure 23. Upconversion photoluminescence spectra of bare and silanized a) NaYF₄: Yb³⁺, Er³⁺ and b) NaYF₄: Yb³⁺, Tm³⁺ nanophosphors in H₂O and D₂O. (IV)

To find a reason for the high quenching efficiency of water, the upconversion luminescence decays were measured in the two solvents. The quenching efficiencies of water were calculated using Equation 3, where $\tau(\text{DA})$ is the lifetime of the UCNP in water and $\tau(\text{D})$ is the lifetime in D₂O. For NaYF₄: Yb³⁺, Er³⁺ nanophosphors the luminescence lifetimes decreased in water by 53 % at 550 nm (Figure 24a) and 11 % at 660 nm, whereas for NaYF₄: Yb³⁺, Tm³⁺ nanophosphors the decrease was 5–25 % at 470 nm (Figure 24b), 650 nm and 800 nm. This small decrease in decays was not enough to explain the strong upconversion intensity quenching (up to 99.9 %). The main decay fractions were the shorter ones, and the amplitude fraction decreased in water. Thus, the shorter decay probably originates from the surface part of the nanophosphor which is more affected by the surface quenchers. When the quenchers were not present in D₂O, the amplitude fraction of the shorter decay was nearly 100 %. However, for the luminescence of NaYF₄: Yb³⁺, Tm³⁺ nanophosphors only one lifetime was found, which was not significantly changed in the presence of water. The doping concentration of Tm³⁺ is significantly lower than that of Er³⁺ in NaYF₄: Yb³⁺, Er³⁺ nanophosphors and, thus, there are less Tm³⁺ dopants near the surface of the UCNPs. Furthermore, as illustrated in the energy level diagram in Figure 3, no direct relaxations occur from the emissive levels of Tm³⁺ dopants in the presence of high energy OH-vibrations as the vibrational relaxations in NaYF₄: Yb³⁺, Tm³⁺ nanophosphors occur only in the intermediate energy levels and, further, the energy difference between those levels are too small for OH-vibrations. Therefore, Tm³⁺ dopants are less affected by the quenching effect of water.

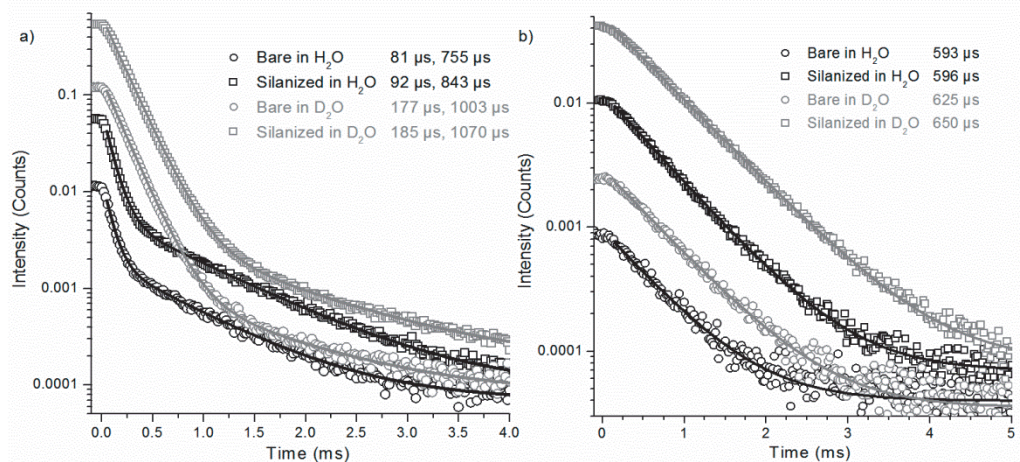


Figure 24. Upconversion photoluminescence decay curves of bare and silanized nanophosphors upon 980-nm excitation in H₂O and D₂O: a) NaYF₄: Yb³⁺, Er³⁺ at 544 nm and b) NaYF₄: Yb³⁺, Tm³⁺ nanophosphors at 470 nm. (IV)

The effect of excitation power density on the quenching efficiency of water was studied by measuring the upconversion luminescence spectrum of bare NaYF₄: Yb³⁺, Er³⁺ in both water and D₂O using different excitation powers ranging from 57 to 85 W/cm². The integrated intensities of the spectra were plotted against the excitation power densities in a log–log curve (Figure 25). For UCNPs in D₂O, the slopes of the power density dependency curves, from which the number of the excitation photons required to produce the upconversion photoluminescence is obtained according to Equation 2, were 2.1 and 2.6 for the green and red emission, respectively; the values are similar to those reported in literature (Wang *et al.*, 2009b). In the presence of the high-energy OH-vibrations, the slopes increased to 5.4 and 5.7, respectively. No previous reports on the excitation power density dependencies of the upconversion photoluminescence in water were found. Although the range of power densities was small, this clearly demonstrates the high quenching effect of water on upconversion photoluminescence.

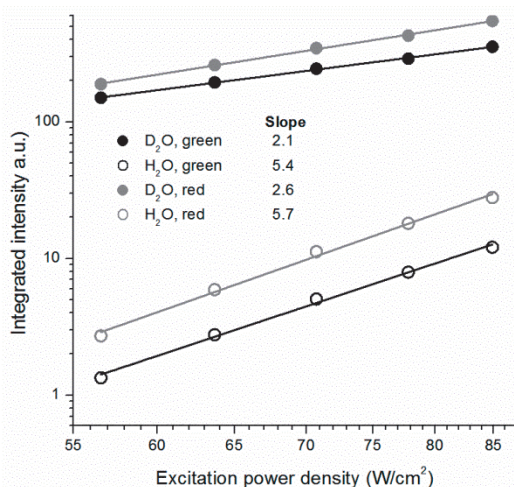


Figure 25. Intensities of the red (636–684 nm, gray symbols) and green (510–565 nm, black symbols) upconversion emission peaks in D₂O or in H₂O plotted together with excitation power density in a log–log curve. (IV)

In the original publication IV, also down-shifting emission decays were measured from the UCNPs. The fluorescence lifetimes of erbium dopants of NaYF₄: Yb³⁺, Er³⁺ nanophosphors were measured at 550 nm and 655 nm upon 380-nm excitation. The obtained decay times suggested that the green emissive state ⁴S_{3/2} is indeed quenched by multiphonon relaxation due to the OH-vibrations, but the red emissive state ⁴F_{9/2} is not directly affected by water. However, also the red upconversion luminescence intensity is strongly quenched by water. To find a reason for that, the luminescence decay of the excited state of ytterbium dopant in both NaYF₄: Yb³⁺, Er³⁺ and NaYF₄: Yb³⁺, Tm³⁺ nanophosphors was also measured at 980 nm upon 930-nm excitation (Figure 26). The experiment clearly revealed that it is the deactivation of the ²F_{5/2} state of the Yb³⁺ sensitizer ions by water that causes the strong quenching of upconversion photoluminescence. The directly excited luminescence decays of NaYF₄: Yb³⁺, Er³⁺ and NaYF₄: Yb³⁺, Tm³⁺ nanophosphors decreased by 73 % and 54 % in water, respectively, when compared to the decays in D₂O. Silica shell did not significantly prevent the quenching. Because upconversion is a multiphoton process, the deactivation of the sensitizer ion Yb³⁺ has a very strong quenching effect on the upconversion emission, since the excitation of the activator via ETU becomes more cumbersome.

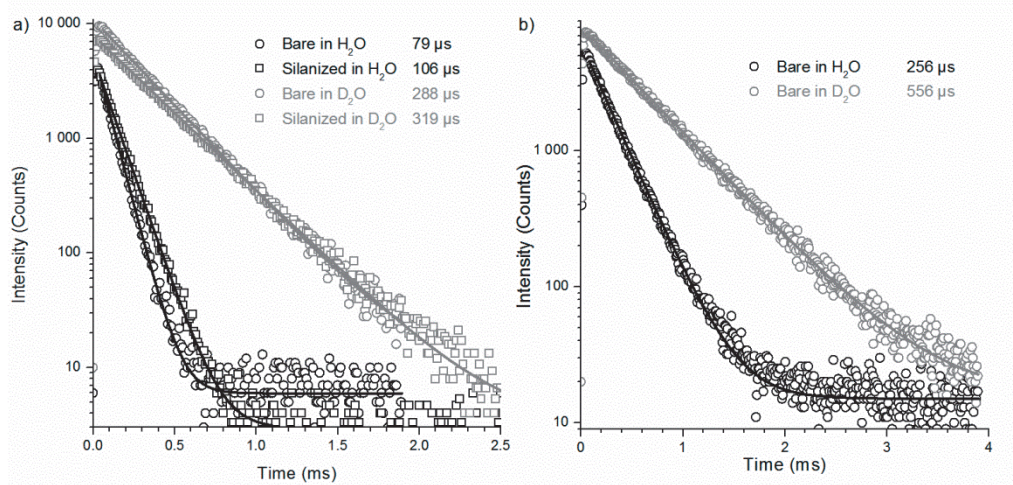


Figure 26. Decay curves of luminescence emission of a) bare and silanized NaYF₄: Yb³⁺, Er³⁺ and b) bare NaYF₄: Yb³⁺, Tm³⁺ nanophosphors at 980 nm upon 930 nm excitation in H₂O and in D₂O. (IV)

According to the obtained results, the whole volume of the UCNP seems to be susceptible to the water-based quenching. This is due to the higher number of Yb³⁺ ions (compared to the number of activators), and shorter distance between individual Yb ions which causes an efficient Yb–Yb energy migration from the core of the nanophosphor to the surface, where the energy is coupled with the vibrational modes of the environment (Gargas *et al.*, 2014; Tu *et al.*, 2015).

To produce more efficiently luminescing upconverting nanophosphors for bioanalytical assays, which are always done in aqueous environments, their surface must be shielded from water to prevent the Yb–Yb energy migration and the subsequent efficient luminescence quenching. Because the lanthanide dopant ions are the ones mostly affected by water, a core-shell structure with the luminescent dopants in the core and an “inactive” shell of NaYF₄ surrounding them would enhance the upconversion luminescence in water. However, a shell would inevitably increase the size of the nanophosphors. Another option would be a dense layer of hydrophobic or amphiphilic ligands which would prevent the water from reaching the sensitive lanthanide ions on the surface. This would, however, also require an additional hydrophilic layer to render the nanophosphors water-dispersible. An additional problem with this method is that the OH-, CH- and NH-vibrations of the ligand can also quench the luminescence of UCNP. One option is to replace the CH oscillators in the ligands with CF- or CD-bonds, which should reduce the non-radiative deactivation, although the water-dispersibility of UCNP with fluorinated ligand capping becomes an additional challenge (Hasegawa *et al.*, 2000; Werts, 2005).

6 CONCLUSIONS AND FUTURE PROSPECTS

The applicability of photon upconversion in bioanalytical assays has already been well established with bulk phosphors. In the meanwhile, synthetic methods for producing nanosized UCNPs have emerged. The decreasing particle size enables even higher specific activity compared to the bulk and brings more opportunities for the exploitation of this label technology. In this study, the unique physical properties of nanosized UCNPs were exploited in the development of a highly selective separation method for UCNP-bioconjugates, and their unique optical properties were used for the development of a pH-nanosensor for the intracellular sensing and imaging of pH, and for the quantification of folic acid in whole blood samples with a homogeneous UC-RET-based assay. In addition, the mechanism of the quenching effect of water on photon upconversion was studied.

The main conclusions based on the original publications are:

- I As the synthetic methods develop, the particle size of UCNPs starts to approach the size of biomolecules to which they must be conjugated for bioanalytical applications. The purification of the bioconjugates from the free biomolecules is essential for high specific activity, but traditional separation methods become cumbersome. The intrinsic weak paramagnetism of the lanthanide dopants provided the opportunity for the development of a highly selective separation method utilizing a high gradient magnetic separation system. The magnetic field between two strong permanent supermagnets was amplified with a magnetizable steel wool matrix by producing high magnetic gradients on the surface of the steel wool fibers. Even though the highly magnetically susceptible Er^{3+} ions only take up 3 mol% of all the rare earth elements in the nanophosphor, the UCNPs could be captured with HGMS while non-magnetic materials, such as excess biomolecules, flowed through. The UCNPs were eluted only after the magnetic field was removed. The developed separation method was highly selective, fast, and gentle for biomolecules, and the purification of the UCNP-bioconjugates improved their specific activity.
- II The high penetration depth of near-infrared radiation and the lack of autofluorescence with upconverting nanophosphor labels together with high photostability enable their use in intracellular sensing. A simple, fast, and sensitive pH-nanosensor for a pH-range of 3–6.7 was developed based on UC-RET between an UCNP and a fluorogenic pH-dependent dye pHrodo™ Red conjugated to the UCNP surface. The dual-wavelength referenced nanosensor was applied for imaging pH inside live HeLa cells. The UCNPs were internalized by the cells and no cytotoxic effects were found. An acidic pH of endosomes was imaged with a confocal fluorescence microscope. Thus, the developed pH-nanosensor is applicable to intracellular pH sensing after extensive calibration experiments.

- III** Homogeneous bioanalytical assays straight in an unprocessed whole blood sample would be valuable for a point-of-care setting. However, the use of conventional fluorescent labels is limited due to the strong light absorption by whole blood and the autofluorescence background from biological material. The utilization of the red emission peak of NaYF₄: Yb³⁺, Er³⁺ nanophosphors and a near-infrared fluorescent acceptor in an UC-RET-based assay enables both excitation and detection at optically transparent window of biomaterials, as established before. Furthermore, the anti-Stokes detection eliminates the Stokes-shifted autofluorescence. These unique properties of UCNPs were exploited in developing a homogeneous assay for the quantification of whole blood folic acid. The assay could be used with a large range of sample folate concentrations and it produced comparable results with an established heterogeneous folate assay based on the DELFIA technology. However, there was high variation in upconversion photoluminescence intensities, probably caused by UCNP aggregation due to irregular or blotchy surface silica layer, which caused high variation also in the sensitized acceptor emission. This should be minimized by improving the surface coating. In addition, a comparison of the developed assay to a standard commercial assay in use should be performed for final assay validation.
- IV** Bioanalytical applications are performed in aqueous environments and the inorganic UCNPs must be rendered water-dispersible. However, water is known to quench the upconversion luminescence of nanosized UCNPs but the mechanism behind the efficient quenching has not been clear. To find the mechanism involved, extensive studies were performed by the means of luminescence lifetime measurements. It has been suggested that the high-energy OH-vibrations in water increase the rate of the non-radiative relaxation of excited Er³⁺ dopants causing the quenching of upconversion luminescence, but this was found to be only a part of the mechanism. The main reason for the efficient quenching was the non-radiative deactivation of the Yb³⁺ sensitizer ion. The third vibrational overtone of the OH-stretching can bridge the energy gap of an excited Yb³⁺ ion causing a relaxation to ground state. Additionally, the Yb–Yb energy migration can transfer the excited energy in the core of the UCNP to the surface, where it is deactivated by water. Thus, the whole nanophosphor volume can be susceptible for quenching and the deactivation of the Yb³⁺ sensitizer ion has a very strong quenching effect on the upconversion photoluminescence intensity. This is a major finding as regards the development of brightly luminescent UCNPs.

In conclusion, the unique physical and optical properties of UCNPs provide opportunities for the development of sensitive, high-specific-activity labels for both optical sensing and bioanalytical applications also in difficult sample matrices. The presented homogeneous sensing applications can still be improved by the means of optimal surface coating, which reduces the particle aggregation and nonspecific binding, and increases the binding capacity. Thus, the surface chemistry of UCNPs

still remains an important object of research. Lately, also commercial sources of the UCNP materials and detection instruments have emerged, which will undoubtedly accelerate the development of UCNPs towards an established label technology and its commercial exploitation.

However, there is still potential for improvement in the upconversion photoluminescence brightness by the efficient passivation of the UCNP surface to prevent the environmental quenching effects. At the moment, intense development and study of core-shell-type UCNPs for the improvement of the upconversion photoluminescence efficiency is on-going. The lifetime measurement of the directly excited Yb^{3+} sensitizer emission could be used as an efficient tool for determining the ability of the shell to protect the core luminescence from the quenching effect of water. Also other surface passivation methods via incorporation of hydrophobic or amphiphilic ligands are being developed. In addition to the surface passivation, strategies, such as plasmon enhancement and broadband sensitization, have been explored to increase the quantum yield of the upconversion photoluminescence. The achievement of this goal is probably the most important research topic at the moment, and when successful, it would significantly increase the potential of UCNPs as a label technology.

ACKNOWLEDGEMENTS

This study was carried out at the Department of Biotechnology, University of Turku, during the years 2012–2015. Financial support from the National Doctoral Programme of Advanced Diagnostic Technologies and Applications (DIA-NET), the Academy of Finland, and the Finnish Funding Agency for Technology and Innovation (Tekes) is gratefully acknowledged.

I wish to thank the professors of the Department of Biotechnology, Professor Emeritus Timo Lövgren, Professor Kim Pettersson, and Professor Tero Soukka for giving me the opportunity to work at the department and carry out my doctoral studies in the DIA-NET doctoral program.

My deepest gratitude goes first and foremost to my supervisor Tero Soukka whose intelligence and expertise in everything (it seems) are enviable, and his enthusiasm for science and dedication to his students makes him the best supervisor one could have. I would also like to express my appreciation for giving me responsibilities in research projects and in writing funding applications, from which I have learned a lot. I also want to thank him for giving me opportunities to travel abroad for conferences, summer schools and a researcher exchange.

I wish to extend my gratitude to my other supervisor Adjunct Professor Mika Lastusaari and to my thesis committee advisors Dr. Terhi Riuttamäki, Dr. Katri Kuningas, and Dr. Michael Schäferling for your guidance.

I am extremely grateful to Dr. Harri Takalo and Professor Artur Bednarkiewicz for thoroughly reviewing this thesis. Their invaluable comments and suggestions helped improving the thesis. Anu Toivonen is gratefully thanked for reviewing the language of the thesis.

The original publications I owe to my hard-working and talented co-authors: Oskari Salovaara, Leena Mattsson, Satu Lahtinen, Timo Valta, Dr. Terhi Riuttamäki, Dr. Tuomas Näreoja, Sami Nylund, Sami Koho, Professor Jessica Rosenholm, Dr. Michael Schäferling, Krista Korpi, Sami Blom, Dr. Qi Wang, Dr. Iko Hyppänen, Niina Perälä, Riikka Peltomaa, Martin Kaiser, Dr. Christian Würth, Simon Christ, and Dr. Ute Resch-Genger are sincerely thanked for their vital contributions.

I have had the privilege to work in, in my humble opinion, the best projects (LEAP, INFRA, UPCORE, UPSHELL) in our department with the best group of people. There are too lot of us to list here, but I would like to thank each and every one of you for all the fun times in the lab and outside it. Dr. Terhi Riuttamäki and Dr. Johanna Pyylampi were my role models who I followed into this crazy idea called doctoral studies. Satu Lahtinen and Leena Mattsson are gratefully acknowledged for being my right-hand persons in the lab whose help I could always count on: thank you for

sharing all the success and failure in research. None of this would have been possible without our own synthesis wizard, Emilia Palo, who has prepared a large stash of nanosized upconverting phosphors for our studies. My sincere gratitude goes also to Timo Valta for the peer support during this whole thesis project. It was very helpful to have someone with the same thesis schedule, to share the stress, and to celebrate the reaching of both smaller and bigger milestones with someone. And thanks for the dinner company every night at 5 PM in the coffee room during the writing process. Dr. Henna Päckilä and the exemplarily organized thesis folder of Dr. Johanna Pyylampi were very helpful when arranging everything regarding the dissertation.

I would like to thank Dr. Johanna Pyylampi, Marja-Leena Järvenpää, Timo Valta, Sami Blom, Henna Savela, Juho Terrijärvi, and Maria Lahti for your company in our own, dark office corner in the “maisemakonttori”, and Dr. Henna Päckilä for sharing “the better office with a view and a door” with me. Thank you for sharing laughs and troubles, concerning either research or personal life. I wish to thank my fellow DIA-NET trainees Dr. Ari Lehmusvuori, Dr. Tuomas Huovinen, Dr. Minna Ylihärsilä, Marika Heikkinen, Dr. Tanja Savukoski, and Sami Blom, as well as the coordinators Dr. Johanna Pyylampi, Dr. Mari Peltola, and Dr. Saara Wittfooth for welcoming me into the DIA-NET family. I wish to thank all previous and present staff members at the Department of Biotechnology for providing a pleasant atmosphere and great laughs at coffee breaks.

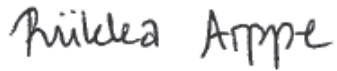
While studying upconverting nanophosphors, I have had opportunities to learn to use multiple transmission or scanning electron microscopes. The guidance of Professor Janne Ruokolainen and Dr. Hua Jiang (Nanomicroscopy center, Aalto University), and Dr. Markus Peurla (Laboratory of Electron Microscopy, University of Turku) in electron microscopy is gratefully acknowledged. I would also like to thank Oskari and Leena for their company during the long imaging sessions. While spending hours and hours in a cold, dark room staring at black dots in a screen, we started to see shapes, such as a walking duck in boots, a dolphin, a Moomin, or a bird and its nestling, in the images.

I am extremely thankful to my dear friends for the life outside the thesis project. I am very lucky to have such great friends with whom to relax every now and then. Thank you Heidi for your phone calls (even though they do not last for two hours any more or come as often as twelve years ago): our friendship has lasted as long as I can remember in spite of the long distance and I am sure it will last for the rest of our lives. Thank you also for giving me a lovely god-daughter. Huge thanks are also given to Henna S. and Emi for ”Marttaillat” (we should have those more often) and fun company during lunch breaks together with Timo; to Etvi, Jari-Matti, Veikko, Timpe, and Mikko for our mutual interest in progressive metal music and for your company at gigs; to Leena and Juho for all the cat GIFs; to Satu, Merja, and Laura for the pole dancing club; and to Nina, Risto, and other spouses for the fun get-togethers.

Acknowledgements

Lopuksi vielä kiitokset perheelleni kannustuksesta ja konnanhoitoavusta ulkomaanreissujen aikana: äiti, isä, Antti, sekä Milja ja Iisko, ja maailman parhaat siskonlapset Immi, Pilvi ja Anselmi. Kiitos, kun välillä käänsitte tädin ajatukset pois väitöskirjasta tärkeämpiin asioihin, kuten Disneyn prinsessoihin.

Turku, June 2015

A handwritten signature in dark ink, reading "Riikka Arppe". The script is cursive and fluid, with the first name "Riikka" and the last name "Arppe" clearly distinguishable.

Riikka Arppe

REFERENCES

- Abdul Jalil, R. and Zhang, Y. (2008) Biocompatibility of silica coated NaYF₄ upconversion fluorescent nanocrystals. *Biomaterials* **29**: 4122-4128.
- Abel, K.A., Boyer, J.-C., Andrei, C.M. and van Veggel, F.C.J.M. (2011) Analysis of the shell thickness distribution on NaYF₄/NaGdF₄ core/shell nanocrystals by EELS and EDS. *The Journal of Physical Chemistry Letters* **2**: 185-189.
- Achatz, D.E., Meier, R.J., Fischer, L.H. and Wolfbeis, O.S. (2011) Luminescent sensing of oxygen using a quenchable probe and upconverting nanoparticles. *Angewandte Chemie International Edition* **50**: 260-263.
- Adamczyk, M., Fino, J.R., Mattingly, P.G., Moore, J.A. and Pan, Y. (2004) Chemiluminescence quenching of pterioic acid-N-sulfonyl-acridinium-9-carboxamide conjugates by folate binding protein. *Bioorganic & Medicinal Chemistry Letters* **14**: 2313-2317.
- Aebischer, A., Hostettler, M., Hauser, J., Krämer, K., Weber, T., Güdel, H.U. and Bürgi, H.-B. (2006) Structural and spectroscopic characterization of active sites in a family of light-emitting sodium lanthanide tetrafluorides. *Angewandte Chemie International Edition* **45**: 2802-2806.
- Ali, R., Saleh, S.M., Meier, R.J., Azab, H.A., Abdelgawad, I.I. and Wolfbeis, O.S. (2010) Upconverting nanoparticle based optical sensor for carbon dioxide. *Sensors and Actuators B: Chemical* **150**: 126-131.
- Amos, R.J., Dawson, D.W., Fish, D.I., Leeming, R.J. and Linnell, J.C. (1994) Guidelines on the investigation and diagnosis of cobalamin and folate deficiencies. *Clinical & Laboratory Haematology* **16**: 101-115.
- Anderson, R.B., Smith, S.J., May, P.S. and Berry, M.T. (2014) Revisiting the NIR-to-visible upconversion mechanism in β -NaYF₄:Yb³⁺,Er³⁺. *The Journal of Physical Chemistry Letters* **5**: 36-42.
- Appling, D.R. (1991) Compartmentation of folate-mediated one-carbon metabolism in eukaryotes. *The Journal of the Federation of American Societies for Experimental Biology* **5**: 2645-2651.
- Arshady, R. and Mosbach, K. (1981) Synthesis of substrate-selective polymers by host-guest polymerization. *Die Makromolekulare Chemie* **182**: 687-692.
- Auzel, F. (1966) Compteur quantique par transfert d'energie entre deux ions de terres rares dans un tungstate mixte et dans un verre. *Comptes Rendus Hebdomadaires Des Seances De L Academie Des Sciences Serie B* **262**: 1016-&.
- Auzel, F. (2004) Upconversion and anti-Stokes processes with f and d ions in solids. *Chemical Reviews* **104**: 139-173.
- Bagwe, R.P., Hilliard, L.R. and Tan, W. (2006) Surface modification of silica nanoparticles to reduce aggregation and nonspecific binding. *Langmuir* **22**: 4357-4362.
- Beyazit, S., Ambrosini, S., Marchyk, N., Palo, E., Kale, V., Soukka, T., Tse Sum Bui, B. and Haupt, K. (2014) Versatile synthetic strategy for coating upconverting nanoparticles with polymer shells through localized photopolymerization by using the particles as internal light sources. *Angewandte Chemie International Edition* **53**: 8919-8923.
- Bogdan, N., Vetrone, F., Ozin, G.A. and Capobianco, J.A. (2011) Synthesis of ligand-free colloiddally stable water dispersible brightly luminescent lanthanide-doped upconverting nanoparticles. *Nano Letters* **11**: 835-840.
- Bogdan, N., Vetrone, F., Roy, R. and Capobianco, J.A. (2010) Carbohydrate-coated lanthanide-doped upconverting nanoparticles for lectin recognition. *Journal of Materials Chemistry* **20**: 7543-7550.
- Botto, L.D., Moore, C.A., Khoury, M.J. and Erickson, J.D. (1999) Neural-tube defects. *New England Journal of Medicine* **341**: 1509-1519.
- Boyer, J.-C., Manseau, M.-P., Murray, J.I. and van Veggel, F.C.J.M. (2010) Surface modification of upconverting NaYF₄ nanoparticles with PEG-phosphate ligands for NIR (800 nm) biolabeling within the biological window. *Langmuir* **26**: 1157-1164.
- Boyer, J.-C. and van Veggel, F.C.J.M. (2010) Absolute quantum yield measurements of colloidal NaYF₄: Er³⁺, Yb³⁺ upconverting nanoparticles. *Nanoscale* **2**: 1417-1419.
- Boyer, J.-C., Vetrone, F., Cuccia, L.A. and Capobianco, J.A. (2006) Synthesis of colloidal upconverting NaYF₄ nanocrystals doped with Er³⁺, Yb³⁺ and Tm³⁺, Yb³⁺ via thermal decomposition of lanthanide trifluoroacetate precursors. *Journal of the American Chemical Society* **128**: 7444-7445.
- Budijono, S.J., Shan, J., Yao, N., Miura, Y., Hoye, T., Austin, R.H., Ju, Y. and Prud'homme, R.K.

- (2010) Synthesis of stable block-copolymer-protected $\text{NaYF}_4\text{:Yb}^{3+}, \text{Er}^{3+}$ up-converting phosphor nanoparticles. *Chemistry of Materials* **22**: 311-318.
- Cao, T., Yang, T., Gao, Y., Yang, Y., Hu, H. and Li, F. (2010) Water-soluble $\text{NaYF}_4\text{:Yb/Er}$ upconversion nanophosphors: Synthesis, characteristics and application in bioimaging. *Inorganic Chemistry Communications* **13**: 392-394.
- Cao, T., Yang, Y., Gao, Y., Zhou, J., Li, Z. and Li, F. (2011) High-quality water-soluble and surface-functionalized upconversion nanocrystals as luminescent probes for bioimaging. *Biomaterials* **32**: 2959-2968.
- Chatterjee, D.K., Rufaihah, A.J. and Zhang, Y. (2008) Upconversion fluorescence imaging of cells and small animals using lanthanide doped nanocrystals. *Biomaterials* **29**: 937-943.
- Chen, F., Zhang, S., Bu, W., Chen, Y., Xiao, Q., Liu, J., Xing, H., Zhou, L., Peng, W. and Shi, J. (2012) A uniform sub-50 nm-sized magnetic/upconversion fluorescent bimodal imaging agent capable of generating singlet oxygen by using a 980 nm laser. *Chemistry - A European Journal* **18**: 7082-7090.
- Chen, G., Qiu, H., Prasad, P.N. and Chen, X. (2014) Upconversion nanoparticles: Design, nanochemistry, and applications in theranostics. *Chemical Reviews* **114**: 5161-5214.
- Chen, G., Yang, C. and Prasad, P.N. (2013) Nanophotonics and nanochemistry: Controlling the excitation dynamics for frequency up- and down-conversion in lanthanide-doped nanoparticles. *Accounts of Chemical Research* **46**: 1474-1486.
- Chen, J. and Zhao, J.X. (2012) Upconversion nanomaterials: Synthesis, mechanism, and applications in sensing. *Sensors* **12**: 2414-2435.
- Chen, Z., Chen, H., Hu, H., Yu, M., Li, F., Zhang, Q., Zhou, Z., Yi, T. and Huang, C. (2008) Versatile synthesis strategy for carboxylic acid-functionalized upconverting nanophosphors as biological labels. *Journal of the American Chemical Society* **130**: 3023-3029.
- Chivian, J.S., Case, W.E. and Eden, D.D. (1979) The photon avalanche: A new phenomenon in Pr^{3+} -based infrared quantum counters. *Applied Physics Letters* **35**: 124-125.
- Choi, S.-W. and Mason, J.B. (2000) Folate and carcinogenesis: An integrated scheme 1-3. *The Journal of Nutrition* **130**: 129-132.
- Corstjens, P.L., Li, S., Zuiderwijk, M., Kardos, K., Abrams, W.R., Niedbala, R.S. and Tanke, H.J. (2005) Infrared up-converting phosphors for bioassays. *IEE proceedings Nanobiotechnology* **152**: 64-72.
- DaCosta, M.V., Doughan, S., Han, Y. and Krull, U.J. (2014) Lanthanide upconversion nanoparticles and applications in bioassays and bioimaging: a review. *Analytica Chimica Acta* **832**: 1-33.
- Darbandi, M. and Nann, T. (2006) One-pot synthesis of YF_3 @silica core/shell nanoparticles. *Chemical Communications*: 776-778.
- del Barrio, M., de Marcos, S., Cebolla, V., Heiland, J., Wilhelm, S., Hirsch, T. and Galbán, J. (2014) Enzyme-induced modulation of the emission of upconverting nanoparticles: Towards a new sensing scheme for glucose. *Biosensors and Bioelectronics* **59**: 14-20.
- Deng, H., Yang, S., Xiao, S., Gong, H.-M. and Wang, Q.-Q. (2008) Controlled synthesis and upconverted avalanche luminescence of cerium(III) and neodymium(III) orthovanadate nanocrystals with high uniformity of size and shape. *Journal of the American Chemical Society* **130**: 2032-2040.
- Diamente, P.R., Raudsepp, M. and van Veggel, F.C.J.M. (2007) Dispersible Tm^{3+} -doped nanoparticles that exhibit strong 1.47 μm photoluminescence. *Advanced Functional Materials* **17**: 363-368.
- Dong, A., Ye, X., Chen, J., Kang, Y., Gordon, T., Kikkawa, J.M. and Murray, C.B. (2011) A generalized ligand-exchange strategy enabling sequential surface functionalization of colloidal nanocrystals. *Journal of the American Chemical Society* **133**: 998-1006.
- Dong, H., Sun, L.-D. and Yan, C.-H. (2015) Energy transfer in lanthanide upconversion studies for extended optical applications. *Chemical Society Reviews* **44**: 1608-1634.
- Dong, J. and Zink, J.I. (2014) Taking the temperature of the interiors of magnetically heated nanoparticles. *ACS Nano* **8**: 5199-5207.
- Engel, W.D. and Khanna, P.L. (1992) CEDIA in vitro diagnostics with a novel homogeneous immunoassay technique: Current status and future prospects. *Journal of Immunological Methods* **150**: 99-102.
- Ermolaev, V.L. and Sveshnikova, E.B. (1994) The application of luminescence-kinetic methods in the study of the formation of lanthanide ion complexes in solution. *Russian Chemical Reviews* **63**: 905.

- Erni, R., Rossell, M.D., Kisielowski, C. and Dahmen, U. (2009) Atomic-resolution imaging with a sub-50-pm electron probe. *Physical Review Letters* **102**: 096101.
- Esipova, T.V., Ye, X., Collins, J.E., Sakadžić, S., Mandeville, E.T., Murray, C.B. and Vinogradov, S.A. (2012) Dendritic upconverting nanoparticles enable in vivo multiphoton microscopy with low-power continuous wave sources. *Proceedings of the National Academy of Sciences* **109**: 20826-20831.
- Evans, C.H. and Tew, W.P. (1981) Isolation of biological materials by use of erbium (III)-induced magnetic susceptibilities. *Science* **213**: 653-654.
- Förster, T. (1948) Zwischenmolekulare Energiewanderung und Fluoreszenz. *Annalen der Physik* **437**: 55-75.
- Gai, S., Yang, P., Li, C., Wang, W., Dai, Y., Niu, N. and Lin, J. (2010) Synthesis of magnetic, up-conversion luminescent, and mesoporous core-shell-structured nanocomposites as drug carriers. *Advanced Functional Materials* **20**: 1166-1172.
- Gargas, D.J., Chan, E.M., Ostrowski, A.D., Aloni, S., Altoe, M.V.P., Barnard, E.S., Sanii, B., Urban, J.J., Milliron, D.J., Cohen, B.E. and Schuck, P.J. (2014) Engineering bright sub-10-nm upconverting nanocrystals for single-molecule imaging. *Nature Nanotechnology* **9**: 300-305.
- Givas, J.K. and Gutcho, S. (1975) pH dependence of the binding of folates to milk binder in radioassay of folates. *Clinical Chemistry* **21**: 427-428.
- Gnach, A. and Bednarkiewicz, A. (2012) Lanthanide-doped up-converting nanoparticles: Merits and challenges. *Nano Today* **7**: 532-563.
- Gorris, H.H., Ali, R., Saleh, S.M. and Wolfbeis, O.S. (2011) Tuning the dual emission of photon-upconverting nanoparticles for ratiometric multiplexed encoding. *Advanced Materials* **23**: 1652-1655.
- Graf, C., Vossen, D.L.J., Imhof, A. and van Blaaderen, A. (2003) A general method to coat colloidal particles with silica. *Langmuir* **19**: 6693-6700.
- Greenwood, N.N. and Earnshaw, A. (1997) *Chemistry of the elements*, Pergamon press, Oxford.
- Haase, M. and Schäfer, H. (2011) Upconverting nanoparticles. *Angewandte Chemie International Edition* **50**: 5808-5829.
- Hampl, J., Hall, M., Mufti, N.A., Yao, Y.M., MacQueen, D.B., Wright, W.H. and Cooper, D.E. (2001) Upconverting phosphor reporters in immunochromatographic assays. *Analytical Biochemistry* **288**: 176-187.
- Han, J. and Burgess, K. (2009) Fluorescent indicators for intracellular pH. *Chemical Reviews* **110**: 2709-2728.
- Hasegawa, Y., Ohkubo, T., Sogabe, K., Kawamura, Y., Wada, Y., Nakashima, N. and Yanagida, S. (2000) Luminescence of novel neodymium sulfonylamine complexes in organic media. *Angewandte Chemie International Edition* **39**: 357-360.
- Haupt, K., Linares, A.V., Bompert, M. and Tse Sum Bui, B. (2012) Molecularly imprinted polymers, in *Molecular Imprinting* (Haupt, K. ed) pp 1-28, Springer Berlin Heidelberg.
- He, X., Li, Z., Jia, X., Wang, K. and Yin, J. (2013) A highly selective sandwich-type FRET assay for ATP detection based on silica coated photon upconverting nanoparticles and split aptamer. *Talanta* **111**: 105-110.
- Heer, S., Kömpe, K., Güdel, H.U. and Haase, M. (2004) Highly efficient multicolour upconversion emission in transparent colloids of lanthanide-doped NaYF₄ nanocrystals. *Advanced Materials* **16**: 2102-2105.
- Hemmilä, I. (1985) Fluoroimmunoassays and immunofluorometric assays. *Clinical Chemistry* **31**: 359-370.
- Herbert, V., Larrabee, A.R. and Buchanan, J.M. (1962) Studies on the identification of a folate compound of human serum. *The Journal of Clinical Investigation* **41**: 1134-1138.
- Hlaváček, A., Sedlmeier, A., Skládal, P. and Gorris, H.H. (2014) Electrophoretic characterization and purification of silica-coated photon-upconverting nanoparticles and their bioconjugates. *ACS Applied Materials & Interfaces* **6**: 6930-6935.
- Hu, H., Yu, M., Li, F., Chen, Z., Gao, X., Xiong, L. and Huang, C. (2008) Facile epoxidation strategy for producing amphiphilic up-converting rare-earth nanophosphors as biological labels. *Chemistry of Materials* **20**: 7003-7009.
- Hyppänen, I., Hölsä, J., Kankare, J., Lastusaari, M., Malkamäki, M. and Pihlgren, L. (2009) The effect of Y³⁺ co-doping on the persistent up-conversion luminescence of the ZrO₂:Yb³⁺,Er³⁺ nanomaterials. *Journal of Luminescence* **129**: 1739-1743.
- Jana, N.R., Earhart, C. and Ying, J.Y. (2007) Synthesis of water-soluble and functionalized

- nanoparticles by silica coating. *Chemistry of Materials* **19**: 5074-5082.
- Jiang, G., Pichaandi, J., Johnson, N.J.J., Burke, R.D. and van Veggel, F.C.J.M. (2012) An effective polymer cross-linking strategy to obtain stable dispersions of upconverting NaYF₄ nanoparticles in buffers and biological growth media for biolabeling applications. *Langmuir* **28**: 3239-3247.
- Jiang, S., Win, K.Y., Liu, S., Teng, C.P., Zheng, Y. and Han, M.-Y. (2013) Surface-functionalized nanoparticles for biosensing and imaging-guided therapeutics. *Nanoscale* **5**: 3127-3148.
- Jiang, S., Zhang, Y., Lim, K.M., Sim, E., K. W. and Ye, L. (2009) NIR-to-visible upconversion nanoparticles for fluorescent labeling and targeted delivery of siRNA. *Nanotechnology* **20**: 155101.
- Johnson, N.J.J., Sangeetha, N.M., Boyer, J.-C. and van Veggel, F.C.J.M. (2010) Facile ligand-exchange with polyvinylpyrrolidone and subsequent silica coating of hydrophobic upconverting β -NaYF₄:Yb³⁺/Er³⁺ nanoparticles. *Nanoscale* **2**: 771-777.
- Joubert, M.-F. (1999) Photon avalanche upconversion in rare earth laser materials. *Optical Materials* **11**: 181-203.
- Kamimura, M., Miyamoto, D., Saito, Y., Soga, K. and Nagasaki, Y. (2008) Design of poly(ethylene glycol)/streptavidin coimmobilized upconversion nanophosphors and their application to fluorescence biolabeling. *Langmuir* **24**: 8864-8870.
- Khanna, P.L., Dworschack, R.T., Manning, W.B. and Harris, J.D. (1989) A new homogenous enzyme immunoassay using recombinant enzyme fragments. *Clinica Chimica Acta* **185**: 231-239.
- Krämer, K.W., Biner, D., Frei, G., Güdel, H.U., Hehlen, M.P. and Lüthi, S.R. (2004) Hexagonal sodium yttrium fluoride based green and blue emitting upconversion phosphors. *Chemistry of Materials* **16**: 1244-1251.
- Kumar, M., Guo, Y. and Zhang, P. (2009) Highly sensitive and selective oligonucleotide sensor for sickle cell disease gene using photon upconverting nanoparticles. *Biosensors and Bioelectronics* **24**: 1522-1526.
- Kumar, M. and Zhang, P. (2009) Highly sensitive and selective label-free optical detection of DNA hybridization based on photon upconverting nanoparticles. *Langmuir* **25**: 6024-6027.
- Kumar, M. and Zhang, P. (2010) Highly sensitive and selective label-free optical detection of mercuric ions using photon upconverting nanoparticles. *Biosensors and Bioelectronics* **25**: 2431-2435.
- Kuningas, K., Pääkilä, H., Ukonaho, T., Rantanen, T., Lövgren, T. and Soukka, T. (2007) Upconversion fluorescence enables homogeneous immunoassay in whole blood. *Clinical Chemistry* **53**: 145-146.
- Kuningas, K., Rantanen, T., Lövgren, T. and Soukka, T. (2005a) Enhanced photoluminescence of up-converting phosphors in a solid phase bioaffinity assay. *Analytica Chimica Acta* **543**: 130-136.
- Kuningas, K., Rantanen, T., Ukonaho, T., Lövgren, T. and Soukka, T. (2005b) Homogeneous assay technology based on upconverting phosphors. *Analytical Chemistry* **77**: 7348-7355.
- Kuningas, K., Ukonaho, T., Pääkilä, H., Rantanen, T., Rosenberg, J., Lövgren, T. and Soukka, T. (2006) Upconversion fluorescence resonance energy transfer in a homogeneous immunoassay for estradiol. *Analytical Chemistry* **78**: 4690-4696.
- Li, C., Quan, Z., Yang, J., Yang, P. and Lin, J. (2007) Highly uniform and monodisperse β -NaYF₄:Ln³⁺ (Ln = Eu, Tb, Yb/Er, and Yb/Tm) hexagonal microprism crystals: Hydrothermal synthesis and luminescent properties. *Inorganic Chemistry* **46**: 6329-6337.
- Li, H., Sun, D.-e., Liu, Y. and Liu, Z. (2014a) An ultrasensitive homogeneous aptasensor for kanamycin based on upconversion fluorescence resonance energy transfer. *Biosensors and Bioelectronics* **55**: 149-156.
- Li, H. and Wang, L. (2013) NaYF₄:Yb³⁺/Er³⁺ nanoparticle-based upconversion luminescence resonance energy transfer sensor for mercury(II) quantification. *Analyst* **138**: 1589-1595.
- Li, L.-L., Wu, P., Hwang, K. and Lu, Y. (2013) An exceptionally simple strategy for DNA-functionalized up-conversion nanoparticles as biocompatible agents for nanoassembly, DNA delivery, and imaging. *Journal of the American Chemical Society* **135**: 2411-2414.
- Li, L.-L., Zhang, R., Yin, L., Zheng, K., Qin, W., Selvin, P.R. and Lu, Y. (2012) Biomimetic surface engineering of lanthanide-doped upconversion nanoparticles as versatile bioprobes. *Angewandte Chemie International Edition* **51**: 6121-6125.
- Li, X., Wu, Y., Liu, Y., Zou, X., Yao, L., Li, F. and Feng, W. (2014b) Cyclometallated ruthenium complex-modified upconversion nanophosphors for selective detection of Hg²⁺ ions in water. *Nanoscale* **6**: 1020-1028.

- Li, X., Zhang, F. and Zhao, D. (2015) Lab on upconversion nanoparticles: optical properties and applications engineering via designed nanostructure. *Chemical Society Reviews* **44**: 1346-1378.
- Li, Z. and Zhang, Y. (2006) Monodisperse silica-coated polyvinylpyrrolidone/NaYF₄ nanocrystals with multicolor upconversion fluorescence emission. *Angewandte Chemie International Edition* **45**: 7732-7735.
- Li, Z. and Zhang, Y. (2008) An efficient and user-friendly method for the synthesis of hexagonal-phase NaYF₄:Yb, Er/Tm nanocrystals with controllable shape and upconversion fluorescence. *Nanotechnology* **19**: 345606.
- Li, Z., Zhang, Y. and Jiang, S. (2008) Multicolor core/shell-structured upconversion fluorescent nanoparticles. *Advanced Materials* **20**: 4765-4769.
- Li, Z., Zhang, Y., Shuter, B. and Muhammad Idris, N. (2009) Hybrid lanthanide nanoparticles with paramagnetic shell coated on upconversion fluorescent nanocrystals. *Langmuir* **25**: 12015-12018.
- Liang, S., Liu, Y., Tang, Y., Xie, Y., Sun, H., Zhang, H. and Yang, B. (2011) A user-friendly method for synthesizing high-quality NaYF₄:Yb,Er(Tm) nanocrystals in liquid paraffin. *Journal of Nanomaterials*: Article ID 302364.
- Liebherr, R.B., Soukka, T., Wolfbeis, O.S. and Gorris, H.H. (2012) Maleimide activation of photon upconverting nanoparticles for bioconjugation. *Nanotechnology* **23**: 485103.
- Lilja, H., Christensson, A., Dahlen, U., Matikainen, M.T., Nilsson, O., Pettersson, K. and Lövgren, T. (1991) Prostate-specific antigen in serum occurs predominantly in complex with alpha 1-antichymotrypsin. *Clinical Chemistry* **37**: 1618-1625.
- Lim, S.F., Ryu, W.S. and Austin, R.H. (2010) Particle size dependence of the dynamic photophysical properties of NaYF₄:Yb, Er nanocrystals. *Optics Express* **18**: 2309-2316.
- Liu, B., Tan, H. and Chen, Y. (2013a) Upconversion nanoparticle-based fluorescence resonance energy transfer assay for Cr(III) ions in urine. *Analytica Chimica Acta* **761**: 178-185.
- Liu, C., Wang, H., Li, X. and Chen, D. (2009) Monodisperse, size-tunable and highly efficient β -NaYF₄:Yb,Er(Tm) up-conversion luminescent nanospheres: controllable synthesis and their surface modifications. *Journal of Materials Chemistry* **19**: 3546-3553.
- Liu, C., Wang, Z., Jia, H. and Li, Z. (2011a) Efficient fluorescence resonance energy transfer between upconversion nanophosphors and graphene oxide: a highly sensitive biosensing platform. *Chemical Communications* **47**: 4661-4663.
- Liu, F., Zhao, Q., You, H. and Wang, Z. (2013b) Synthesis of stable carboxy-terminated NaYF₄:Yb³⁺, Er³⁺@SiO₂ nanoparticles with ultrathin shell for biolabeling applications. *Nanoscale* **5**: 1047-1053.
- Liu, G. (2015) Advances in the theoretical understanding of photon upconversion in rare-earth activated nanophosphors. *Chemical Society Reviews* **44**: 1635-1652.
- Liu, H., Xu, C.T., Lindgren, D., Xie, H., Thomas, D., Gundlach, C. and Andersson-Engels, S. (2013c) Balancing power density based quantum yield characterization of upconverting nanoparticles for arbitrary excitation intensities. *Nanoscale* **5**: 4770-4775.
- Liu, J., Bu, W., Zhang, S., Chen, F., Xing, H., Pan, L., Zhou, L., Peng, W. and Shi, J. (2012a) Controlled synthesis of uniform and monodisperse upconversion core/mesoporous silica shell nanocomposites for bimodal imaging. *Chemistry (Weinheim an der Bergstrasse, Germany)* **18**: 2335-2341.
- Liu, J., Cheng, J. and Zhang, Y. (2013d) Upconversion nanoparticle based LRET system for sensitive detection of MRSA DNA sequence. *Biosensors and Bioelectronics* **43**: 252-256.
- Liu, Q., Peng, J., Sun, L. and Li, F. (2011b) High-efficiency upconversion luminescent sensing and bioimaging of Hg(II) by chromophoric ruthenium complex-assembled nanophosphors. *ACS Nano* **5**: 8040-8048.
- Liu, Q., Sun, Y., Yang, T., Feng, W., Li, C. and Li, F. (2011c) Sub-10 nm hexagonal lanthanide-doped NaLuF₄ upconversion nanocrystals for sensitive bioimaging in vivo. *Journal of the American Chemical Society* **133**: 17122-17125.
- Liu, X., Deng, R., Zhang, Y., Wang, Y., Chang, H., Huang, L. and Liu, X. (2015) Probing the nature of upconversion nanocrystals: instrumentation matters. *Chemical Society Reviews* **44**: 1479-1508.
- Liu, Y., Tu, D., Zhu, H. and Chen, X. (2013e) Lanthanide-doped luminescent nanoprobe: controlled synthesis, optical spectroscopy, and bioapplications. *Chemical Society Reviews* **42**: 6924-6958.
- Liu, Y., Zhou, S., Tu, D., Chen, Z., Huang, M., Zhu, H., Ma, E. and Chen, X. (2012b) Amine-

References

- functionalized lanthanide-doped zirconia nanoparticles: Optical spectroscopy, time-resolved fluorescence resonance energy transfer biotetection, and targeted imaging. *Journal of the American Chemical Society* **134**: 15083-15090.
- Mader, H.S., Link, M., Achatz, D.E., Uhlmann, K., Li, X. and Wolfbeis, O.S. (2010) Surface-modified upconverting microparticles and nanoparticles for use in click chemistries. *Chemistry – A European Journal* **16**: 5416-5424.
- Mader, H.S. and Wolfbeis, O.S. (2010) Optical ammonia sensor based on upconverting luminescent nanoparticles. *Analytical Chemistry* **82**: 5002-5004.
- Mahalingam, V., Vetrone, F., Naccache, R., Speghini, A. and Capobianco, J.A. (2009) Colloidal $\text{Tm}^{3+}/\text{Yb}^{3+}$ -doped LiYF_4 nanocrystals: multiple luminescence spanning the UV to NIR regions via low-energy excitation. *Advanced Materials* **21**: 4025-4028.
- Mai, H.-X., Zhang, Y.-W., Si, R., Yan, Z.-G., Sun, L.-D., You, L.-P. and Yan, C.-H. (2006) High-quality sodium rare-earth fluoride nanocrystals: Controlled synthesis and optical properties. *Journal of the American Chemical Society* **128**: 6426-6436.
- Mathis, G. (1993) Rare earth cryptates and homogeneous fluorimmunoassays with human sera. *Clinical Chemistry* **39**: 1953-1959.
- Mattsson, L., Wegner, K.D., Hildebrandt, N. and Soukka, T. (2015) Upconverting nanoparticle to quantum dot FRET for homogeneous double-nano biosensors. *RSC Advances* **5**: 13270-13277.
- Max, J.-J. and Chapados, C. (2009) Isotope effects in liquid water by infrared spectroscopy. III. H_2O and D_2O spectra from 6000 to 0 cm^{-1} . *Journal of Chemical Physics* **131**: 184505.
- Meier, R.J., Simbürger, J.M.B., Soukka, T. and Schäferling, M. (2014) Background-free referenced luminescence sensing and imaging of pH using upconverting phosphors and color camera read-out. *Analytical Chemistry* **86**: 5535-5540.
- Miyake, Y., Togashi, H., Tashiro, M., Yamaguchi, H., Oda, S., Kudo, M., Tanaka, Y., Kondo, Y., Sawa, R., Fujimoto, T., Machinami, T. and Ono, A. (2006) Mercury^{II}-mediated formation of thymine-Hg^{II}-thymine base pairs in DNA duplexes. *Journal of the American Chemical Society* **128**: 2172-2173.
- Monguzzi, A., Milani, A., Lodi, L., Trioni, M.I., Tubino, R. and Castiglioni, C. (2009) Vibrational overtones quenching of near infrared emission in Er^{3+} complexes. *New Journal of Chemistry* **33**: 1542-1548.
- Muhr, V., Wilhelm, S., Hirsch, T. and Wolfbeis, O.S. (2014) Upconversion nanoparticles: From hydrophobic to hydrophilic surfaces. *Accounts of Chemical Research* **47**: 3481-3493.
- Naccache, R., Vetrone, F., Mahalingam, V., Cuccia, L.A. and Capobianco, J.A. (2009) Controlled synthesis and water dispersibility of hexagonal phase $\text{NaGdF}_4:\text{Ho}^{3+}/\text{Yb}^{3+}$ nanoparticles. *Chemistry of Materials* **21**: 717-723.
- Ni, D., Zhang, J., Bu, W., Xing, H., Han, F., Xiao, Q., Yao, Z., Chen, F., He, Q., Liu, J., Zhang, S., Fan, W., Zhou, L., Peng, W. and Shi, J. (2014) Dual-targeting upconversion nanoprobe across the blood-brain barrier for magnetic resonance/fluorescence imaging of intracranial glioblastoma. *ACS Nano* **8**: 1231-1242.
- Nyk, M., Kumar, R., Ohulchanskyy, T.Y., Bergey, E.J. and Prasad, P.N. (2008) High contrast in vitro and in vivo photoluminescence bioimaging using near infrared to near infrared up-conversion in Tm^{3+} and Yb^{3+} doped fluoride nanophosphors. *Nano Letters* **8**: 3834-3838.
- Ogawa, M., Kosaka, N., Regino, C.A.S., Mitsunaga, M., Choyke, P.L. and Kobayashi, H. (2010) High sensitivity detection of cancer in vivo using a dual-controlled activation fluorescent imaging probe based on H-dimer formation and pH activation. *Molecular BioSystems* **6**: 888-893.
- Ostrowski, A.D., Chan, E.M., Gargas, D.J., Katz, E.M., Han, G., Schuck, P.J., Milliron, D.J. and Cohen, B.E. (2012) Controlled synthesis and single-particle imaging of bright, sub-10 nm lanthanide-doped upconverting nanocrystals. *ACS Nano* **6**: 2686-2692.
- Peng, J., Wang, Y., Wang, J., Zhou, X. and Liu, Z. (2011) A new biosensor for glucose determination in serum based on up-converting fluorescence resonance energy transfer. *Biosensors and Bioelectronics* **28**: 414-420.
- Peng, J., Xu, W., Teoh, C.L., Han, S., Kim, B., Samanta, A., Er, J.C., Wang, L., Yuan, L., Liu, X. and Chang, Y.-T. (2015) High-efficiency in vitro and in vivo detection of Zn^{2+} by dye-assembled upconversion nanoparticles. *Journal of the American Chemical Society* **137**: 2336-2342.
- Perry, J. and Chanarin, I. (1977) Abnormal folate polyglutamate ratios in untreated pernicious anaemia corrected by therapy. *British Journal of Haematology* **35**: 397-402.

- Pollnau, M., Gamelin, D.R., Lüthi, S.R., Güdel, H.U. and Hehlen, M.P. (2000) Power dependence of upconversion luminescence in lanthanide and transition-metal-ion systems. *Physical Review B* **61**: 3337-3346.
- Prabhakar, N., Näreojä, T., von Haartman, E., Karaman, D.S., Jiang, H., Koho, S., Dolenko, T.A., Hänninen, P.E., Vlasov, D.I., Ralchenko, V.G., Hosomi, S., Vlasov, I.I., Sahlgren, C. and Rosenholm, J.M. (2013) Core-shell designs of photoluminescent nanodiamonds with porous silica coatings for bioimaging and drug delivery II: application. *Nanoscale* **5**: 3713-3722.
- Prorok, K., Bednarkiewicz, A., Cichy, B., Gnach, A., Misiak, M., Sobczyk, M. and Strek, W. (2014) The impact of shell host (NaYF₄/CaF₂) and shell deposition methods on the up-conversion enhancement in Tb³⁺, Yb³⁺ codoped colloidal α -NaYF₄ core-shell nanoparticles. *Nanoscale* **6**: 1855-1864.
- Päkkilä, H., Ylihärsilä, M., Lahtinen, S., Hattara, L., Salminen, N., Arppe, R., Lastusaari, M., Saviranta, P. and Soukka, T. (2012) Quantitative multianalyte microarray immunoassay utilizing upconverting phosphor technology. *Analytical Chemistry* **84**: 8628-8634.
- Qian, H.S., Guo, H.C., Ho, P.C.-L., Mahendran, R. and Zhang, Y. (2009) Mesoporous-silica-coated up-conversion fluorescent nanoparticles for photodynamic therapy. *Small* **5**: 2285-2290.
- Qiu, H., Yang, C., Shao, W., Damasco, J., Wang, X., Ågren, H., Prasad, P. and Chen, G. (2014) Enhanced upconversion luminescence in Yb³⁺/Tm³⁺-codoped fluoride active core/active shell/inert shell nanoparticles through directed energy migration. *Nanomaterials* **4**: 55-68.
- Rakov, N. and Maciel, G.S. (2012) Three-photon upconversion and optical thermometry characterization of Er³⁺:Yb³⁺ co-doped yttrium silicate powders. *Sensors and Actuators B: Chemical* **164**: 96-100.
- Rantanen, T., Järvenpää, M.L., Vuojola, J., Arppe, R., Kuningas, K. and Soukka, T. (2009) Upconverting phosphors in a dual-parameter LRET-based hybridization assay. *Analyst* **134**: 1713-1716.
- Rantanen, T., Järvenpää, M.L., Vuojola, J., Kuningas, K. and Soukka, T. (2008) Fluorescence-quenching-based enzyme-activity assay by using photon upconversion. *Angewandte Chemie International Edition* **47**: 3811-3813.
- Rantanen, T., Päkkilä, H., Jämsen, L., Kuningas, K., Ukonaho, T., Lövgren, T. and Soukka, T. (2007) Tandem dye acceptor used to enhance upconversion fluorescence resonance energy transfer in homogeneous assays. *Analytical Chemistry* **79**: 6312-6318.
- Riseberg, L.A. and Moos, H.W. (1968) Multiphonon orbit-lattice relaxation of excited states of rare-earth ions in crystals. *Physical Review* **174**: 429-438.
- Riuttamäki, T., Hyppänen, I., Kankare, J. and Soukka, T. (2011) Decrease in luminescence lifetime indicating nonradiative energy transfer from upconverting phosphors to fluorescent acceptors in aqueous suspensions. *The Journal of Physical Chemistry C* **115**: 17736-17742.
- Riuttamäki, T. and Soukka, T. (2014) Upconverting phosphor labels for bioanalytical assays, in *Advances in Chemical Bioanalysis* (Matysik, F.-M. ed) pp 155-204, Springer International Publishing.
- Robinson, K., Arheart, K., Refsum, H., Brattström, L., Boers, G., Ueland, P., Rubba, P., Palma-Reis, R., Meleady, R., Daly, L., Witteman, J. and Graham, I. (1998) Low circulating folate and vitamin B6 concentrations: Risk factors for stroke, peripheral vascular disease, and coronary artery disease. *Circulation* **97**: 437-443.
- Rosen, E.L., Buonsanti, R., Llordes, A., Sawvel, A.M., Milliron, D.J. and Helms, B.A. (2012) Exceptionally mild reactive stripping of native ligands from nanocrystal surfaces by using Meerwein's salt. *Angewandte Chemie International Edition* **51**: 684-689.
- Rubner, M.M., Achatz, D.E., Mader, H.S., Stolwijk, J.A., Wegener, J., Harms, G.S., Wolfbeis, O.S. and Wagenknecht, H.-A. (2012) DNA "nanolamps": "Clicked" DNA conjugates with photon upconverting nanoparticles as highly emissive biomaterial. *ChemPlusChem* **77**: 129-134.
- Saleh, S.M., Ali, R., Hirsch, T. and Wolfbeis, O.S. (2011a) Detection of biotin-avidin affinity binding by exploiting a self-referenced system composed of upconverting luminescent nanoparticles and gold nanoparticles. *Journal of Nanoparticle Research* **13**: 4603-4611.
- Saleh, S.M., Ali, R. and Wolfbeis, O.S. (2011b) Quenching of the luminescence of upconverting luminescent nanoparticles by heavy metal ions. *Chemistry - A European Journal* **17**: 14611-14617.
- Santra, S., Tapeç, R., Theodoropoulou, N., Dobson, J., Hebard, A. and Tan, W. (2001) Synthesis and characterization of silica-coated iron oxide nanoparticles in microemulsion: The effect of nonionic surfactants. *Langmuir* **17**: 2900-2906.

- Schietinger, S., Menezes, L.d.S., Lauritzen, B. and Benson, O. (2009) Observation of size dependence in multicolor upconversion in single Yb^{3+} , Er^{3+} codoped NaYF_4 nanocrystals. *Nano Letters* **9**: 2477-2481.
- Schäfer, H., Ptacek, P., Kömpe, K. and Haase, M. (2007) Lanthanide-doped NaYF_4 nanocrystals in aqueous solution displaying strong up-conversion emission. *Chemistry of Materials* **19**: 1396-1400.
- Schäferling, M. and Duerkop, A. (2008) Intrinsically referenced fluorimetric sensing and detection schemes: Methods, advantages and applications, in *Standardization and Quality Assurance in Fluorescence Measurements I* (Resch-Genger, U. ed) pp 373-414, Springer Berlin Heidelberg.
- Sedlmeier, A., Achatz, D.E., Fischer, L.H., Gorris, H.H. and Wolfbeis, O.S. (2012) Photon upconverting nanoparticles for luminescent sensing of temperature. *Nanoscale* **4**: 7090-7096.
- Sedlmeier, A. and Gorris, H.H. (2015) Surface modification and characterization of photon-upconverting nanoparticles for bioanalytical applications. *Chemical Society Reviews* **44**: 1526-1560.
- Selvin, P.R. (1996) Lanthanide-based resonance energy transfer. *IEEE Journal of Selected Topics in Quantum Electronics* **2**: 1077-1087.
- Shan, J., Uddi, M., Wei, R., Yao, N. and Ju, Y. (2010a) The hidden effects of particle shape and criteria for evaluating the upconversion luminescence of the lanthanide doped nanophosphors. *The Journal of Physical Chemistry C* **114**: 2452-2461.
- Shan, J., Uddi, M., Yao, N. and Ju, Y. (2010b) Anomalous Raman scattering of colloidal Yb^{3+} , Er^{3+} codoped NaYF_4 nanophosphors and dynamic probing of the upconversion luminescence. *Advanced Functional Materials* **20**: 3530-3537.
- Singh, S.K., Kumar, K. and Rai, S.B. (2009) $\text{Er}^{3+}/\text{Yb}^{3+}$ codoped Gd_2O_3 nano-phosphor for optical thermometry. *Sensors and Actuators A: Physical* **149**: 16-20.
- Snow, C.F. (1999) Laboratory diagnosis of vitamin B12 and folate deficiency: A guide for the primary care physician. *Archives of Internal Medicine* **159**: 1289-1298.
- Song, K., Kong, X., Liu, X., Zhang, Y., Zeng, Q., Tu, L., Shi, Z. and Zhang, H. (2012) Aptamer optical biosensor without bio-breakage using upconversion nanoparticles as donors. *Chemical Communications* **48**: 1156-1158.
- Soukka, T., Kuningas, K., Rantanen, T., Haaslahti, V. and Lövgren, T. (2005) Photochemical characterization of up-converting inorganic lanthanide phosphors as potential labels. *Journal of Fluorescence* **15**: 513-528.
- Soukka, T., Rantanen, T. and Kuningas, K. (2008) Photon upconversion in homogeneous fluorescence-based bioanalytical assays. *Annals of the New York Academy of Sciences* **1130**: 188-200.
- Sperling, R.A. and Parak, W.J. (2010) Surface modification, functionalization and bioconjugation of colloidal inorganic nanoparticles. *Philosophical Transactions of the Royal Society of London A: Mathematical, Physical and Engineering Sciences* **368**: 1333-1383.
- Stavola, M. and Dexter, D.L. (1979) Energy transfer and two-center optical transitions involving rare-earth and OH^- impurities in condensed matter. *Physical Review B* **20**: 1867-1885.
- Stöber, W., Fink, A. and Bohn, E. (1968) Controlled growth of monodisperse silica spheres in the micron size range. *Journal of Colloid and Interface Science* **26**: 62-69.
- Su, Q., Han, S., Xie, X., Zhu, H., Chen, H., Chen, C.-K., Liu, R.-S., Chen, X., Wang, F. and Liu, X. (2012) The effect of surface coating on energy migration-mediated upconversion. *Journal of the American Chemical Society* **134**: 20849-20857.
- Sun, L.-N., Peng, H., Stich, M.I.J., Achatz, D. and Wolfbeis, O.S. (2009) pH sensor based on upconverting luminescent lanthanide nanorods. *Chemical Communications*: 5000-5002.
- Suyver, J.F., Aebischer, A., Biner, D., Gerner, P., Grimm, J., Heer, S., Krämer, K.W., Reinhard, C. and Güdel, H.U. (2005a) Novel materials doped with trivalent lanthanides and transition metal ions showing near-infrared to visible photon upconversion. *Optical Materials* **27**: 1111-1130.
- Suyver, J.F., Aebischer, A., García-Revilla, S., Gerner, P. and Güdel, H.U. (2005b) Anomalous power dependence of sensitized upconversion luminescence. *Physical Review B* **71**: 125123.
- Suyver, J.F., Grimm, J., Krämer, K.W. and Güdel, H.U. (2005c) Highly efficient near-infrared to visible up-conversion process in NaYF_4 : Er^{3+} , Yb^{3+} . *Journal of Luminescence* **114**: 53-59.
- Suyver, J.F., Grimm, J., van Veen, M.K., Biner, D., Krämer, K.W. and Güdel, H.U. (2006) Upconversion spectroscopy and properties of NaYF_4 doped with Er^{3+} , Tm^{3+} and/or Yb^{3+} . *Journal of Luminescence* **117**: 1-12.

- Tu, L., Liu, X., Wu, F. and Zhang, H. (2015) Excitation energy migration dynamics in upconversion nanomaterials. *Chemical Society Reviews* **44**: 1331-1345.
- Ullman, E.F. (1999) Homogeneous immunoassays: Historical perspective and future promise. *Journal of Chemical Education* **76**: 781.
- Valta, T., Kale, V., Soukka, T. and Horn, C. (2015) Near-infrared excited ultraviolet emitting upconverting phosphors as an internal light source in dry chemistry test strips for glucose sensing. *Analyst* **140**: 2638-2643.
- van Dijk, J.M.F. and Schuurmans, M.F.H. (1983) On the nonradiative and radiative decay rates and a modified exponential energy gap law for 4f-4f transitions in rare-earth ions. *The Journal of Chemical Physics* **78**: 5317-5323.
- Vedvik, K.L., Eliason, H.C., Hoffman, R.L., Gibson, J.R., Kupcho, K.R., Somberg, R.L. and Vogel, K.W. (2004) Overcoming compound interference in fluorescence polarization-based kinase assays using far-red tracers. *Assay and Drug Development Technologies* **2**: 193-203.
- Vetrone, F., Mahalingam, V. and Capobianco, J.A. (2009) Near-infrared-to-blue upconversion in colloidal $\text{BaYF}_5\text{:Tm}^{3+}$, Yb^{3+} nanocrystals. *Chemistry of Materials* **21**: 1847-1851.
- Vetrone, F., Naccache, R., Morgan, C.G. and Capobianco, J.A. (2010a) Luminescence resonance energy transfer from an upconverting nanoparticle to a fluorescent phycobiliprotein. *Nanoscale* **2**: 1185-1189.
- Vetrone, F., Naccache, R., Zamarrón, A., Juarraz de la Fuente, A., Sanz-Rodríguez, F., Martínez Maestro, L., Martín Rodríguez, E., Jaque, D., García Solé, J. and Capobianco, J.A. (2010b) Temperature sensing using fluorescent nanothermometers. *ACS Nano* **4**: 3254-3258.
- Vuojola, J., Riittamäki, T., Kulta, E., Arppe, R. and Soukka, T. (2012) Fluorescence-quenching-based homogeneous caspase-3 activity assay using photon upconversion. *Analytica Chimica Acta* **725**: 67-73.
- Wang, C., Tao, H., Cheng, L. and Liu, Z. (2011a) Near-infrared light induced in vivo photodynamic therapy of cancer based on upconversion nanoparticles. *Biomaterials* **32**: 6145-6154.
- Wang, F., Banerjee, D., Liu, Y., Chen, X. and Liu, X. (2010a) Upconversion nanoparticles in biological labeling, imaging, and therapy. *Analyst* **135**: 1839-1854.
- Wang, F., Deng, R., Wang, J., Wang, Q., Han, Y., Zhu, H., Chen, X. and Liu, X. (2011b) Tuning upconversion through energy migration in core-shell nanoparticles. *Nature Materials* **10**: 968-973.
- Wang, F., Han, Y., Lim, C.S., Lu, Y., Wang, J., Xu, J., Chen, H., Zhang, C., Hong, M. and Liu, X. (2010b) Simultaneous phase and size control of upconversion nanocrystals through lanthanide doping. *Nature* **463**: 1061-1065.
- Wang, F. and Liu, X. (2008) Upconversion multicolor fine-tuning: Visible to near-infrared emission from lanthanide-doped NaYF_4 nanoparticles. *Journal of the American Chemical Society* **130**: 5642-5643.
- Wang, F. and Liu, X. (2009) Recent advances in the chemistry of lanthanide-doped upconversion nanocrystals. *Chemical Society Reviews* **38**: 976-989.
- Wang, F. and Liu, X. (2014) Multicolor tuning of lanthanide-doped nanoparticles by single wavelength excitation. *Accounts of Chemical Research* **47**: 1378-1385.
- Wang, F., Wang, J. and Liu, X. (2010c) Direct evidence of a surface quenching effect on size-dependent luminescence of upconversion nanoparticles. *Angewandte Chemie International Edition* **49**: 7456-7460.
- Wang, J., Wang, F., Wang, C., Liu, Z. and Liu, X. (2011c) Single-band upconversion emission in lanthanide-doped KMnF_3 nanocrystals. *Angewandte Chemie International Edition* **50**: 10369-10372.
- Wang, J., Wang, F., Xu, J., Wang, Y., Liu, Y., Chen, X., Chen, H. and Liu, X. (2010d) Lanthanide-doped LiYF_4 nanoparticles: Synthesis and multicolor upconversion tuning. *Comptes Rendus Chimie* **13**: 731-736.
- Wang, L., Yan, R., Huo, Z., Wang, L., Zeng, J., Bao, J., Wang, X., Peng, Q. and Li, Y. (2005) Fluorescence resonant energy transfer biosensor based on upconversion-luminescent nanoparticles. *Angewandte Chemie International Edition* **44**: 6054-6057.
- Wang, L., Zhang, Y. and Zhu, Y. (2010e) One-pot synthesis and strong near-infrared upconversion luminescence of poly(acrylic acid)-functionalized $\text{YF}_3\text{:Yb}^{3+}/\text{Er}^{3+}$ nanocrystals. *Nano Research* **3**: 317-325.
- Wang, M., Abbineni, G., Clevenger, A., Mao, C. and Xu, S. (2011d) Upconversion nanoparticles: synthesis, surface modification and biological

- applications. *Nanomedicine: Nanotechnology, Biology, and Medicine* **7**: 710-729.
- Wang, M., Hou, W., Mi, C.-C., Wang, W.-X., Xu, Z.-R., Teng, H.-H., Mao, C.-B. and Xu, S.-K. (2009a) Immunoassay of goat antihuman immunoglobulin G antibody based on luminescence resonance energy transfer between near-infrared responsive $\text{NaYF}_4:\text{Yb}, \text{Er}$ upconversion fluorescent nanoparticles and gold nanoparticles. *Analytical Chemistry* **81**: 8783-8789.
- Wang, Y.-F., Liu, G.-Y., Sun, L.-D., Xiao, J.-W., Zhou, J.-C. and Yan, C.-H. (2013a) Nd^{3+} -sensitized upconversion nanophosphors: Efficient in vivo bioimaging probes with minimized heating effect. *ACS Nano* **7**: 7200-7206.
- Wang, Y., Bao, L., Liu, Z. and Pang, D.-W. (2011e) Aptamer biosensor based on fluorescence resonance energy transfer from upconverting phosphors to carbon nanoparticles for thrombin detection in human plasma. *Analytical Chemistry* **83**: 8130-8137.
- Wang, Y., Shen, P., Li, C., Wang, Y. and Liu, Z. (2012) Upconversion fluorescence resonance energy transfer based biosensor for ultrasensitive detection of matrix metalloproteinase-2 in blood. *Analytical Chemistry* **84**: 1466-1473.
- Wang, Y., Tu, L., Zhao, J., Sun, Y., Kong, X. and Zhang, H. (2009b) Upconversion luminescence of $\beta\text{-NaYF}_4:\text{Yb}^{3+}, \text{Er}^{3+}$ @ $\beta\text{-NaYF}_4$ core/shell nanoparticles: Excitation power density and surface dependence. *The Journal of Physical Chemistry C* **113**: 7164-7169.
- Wang, Y., Wang, H., Liu, D., Song, S., Wang, X. and Zhang, H. (2013b) Graphene oxide covalently grafted upconversion nanoparticles for combined NIR mediated imaging and photothermal/photodynamic cancer therapy. *Biomaterials* **34**: 7715-7724.
- Wang, Y., Wu, Z. and Liu, Z. (2013c) Upconversion fluorescence resonance energy transfer biosensor with aromatic polymer nanospheres as the label-free energy acceptor. *Analytical Chemistry* **85**: 258-264.
- Weidgans, B.M., Krause, C., Klimant, I. and Wolfbeis, O.S. (2004) Fluorescent pH sensors with negligible sensitivity to ionic strength. *Analyst* **129**: 645-650.
- Wermuth, M., Riedener, T. and Güdel, H.U. (1998) Spectroscopy and upconversion mechanisms of $\text{CsCdBr}_3:\text{Dy}^{3+}$. *Physical Review B* **57**: 4369-4376.
- Werts, M.H. (2005) Making sense of lanthanide luminescence. *Science Progress* **88**: 101-131.
- Wilhelm, S., del Barrio, M., Heiland, J., Himmelstoß, S.F., Galbán, J., Wolfbeis, O.S. and Hirsch, T. (2014) Spectrally matched upconverting luminescent nanoparticles for monitoring enzymatic reactions. *ACS Applied Materials & Interfaces* **6**: 15427-15433.
- Wilhelm, S., Hirsch, T., Patterson, W.M., Scheucher, E., Mayr, T. and Wolfbeis, O.S. (2013) Multicolor upconversion nanoparticles for protein conjugation. *Theranostics* **3**: 239-248.
- Wilhelm, S., Hirsch, T., Scheucher, E., Mayr, T. and Wolfbeis, O.S. (2011) Magnetic nanosensor particles in luminescence upconversion capability. *Angewandte Chemie International Edition* **50**: A59-62.
- Wilhelm, S., Kaiser, M., Wurth, C., Heiland, J., Carrillo-Carrion, C., Muhr, V., Wolfbeis, O.S., Parak, W.J., Resch-Genger, U. and Hirsch, T. (2015) Water dispersible upconverting nanoparticles: effects of surface modification on their luminescence and colloidal stability. *Nanoscale* **7**: 1403-1410.
- Wong, H.-T., Vetrone, F., Naccache, R., Chan, H.L.W., Hao, J. and Capobianco, J.A. (2011) Water dispersible ultra-small multifunctional $\text{KGdF}_4:\text{Tm}^{3+}, \text{Yb}^{3+}$ nanoparticles with near-infrared to near-infrared upconversion. *Journal of Materials Chemistry* **21**: 16589-16596.
- Wu, S., Han, G., Milliron, D.J., Aloni, S., Altoe, V., Talapin, D.V., Cohen, B.E. and Schuck, P.J. (2009) Non-blinking and photostable upconverted luminescence from single lanthanide-doped nanocrystals. *Proceedings of the National Academy of Sciences* **106**: 10917-10921.
- Wu, Y.-M., Cen, Y., Huang, L.-J., Yu, R.-Q. and Chu, X. (2014) Upconversion fluorescence resonance energy transfer biosensor for sensitive detection of human immunodeficiency virus antibodies in human serum. *Chemical Communications* **50**: 4759-4762.
- Würth, C., Grabolle, M., Pauli, J., Spieles, M. and Resch-Genger, U. (2013) Relative and absolute determination of fluorescence quantum yields of transparent samples. *Nature Protocols* **8**: 1535-1550.
- Xie, L., Qin, Y. and Chen, H.-Y. (2012) Polymeric optodes based on upconverting nanorods for fluorescent measurements of pH and metal ions in blood samples. *Analytical Chemistry* **84**: 1969-1974.

- Xie, L., Qin, Y. and Chen, H.-Y. (2013) Direct fluorescent measurement of blood potassium with polymeric optical sensors based on upconverting nanomaterials. *Analytical Chemistry* **85**: 2617-2622.
- Xiong, L., Yang, T., Yang, Y., Xu, C. and Li, F. (2010) Long-term in vivo biodistribution imaging and toxicity of polyacrylic acid-coated upconversion nanophosphors. *Biomaterials* **31**: 7078-7085.
- Xu, C.T., Zhan, Q., Liu, H., Somesfalean, G., Qian, J., He, S. and Andersson-Engels, S. (2013) Upconverting nanoparticles for pre-clinical diffuse optical imaging, microscopy and sensing: Current trends and future challenges. *Laser & Photonics Reviews* **7**: 663-697.
- Yang, T., Sun, Y., Liu, Q., Feng, W., Yang, P. and Li, F. (2012) Cubic sub-20 nm NaLuF₄-based upconversion nanophosphors for high-contrast bioimaging in different animal species. *Biomaterials* **33**: 3733-3742.
- Yang, Y., Sun, Y., Cao, T., Peng, J., Liu, Y., Wu, Y., Feng, W., Zhang, Y. and Li, F. (2013) Hydrothermal synthesis of NaLuF₄:¹⁵³Sm,Yb,Tm nanoparticles and their application in dual-modality upconversion luminescence and SPECT bioimaging. *Biomaterials* **34**: 774-783.
- Yao, C., Wang, P., Zhou, L., Wang, R., Li, X., Zhao, D. and Zhang, F. (2014) Highly biocompatible zwitterionic phospholipids coated upconversion nanoparticles for efficient bioimaging. *Analytical Chemistry* **86**: 9749-9757.
- Yao, L., Zhou, J., Liu, J., Feng, W. and Li, F. (2012) Iridium-complex-modified upconversion nanophosphors for effective LRET detection of cyanide anions in pure water. *Advanced Functional Materials* **22**: 2667-2672.
- Ye, W.W., Tsang, M.-K., Liu, X., Yang, M. and Hao, J. (2014) Upconversion luminescence resonance energy transfer (LRET)-based biosensor for rapid and ultrasensitive detection of avian influenza virus H7 subtype. *Small* **10**: 2390-2397.
- Ye, X., Collins, J.E., Kang, Y., Chen, J., Chen, D.T.N., Yodh, A.G. and Murray, C.B. (2010) Morphologically controlled synthesis of colloidal upconversion nanophosphors and their shape-directed self-assembly. *Proceedings of the National Academy of Sciences* **107**: 22430-22435.
- Yi, G.-S. and Chow, G.-M. (2007) Water-soluble NaYF₄:Yb,Er(Tm)/NaYF₄/polymer core/shell/shell nanoparticles with significant enhancement of upconversion fluorescence. *Chemistry of Materials* **19**: 341-343.
- Yi, G., Sun, B., Yang, F., Chen, D., Zhou, Y. and Cheng, J. (2002) Synthesis and characterization of high-efficiency nanocrystal up-conversion phosphors: Ytterbium and erbium codoped lanthanum molybdate. *Chemistry of Materials* **14**: 2910-2914.
- Yi, G.S. and Chow, G.M. (2006) Synthesis of hexagonal-phase NaYF₄:Yb,Er and NaYF₄:Yb,Tm nanocrystals with efficient up-conversion fluorescence. *Advanced Functional Materials* **16**: 2324-2329.
- Yuan, F., Chen, H., Xu, J., Zhang, Y., Wu, Y. and Wang, L. (2014) Aptamer-based luminescence energy transfer from near-infrared-to-near-infrared upconverting nanoparticles to gold nanorods and its application for the detection of thrombin. *Chemistry – A European Journal* **20**: 2888-2894.
- Zeng, J.H., Su, J., Li, Z.H., Yan, R.X. and Li, Y.D. (2005) Synthesis and upconversion luminescence of hexagonal-phase NaYF₄:Yb, Er³⁺ phosphors of controlled size and morphology. *Advanced Materials* **17**: 2119-2123.
- Zeng, S., Tsang, M.-K., Chan, C.-F., Wong, K.-L. and Hao, J. (2012) PEG modified BaGdF₅:Yb/Er nanoprobe for multi-modal upconversion fluorescent, in vivo X-ray computed tomography and biomagnetic imaging. *Biomaterials* **33**: 9232-9238.
- Zhan, Q., Qian, J., Liang, H., Somesfalean, G., Wang, D., He, S., Zhang, Z. and Andersson-Engels, S. (2011) Using 915 nm laser excited Tm³⁺/Er³⁺/Ho³⁺-doped NaYbF₄ upconversion nanoparticles for in vitro and deeper in vivo bioimaging without overheating irradiation. *ACS Nano* **5**: 3744-3757.
- Zhang, C., Yuan, Y., Zhang, S., Wang, Y. and Liu, Z. (2011) Biosensing platform based on fluorescence resonance energy transfer from upconverting nanocrystals to graphene oxide. *Angewandte Chemie International Edition* **50**: 6851-6854.
- Zhang, F., Che, R., Li, X., Yao, C., Yang, J., Shen, D., Hu, P., Li, W. and Zhao, D. (2012a) Direct imaging the upconversion nanocrystal core/shell structure at the subnanometer level: Shell thickness dependence in upconverting optical properties. *Nano Letters* **12**: 2852-2858.
- Zhang, F., Wan, Y., Yu, T., Zhang, F., Shi, Y., Xie, S., Li, Y., Xu, L., Tu, B. and Zhao, D. (2007) Uniform nanostructured arrays of sodium rare-earth fluorides for highly efficient multicolor upconversion luminescence. *Angewandte Chemie International Edition* **46**: 7976-7979.

- Zhang, J., Li, B., Zhang, L. and Jiang, H. (2012b) An optical sensor for Cu(II) detection with upconverting luminescent nanoparticles as an excitation source. *Chemical Communications* **48**: 4860-4862.
- Zhang, Q., Song, K., Zhao, J., Kong, X., Sun, Y., Liu, X., Zhang, Y., Zeng, Q. and Zhang, H. (2009) Hexanedioic acid mediated surface-ligand-exchange process for transferring NaYF₄:Yb/Er (or Yb/Tm) up-converting nanoparticles from hydrophobic to hydrophilic. *Journal of Colloid and Interface Science* **336**: 171-175.
- Zhao, J., Lu, Z., Yin, Y., McRae, C., Piper, J.A., Dawes, J.M., Jin, D. and Goldys, E.M. (2013) Upconversion luminescence with tunable lifetime in NaYF₄:Yb,Er nanocrystals: role of nanocrystal size. *Nanoscale* **5**: 944-952.
- Zhao, J., Sun, Y., Kong, X., Tian, L., Wang, Y., Tu, L., Zhao, J. and Zhang, H. (2008) Controlled synthesis, formation mechanism, and great enhancement of red upconversion luminescence of NaYF₄:Yb³⁺, Er³⁺ nanocrystals/submicroplates at low doping level. *The Journal of Physical Chemistry B* **112**: 15666-15672.
- Zheng, W., Huang, P., Tu, D., Ma, E., Zhu, H. and Chen, X. (2015) Lanthanide-doped upconversion nano-bioprobes: electronic structures, optical properties, and biodetection. *Chemical Society Reviews* **44**: 1379-1415.
- Zhou, F., Noor, M.O. and Krull, U.J. (2014) Luminescence resonance energy transfer-based nucleic acid hybridization assay on cellulose paper with upconverting phosphor as donors. *Analytical Chemistry* **86**: 2719-2726.
- Zhou, H.-P., Xu, C.-H., Sun, W. and Yan, C.-H. (2009) Clean and flexible modification strategy for carboxyl/aldehyde-functionalized upconversion nanoparticles and their optical applications. *Advanced Functional Materials* **19**: 3892-3900.
- Zhou, J., Yu, M., Sun, Y., Zhang, X., Zhu, X., Wu, Z., Wu, D. and Li, F. (2011) Fluorine-18-labeled Gd³⁺/Yb³⁺/Er³⁺ co-doped NaYF₄ nanophosphors for multimodality PET/MR/UCL imaging. *Biomaterials* **32**: 1148-1156.
- Zou, W., Visser, C., Maduro, J.A., Pshenichnikov, M.S. and Hummelen, J.C. (2012) Broadband dye-sensitized upconversion of near-infrared light. *Nature Photonics* **6**: 560-564.